INTRA-BODY MOLECULAR COMMUNICATIONS: A THEORETICAL STUDY ON SYNAPTIC MULTIPLE-ACCESS CHANNEL

A THESIS SUBMITTED TO
THE GRADUATE SCHOOL OF SCIENCES AND ENGINEERING
OF
KOC UNIVERSITY

BY

DERYA MALAK

IN PARTIAL FULFILLMENT OF THE REQUIREMENTS
FOR
THE DEGREE OF MASTER OF SCIENCE
IN
ELECTRICAL AND ELECTRONICS ENGINEERING

FEBRUARY 2013

Koç University

Graduate School of Sciences and Engineering

This is to certify that I have examined this copy of a master's thesis by

Derya Malak

and have found that it is complete and satisfactory in all respects,

and that any and all revisions required by the final

examining committee have been made.

Committee Members:

_____

Özgür B. Akan, Ph. D. (Advisor)

_____

Kemal S. Türker, Ph. D.

_____

Alper Tunga Erdoğan, Ph. D.

Date: _____

Anneme ve Babama,

Mediha Malak ve Ahmet Haşim Malak.

ABSTRACT

Molecular communication is a novel nanoscale communication paradigm, in which information is encoded in messenger molecules for transmission and reception. Indeed, human body is a large-scale heterogeneous communication network of nanonetworks composed of interacting nanomachines, i.e., cells, whose functionalities primarily depend on nanoscale molecular communications. In this thesis, we introduce the elementary models for significant intra-body molecular communication channels, and then, discuss molecular nanonetworks belonging to multi-terminal extensions of channel models. Our objective is to learn from the elegant molecular communication mechanisms inside us for engineering practical communication techniques for emerging nanonetworks. Besides, we aim to pave the way for the advancement of revolutionary diagnosis and treatment techniques inspired from information and communication technologies, which is promising for future nanomedicine and bio-inspired molecular communication applications. Furthermore, we model the multiple-access synaptic communication channel, and analyze the synaptic transmission performance by incorporating the role of presynaptic input correlation. Using this model, we concentrate on the disorders characterized by abnormalities in the synaptic terminals and connections, and establish relations between neural diseases and synaptic communication problems. Additionally, we investigate the multiuser interference in synaptic communication channel and provide a performance analysis for the postsynaptic rate. Moreover, we investigate the performance, i.e., rate and delay, tradeoffs in messenger based molecular nanonetworks, and analyze a molecular network coding scheme to investigate the communication rate improvement.

ÖZET

Moleküler haberleşme, bilginin iletiminin ve alımının taşıyıcı moleküllerin kodlanmasıyla gerçekleştirildiği yenilikçi bir nano-ölçekli haberleşme yöntemidir. Gerçekte, insan vücudu da işlevselliği temel olarak nano-ölçekte moleküler haberleşmeye dayanan etkileşim halindeki nanomakinelerin, hücrelerin, oluşturduğu nanoağları içeren çok yapımlı ve büyük ölçekte bir haberleşme ağıdır. Bu tezde, insan vücudu içindeki önemli moleküler haberleşme kanalları için temel modelleri tanıtıp, sonrasında, bu kanal modellerine dayanarak genişletilmiş çoklu-uçlu moleküler ağları ele alıyoruz. Amacımız, vücut içindeki eksiksiz moleküler haberleşme mekanizmalarını öğrenerek yeni geliştirilen nanoağlar için pratik haberleşme teknikleri geliştirmektir. Ayrıca, bilgi ve haberleşme teknolojilerinden esinlenen devrim niteliğinde tanı ve tedavi tekniklerinin geliştirilmesinin yolunu açmaktır. Bu da gelecek-nesil nanotıp ve biyolojik-esinli moleküler haberleşme uygulamaları için umut vericidir. Bu çalışmada ayrıca, presinaptik girdi korelasyonunun rolü dahil edilerek çoklu-erişimli sinaptik haberleşme kanalı modellenmekte, ve sinaptik haberleşme başarımı analiz edilmektedir. Bu model kullanılarak, sinaptik uçlardaki ve bağlantılardaki anormalliklerle karakterize sağlık bozukluklarına ağırlık verilip, sinirsel hastalıklar ve sinaptik haberleşme problemleri arasındaki bağlantılar kurulabilmektedir. Bunlara ek olarak, çoklu-erişimli sinaptik haberleşme kanalındaki girişimi inceleyerek alıcı uçtaki iletim başarımı performansını analiz ediyoruz. Bunlara ilave olarak, bu çalışma, taşıyıcı-tabanlı moleküler nanoağlarda bilgi aktarım hızı ve gecikme başarımı ödünleşimlerinin araştırılmasını da kapsamaktadır. Haberleşme hızındaki artışı gözlemlemek amacıyla, yeni bir moleküler ağ kodlama yöntemi geliştirilmiş ve analiz edilmiştir.

ACKNOWLEDGMENTS

I would like to thank my advisor Prof. Özgür B. Akan for his everlasting support and guidance even before I started my MS study. He has taught me that hard work and effort pay off, and life is a race against time. Without his invaluable support and time, it would be impossible to complete this thesis.

I would like to thank Prof. Alper Tunga Erdoğan and Prof. Kemal S. Türker for participating in my thesis jury and giving me invaluable feedback.

I want to thank the Next-generation and Wireless Communications Laboratory members. I am very grateful to their friendship and collaboration during last two years. I also thank Murat for being my collaborator, my friend and my love with his constant help and compassion. I would also like to thank my old friends Gonca and Elifcan for their love, support and for the good old times.

I want to thank my mathematics teacher İbrahim Gürdal in Malatya Science High School for his enthusiasm and encouraging me to study Electrical Engineering.

I want to acknowledge the support of TÜBİTAK and Koç University, which made the completion of this thesis possible.

Finally, I would like to thank my parents, Mediha Malak and Ahmet Haşim Malak. My mother has always wanted the best for me, and helped me to discover and realize my objectives. My father has always motivated me to make my own decisions. Their affection and endless support are the greatest motivation and source of happiness for me. Finally, I want to thank my brother for being the most precious friend in the world.

TABLE OF CONTENTS

ABSTRACT iv

ÖZET iv

ACKNOWLEDGMENTS vi

TABLE OF CONTENTS vii

LIST OF FIGURES xiii

ABBREVIATIONS xvi

CHAPTERS

1 INTRODUCTION 1

1.1 Molecular Communications 1

1.2 Biological Nanonetworks 2

1.3 Performance Tradeoffs in Molecular Nanonetworks 3

1.4 Research Objectives and Solutions 3

1.4.1 Molecular Communication Nanonetworks inside Human Body 3

1.4.2 Synaptic Multiple-Access Channel in Hippocampal-Cortical Neurons 4

1.4.3 Adaptive Weight Update in Cortical Neurons and Estimation of Channel Weights in Synaptic Interference Channel 5

1.4.4 Rate-Delay Tradeoff in Molecular Nanonetworks 5

1.5 Thesis Outline 6

2 MOLECULAR COMMUNICATION NANONETWORKS INSIDE HUMAN BODY 8

2.1 Introduction 9

2.2 Intra-body Molecular Communication Channels 13

2.2.1 A General Framework for Molecular Communication Channels 14

2.2.2 Nanoscale Neuro-spike Communication Channel 16
2.2.3 Action Potential-based Cardiomyocyte Molecular Communication Channel 19
2.2.4 Hormonal Molecular Communication Channel 22
2.3 Intra-body Molecular Nanonetworks 25
2.3.1 Nervous Nanonetwork 25
2.3.2 Cardiovascular Molecular Nanonetwork 27
2.3.3 Endocrine Nanonetwork 28
2.4 Network of Intra-body Molecular Nanonetworks 28
2.4.1 Communication among Nervous, Cardiovascular Molecular, and Endocrine Nanonetworks 29
2.4.2 Communication between Nanosensor Networks and Nervous Nanonetwork 30
2.4.2.1 Audio Molecular Nanosensor Network 30
2.4.2.2 Visual Nanosensor Network 31
2.4.2.3 Somatosensory Network 32
2.4.2.4 Olfactory Nanosensor Network 32
2.4.2.5 Gustatory Molecular Nanosensor Network . . 33
2.5 Future Research Avenues 34
2.5.1 Molecular Communication Channels 35
2.5.1.1 ***Nanoscale Neuro-spike Communication Channel*** 36
2.5.1.2 ***Action Potential-based Cardiomyocyte Molecular Communication Channel*** 36
2.5.1.3 ***Hormonal Molecular Communication Channel*** 37
2.5.2 Intra-body Molecular Nanonetworks 37
2.5.2.1 ***Nervous Nanonetwork*** 38
2.5.2.2 ***Cardiovascular Molecular Nanonetwork*** . . 38
2.5.2.3 ***Endocrine Nanonetwork*** 39
2.5.2.4 ***Multi-terminal Molecular Communication inside Us*** 39

2.5.3 Physiology and Underlying Pathology of Intra-body Systems from Communication Theory Perspective 40
2.5.3.1 ***Nervous Nanonetwork:*** 40
2.5.3.2 ***Cardiovascular Nanonetwork:*** 41
2.5.3.3 ***Endocrine Nanonetwork:*** 42
2.5.3.4 ***Nanosensor networks:*** 42
3 A COMMUNICATION THEORETICAL ANALYSIS OF SYNAPTIC MULTIPLE-ACCESS CHANNEL IN HIPPOCAMPAL-CORTICAL NEURONS 44
3.1 Introduction 45
3.2 Model Description 48
3.2.1 Neuronal Firing: The Soma Channel 49
3.2.1.1 Low Pass Filtering 50
3.2.1.2 Point (Sigmoidal) Nonlinearity 50
3.2.1.3 Poisson Encoding 52
3.2.2 Vesicle Release Model 53
3.2.3 Postsynaptic Response with Variability in Vesicle Release 58
3.3 Multiple-Access Neuron Channel 59
3.3.1 Modulated Input Power Spectral Density 61
3.3.2 Multiuser Channel Rate Regions 62
3.4 Performance Evaluation 63
3.4.1 Independent Firing of Neurons 67
3.4.2 Correlated Firing of Neurons 68
3.5 Implications of Synaptic Communication on Neurological Disorders 70
3.5.1 Disorders Characterized by Presynaptic Abnormality . . . 71
3.5.1.1 Action Potential and Neural Transmission Performance 71
3.5.1.2 Vesicle Fusion Rate, Neurotransmitters and Neural Transmission Performance 71
3.5.2 Disorders Characterized by Synaptic Abnormality 72
3.5.2.1 Synaptic Depression 72
3.5.2.2 Abnormal Synaptic Plasticity 72
3.5.3 Disorders Characterized by Postsynaptic Abnormality . . 73

3.5.3.1 Postsynaptic Firing Rate and Neural Disorders 73

3.5.3.2 Postsynaptic Receptor Saturation and Neural Transmission Performance 73

4 ADAPTIVE WEIGHT UPDATE IN CORTICAL NEURONS AND ESTIMATION OF CHANNEL WEIGHTS IN SYNAPTIC INTERFERENCE CHANNEL 74

4.1 Introduction 74

4.2 Background and System Model 77

4.2.1 Background on Neural Signaling 77

4.2.2 Background on Neural Communication 78

4.2.2.1 Transmitting Node: The Presynaptic Neuron . 78

4.2.2.2 Transmission Process: The Synaptic Channel 78

4.2.2.3 Receiving Node: The Postsynaptic Neuron . . 79

4.2.2.4 Processing of Axonal Information 80

4.3 Synaptic Interference Channel 80

4.3.1 Interference Eigenfunctions 80

4.3.2 Single-Input Single-Output Neuron Synaptic Interference Channel 82

4.3.3 Multi-Input Single-Output Neuron Synaptic Interference Channel 83

4.4 Achievable Communication Rates in Synaptic Interference Channel . 83

4.4.1 Single-Input Single-Output Neuron Synaptic Interference Channel 84

4.4.1.1 Total Signal Power at the Output 84

4.4.1.2 Channel Capacity 85

4.4.2 Multi-Input Single-Output Neuron Synaptic Interference Channel 85

4.4.2.1 Total Signal Power at the Output: Multiaccess Channel 85

4.4.2.2 Channel Capacity 86

4.5 Classical Communication Techniques for Avoiding Interference in Neurons 86

4.5.1 Linear Estimation of the Channel Weight in Single Input Neural Channel 86

4.5.2 Linear Estimation of the Channel Weights in Multiple-Access Neural Interference Channel 87
4.6 Power Consumption of the Synaptic Interference Communication Channel 89
4.7 Neural Plasticity (Learning) with Synaptic Conductance Modification 90
4.7.1 Spike Timing Dependent Plasticity (STDP) Algorithm . . 91
4.8 Performance Evaluation 94
4.8.1 SISO Synaptic Interference Channel Performance Analysis 94
4.8.2 MISO Synaptic Interference Channel Performance Analysis 97
5 RATE-DELAY TRADEOFF WITH NETWORK CODING IN MOLECULAR NANONETWORKS 101
5.1 Introduction 102
5.2 A Messenger-Based Molecular Communication Model 104
5.2.1 Information Encoding Process 106
5.2.2 Transmission Process 108
5.2.3 Propagation Process 109
5.2.4 Reception Process 110
5.2.5 Information Decoding Process 112
5.3 Rate-Delay Tradeoff with Network Coding 114
5.3.1 Rate-Delay Tradeoff for Uncoded Case 116
5.3.2 Rate-Delay Tradeoff for Network Coded Case 119
5.4 Simulations 121
5.4.1 Simulation for Uncoded Case 121
5.4.2 Simulation for Network Coded Case 123
6 CONCLUSIONS AND FUTURE RESEARCH DIRECTIONS 125
6.1 Contributions 126
6.1.1 Molecular Communication Nanonetworks inside Human Body 126
6.1.2 Synaptic Multiple-Access Channel in Hippocampal-Cortical Neurons 126
6.1.3 Adaptive Weight Update in Cortical Neurons and Estimation of Channel Weights in Synaptic Interference Channel 127
6.1.4 Rate-Delay Tradeoff in Molecular Nanonetworks 127

6.2 Future Research Directions 127

REFERENCES 129

CURRICULUM VITAE 141

LIST OF FIGURES

FIGURES

Figure 2.1 General molecular communication system with two nodes. 14

Figure 2.2 Realistic channel model for nanoscale neuro-spike communication. 18

Figure 2.3 Cardiomyocyte molecular communication channel. 22

Figure 2.4 Hormonal molecular communication channel. 23

Figure 2.5 Communication architecture for overall nervous network. 26

Figure 3.1 A simplified functional model of neural spike responses [156]. In [156], a Linear-Nonlinear-Poisson (LNP) model for neural responses is proposed, which has been successfully used to describe the neuronal response characteristics. . . . 49

Figure 3.2 The pool-based synapse model. 54

Figure 3.3 Single-input single-output neuro-spike channel model between presynaptic and postsynaptic neuron terminals. 60

Figure 3.4 Multiple-access synaptic communication channel model. 60

Figure 3.5 Multiple-access channel model between presynaptic and postsynaptic neuron terminals. 60

Figure 3.6 (a) Linear approximation for the rate of the Poisson arrival process, and (b) the spike train at the output of the LNP filter under varying firing rates. 64

Figure 3.7 Random vesicle release process in the course of Poisson distributed spike train. 65

Figure 3.8 A segment of the EPSP waveform at the postsynaptic membrane, $E[\lambda] = 15.84$. 65

Figure 3.9 Time dependent neuronal (a) vesicle fusion rate, (b) vesicle release process, and (c) average rate during spike train. 66

Figure 3.10 The achievable rate region for SISO synaptic communication channel under variable vesicle pool conditions. 67

Figure 3.11 The rate region for multiple-access synaptic communication channel under independent firing of presynaptic neurons for a subset $A \subseteq \{1,\ldots,M\}$ of $M = 35$ presynaptic terminals 69

Figure 3.12 The rate region for multiple-access synaptic communication channel under correlated firing of presynaptic neurons for $M = 5$ presynaptic terminals with $\rho = 0 : 0.1 : 0.6$. 70

Figure 3.13 The effects of drugs and diseases on synaptic transmission [118]. 72

Figure 4.1 Spike Timing Dependent Plasticity (STDP). 91

Figure 4.2 Capacity of the SISO neuron channel with respect to noise variance σ^2. . . 94

Figure 4.3 Capacity of the SISO neuron channel with respect to time, which is dependent on the actual dynamics of the synaptic channel weight w for $\sigma^2 = 2.5 \times 10^{-8}$. 96

Figure 4.4 MSE performance of weight estimation of the SISO neuron interference channel for $M_{EX}/M_{IN} = 2.5$. 97

Figure 4.5 Communication rate of the SISO neuron interference channel for various values of M_{EX} and M_{IN}, where $\sigma^2 = 2.5 \times 10^{-8}$. 98

Figure 4.6 MISO synaptic interference channel estimation, (a) MSE for $N_S = 2$, (b) MSE for $N_S = 3$, and (c) MSE for $N_S = 4$, $\sigma^2 = 2.5 \times 10^{-4}$. 98

Figure 4.7 MISO synaptic interference channel communication rate with respect to (a) noise variance σ^2, and (b) channel weight w, where $\sigma^2 = 2.5 \times 10^{-4}$. 99

Figure 4.8 MISO synaptic interference channel capacity for (a) $\sigma = 10^{-4}$, (b) $\sigma = 10^{-3}$, (c) $\sigma = 10^{-2}$, and (d) $\sigma = 10^{-1}$. 100

Figure 4.9 MISO synaptic interference channel capacity for $\sigma^2 = 2.5 \times 10^{-8}$, (a) for $M_{EX} = 10$, (b) for $M_{EX} = 100$, and (c) for $M_{EX} = 1000$. 101

Figure 5.1 Constellation diagram for QMoSK modulation, $n = 2$. 108

Figure 5.2 Particle propagation and detection processes. 109

Figure 5.3 A simple uncoded network mechanism. 113

Figure 5.4 A simple network coding mechanism. 113

Figure 5.5 Delay and rate characteristics with N_P. 122
Figure 5.6 Rate vs delay analysis. 123
Figure 5.7 Rate vs delay analysis in uncoded and coded network cases. 123

ABBREVIATIONS

ICT	Information and Communication Technology
LTI	Linear Time-Invariant
MS	Multiple Sclerosis
CNN	Central Nervous Network
PNN	Peripheral Nervous Network
SoNS	Somatic Nervous Subnetwork
ANS	Autonomic Nervous Subnetwork
SNS	Sympathetic Nervous Subnetwork
PSNS	Parasympathetic Nervous Subnetwork
EPSP	Excitatory Postsynaptic Potential
SA	Sinoatrial
AV	Atrioventricular
SISO	Single-Input Single-Output
MISO	Multi-Input Single-Output
MIMO	Multi-Input Multi-Output
CDF	Cumulative Distribution Function
pdf	Probability Density Function
ACF	Autocorrelation Function

CHAPTER 1

INTRODUCTION

Molecular communication is a novel nanoscale communication paradigm, in which molecules are used to encode, transmit and receive information. Indeed, human body is a large-scale heterogeneous communication network of nanonetworks composed of interacting nanomachines, i.e., cells, whose functionalities primarily depend on nanoscale molecular communications. We introduce the elementary models for significant intra-body molecular communication channels, and then, discuss molecular nanonetworks that are the multi-terminal extensions of these channel models. In addition, we investigate the rate-delay tradeoffs with molecular network coding in messenger based molecular nanonetworks. We also model the multiple-access synaptic communication channel, and analyze the synaptic communication rate by incorporating the role of presynaptic input correlation. Moreover, we analyze the interference in single-input and multiple-access synaptic communication channels. In this chapter, we first introduce the fundamentals and then, present the research objectives and solutions.

1.1 Molecular Communications

Recently, enormous improvements in the field of nanotechnology have enabled the realization of powerful and functional man-made tiny devices inspired from the behavior of atomic and molecular structures. Nanomachines, composed of nanoscale components, are independently operating fullfeatured devices capable of tasks ranging from computing and data storing to sensing and actuation. However, their scarce memory and processing capabilities point out the need for establishment of nanonetworks, i.e., a number of nanomachines communicating to jointly execute application-specific tasks. Several communication paradigms are considered

for use in nanonetworks, however the most promising is molecular communication, where molecules are used to encode, transmit and receive information [3]. One main reason is that molecular communication of nanoscale entities is an existing natural phenomena, and offers a field of study for developing solutions through modeling nanonetworks. Another reason is that nanonetworks can be built upon such phenomena with appropriate tools, thus ensuring feasible engineering solutions.

1.2 Biological Nanonetworks

To realize molecular nanonetworks, foundations of molecular information theory should be established through identification of the existing molecular communication mechanisms, and development of networking techniques for nanomachines, which demand novel engineering efforts. Fortunately, these engineering skills and technology have been prepared within us by the natural evolution in the last several billions of years.

Indeed, human body is a large-scale heterogeneous communication network of nanonetworks composed of interacting nanomachines, i.e., cells, whose functionalities primarily depend on nanoscale molecular communications. Hence, the vital conditions of the human body directly depend on the performance, reliability, and continuous functioning of intrabody molecular nanonetworks. Furthermore, understanding potential disorders caused by communication failures paves the way for the development of ICT-inspired treatment techniques. In addition, establishment of the information theoretical foundations of the existing intra-body molecular communication mechanisms will be a significant step towards the development of implementable architectures and communication techniques for emerging applications of nanonetworks.

Our research starts with the pursuit of bringing groundbreaking molecular communication solutions out by observing and understanding the biological processes we inherently have. Thus, introducing the models for elementary molecular communication channels, i.e., nanoscale neuro-spike communication channel, action potential-based cardiomyocyte molecular communication channel, and hormonal molecular communication channel, and identifying few of vital intra-body molecular nanonetworks to pave the way for the development of innovative communication theoretical solutions for future medicine and bio-inspired techniques for

realization of nanonetworks are main objectives of this thesis.

1.3 Performance Tradeoffs in Molecular Nanonetworks

Since molecular communication inherently exists in nature, it is biocompatible, biostable and it has also the capability of operating at nanoscale. Hence, it may be applied to a wide variety of areas such as environmental applications, which include water and air pollution control, industrial applications, which include development of nanorobots, nano-processors and nano-memory, and medical applications, which are drug delivery, disease treatment and health monitoring [3].

Molecular communication differentiates from standard wireless communication applications with its dramatically higher and varying propagation delays [121], operational uncertainties and proneness to noise and interference. To design nanomachines that compensate these drawbacks, the operation limits of molecular communication systems should be thoroughly investigated.

Molecular communication is unreliable and suffering from long propagation delays, even up to hours [54], due to diffusion of large molecules. Moreover, the nanomachine spends time generating multiple redundant molecules for a single message to guarantee the delivery of the message and preparing them for transmission. This unfortunately yields low rates. Therefore, a joint rate and delay analysis for molecular communication is needed to investigate its capabilities and shortcomings.

1.4 Research Objectives and Solutions

The objectives of our research and the solution approaches are explained in this section.

1.4.1 Molecular Communication Nanonetworks inside Human Body

To realize molecular nanonetworks, the foundations of molecular information theory should be established through identification of the existing molecular communication mechanisms, and architectures and networking techniques for nanomachines should be developed, which

demand novel engineering efforts. Luckily, these engineering skills and technology have been prepared for us by the natural evolution in the last several billions of years. Indeed, the human body is a massive nanoscale molecular communications network as it is composed of billions of interacting nanomachines, i.e., cells. Intra-body biological systems are closely linked to each other and communicate primarily through molecular transactions. Thus, vital activities inside the human body are regulated by everlasting communication performance and operations of intra-body molecular nanonetworks. However, natural intra-body molecular nanonetworks are yet to be explored with the elegant tools of information and communication theories.

In this thesis, first, the elementary models for significant intra-body molecular communication channels, i.e., nanoscale neuro-spike communication channel, action potential-based cardiomyocyte molecular communication channel, hormonal molecular communication channel, are introduced. Next, molecular nanonetworks belonging to multi-terminal extensions of channel models, i.e., nervous, cardiovascular molecular, endocrine nanonetworks are discussed. Furthermore, heterogenous communication network of intra-body molecular nanonetworks together with five senses, i.e., nanosensory networks, is explored from the perspectives of communication and network theories. Moreover, open research challenges, such as extension of molecular channel models to multi-terminal cases, and developing a communication theory perspective to understand the physiology and to capture potential communication failures of intra-body biological systems, are provided. Our objectives are to learn from the elegant molecular communication mechanisms inside us for engineering practical communication techniques for emerging nanonetworks, as well as to pave the way for the advancement of revolutionary diagnosis and treatment techniques inspired from information and communication technologies, which is promising for future nanomedicine and bio-inspired molecular communication applications.

1.4.2 Synaptic Multiple-Access Channel in Hippocampal-Cortical Neurons

Communication between neurons occurs via transmission of neural spike trains through junctional structures, either electrical or chemical synapses, providing connections among nerve terminals. Since neural communication is achieved at synapses, the process of neurotransmission is called synaptic communication. Learning and memory processes are based on

the changes in strength and connectivity of neural networks which usually contain multiple synaptic connections.

In this section, we investigate multiple-access neuro-spike communication channel, in which the neural signal, i.e., the action potential, is transmitted through multiple synaptic paths directed to a common postsynaptic neuron terminal. Synaptic transmission is initiated with random vesicle release process from presynaptic neurons to synaptic paths. Each synaptic channel is characterized by its impulse response and available postsynaptic receptors. Here, we model the multiple-access synaptic communication channel, and investigate the information rate per spike at the postsynaptic neuron, and how postsynaptic rate is enhanced compared to single terminal synaptic communication channel. Furthermore, we analyze the synaptic transmission performance by incorporating the role of correlation among presynaptic terminals, and point out the performance improvement. Finally, we concentrate on the disorders characterized by abnormalities in pre- and postsynaptic terminals and synaptic connections, and establish relations between neural diseases and synaptic communication problems.

1.4.3 Adaptive Weight Update in Cortical Neurons and Estimation of Channel Weights in Synaptic Interference Channel

Synapses can modify their strengths depending on the spike-timing characteristics. Learning occurs via elimination of weak presynaptic inputs, which we call interference canceling.

In this section, using an optimal linear estimation method, we estimate the channel weights for both single-input single-output (SISO) and multi-input single-output (MISO) synaptic interference channels. Then, we derive an optimal learning algorithm minimizing the synaptic channel interference. This analysis is also compared to the natural learning algorithm conducted by neurons. Our results demonstrate that neurons are actually capable of interference canceling and they can achieve rates close to the maximum channel capacity.

1.4.4 Rate-Delay Tradeoff in Molecular Nanonetworks

Molecular communication is a novel nanoscale communication paradigm, in which information is encoded in messenger molecules for transmission and reception. However, molecular communication is unreliable and has highly varying long propagation delays mainly due to

the stochastic behavior of the freely diffusing molecules. Thus, it is essential to analyze its delay characteristics, as well as the tradeoff between the rate and delay, in order to reveal the capabilities and limitations of molecular information transmission in nanonetworks.

In this section, first, a new messenger-based molecular communication model, which includes a nano-transmitter sending information to a nano-receiver, is introduced. The information is encoded on a polyethylene molecule, $CH_3(CHX)_nCH_2F$, where X stands for H and F atoms representing 0 and 1 bits, respectively. The emission of the molecules is modeled by puffing process which is inspired by the alarm pheromone release by animals in dangerous situations. In this work, the rate-delay characteristics of this messenger-based molecular communication model are explored. Then, a Nano-Relay is inserted in the model, which XOR's the incoming messages from two different nanomachines. Performance evaluation shows that indeed, a simple network coding mechanism significantly improves the rate given delay of the system, and vice versa.

1.5 Thesis Outline

This thesis is organized as follows: In Chapter 2, we introduce the elementary models for significant intra-body molecular communication channels, i.e., nanoscale neuro-spike communication channel, action potential-based cardiomyocyte molecular communication channel, and hormonal communication channel. Next, we discuss molecular nanonetworks belonging to multi-terminal extension of channel models, i.e., nervous, cardiovascular molecular, endocrine nanonetworks. Furthermore, heterogenous communication network of intra-body molecular nanonetworks is explored from communication and network theory perspectives, and open research issues are highlighted. In Chapter 3, we model the multiple-access synaptic communication channel, and investigate the information rate per spike at the postsynaptic neuron, and how postsynaptic rate is enhanced compared to single terminal synaptic communication channel. Furthermore, we analyze the synaptic transmission performance by incorporating the role of correlation among presynaptic terminals. Moreover, we establish relations between neural diseases and synaptic communication problems. In Chapter 4, we estimate the channel weights for both single-input single-output (SISO) and multi-input single-output (MISO) synaptic interference channels. Next, we derive an optimal learning algorithm, which minimizes the interference in the synaptic channel in the presence of multiple presynaptic neu-

ron terminals, and analyze the mean square error performance for SISO and MISO synaptic interference channels. Moreover, we provide the natural adaptive weight update algorithm for neurons based on experimental findings. Then, we compare the performance of the natural learning algorithm conducted by neurons to the optimal learning algorithm we developed. Our results demonstrate that neurons are capable of mitigating the interference, and achieve rates close to the capacity. In Chapter 5, we introduce a new messenger-based molecular communication model, which includes a nano-transmitter sending information to a nano-receiver. We explore the rate-delay characteristics of this messenger-based molecular communication, and also show that a simple network coding mechanism significantly improves the communication rate. In Chapter 6, we conclude the thesis underlining the importing points together with the discussion of future issues.

CHAPTER 2

MOLECULAR COMMUNICATION NANONETWORKS INSIDE HUMAN BODY

To realize molecular nanonetworks, the foundations of molecular information theory should be established through identification of the existing molecular communication mechanisms, and architectures and networking techniques for nanomachines should be developed, which demand novel engineering efforts. Luckily, these engineering skills and technology have been prepared for us by the natural evolution in the last several billions of years. Indeed, the human body is a massive nanoscale molecular communications network as it is composed of billions of interacting nanomachines, i.e., cells. Intra-body biological systems are closely linked to each other and communicate primarily through molecular transactions. Thus, vital activities inside the human body are regulated by everlasting communication performance and operations of intra-body molecular nanonetworks. However, natural intra-body molecular nanonetworks are yet to be explored with the elegant tools of information and communication theories. In this chapter, first, the elementary models for significant intra-body molecular communication channels, i.e., nanoscale neuro-spike communication channel, action potential-based cardiomyocyte molecular communication channel, hormonal molecular communication channel, are introduced. Next, molecular nanonetworks belonging to multi-terminal extensions of channel models, i.e., nervous, cardiovascular molecular, endocrine nanonetworks are discussed. Furthermore, heterogenous communication network of intra-body molecular nanonetworks together with five senses, i.e., nanosensory networks, is explored from the perspectives of communication and network theories. Moreover, open research challenges, such as extension of molecular channel models to multi-terminal cases, and developing a communication theory perspective to understand the physiology and to capture potential communication failures of intra-body biological systems, are provided. Our objectives are to learn from the

elegant molecular communication mechanisms inside us for engineering practical communication techniques for emerging nanonetworks, as well as to pave the way for the advancement of revolutionary diagnosis and treatment techniques inspired from information and communication technologies, which is promising for future nanomedicine and bio-inspired molecular communication applications.

2.1 Introduction

Enormous improvements in the field of nanotechnology have enabled the realization of powerful and functional man-made tiny devices inspired from the behavior of atomic and molecular structures, recently. *Nanomachines*, composed of nanoscale components, are independently operating full-featured devices capable of tasks ranging from computing and data storing to sensing and actuation, i.e., they not only function as computers, but also establish connections with the world to detect a physical quantity, as living organisms. In [3], the similarities between nano-machines and living cells are expressed, and the need for communication between nano-machines is highlighted.

Some applications of nanonetworks, among others, are: a number of nanomachines communicating for effective drug delivery [165]; multiple nanosensors deployed on human body to monitor glucose, sodium, and cholesterol [45, 95] to detect the presence of different infectious agents [162]; a set of molecular and nanoscale computing devices, i.e., nanocomputers [150], jointly executing an application-specific task. However, realization of these applications mandates addressing the unique challenges posed by the physical characteristics of nanomachines, e.g., dimensions of nanomachines, scarce memory and processing capabilities, and their operating environment on the nanoscale communications.

Several communication paradigms are considered for use in nanonetworks, but the most promising is *molecular communications*, where molecules are used to encode, transmit and receive information [15]. One of the main reasons is that molecular communication of nanoscale entities is an existing natural phenomena, and offers a field of study for developing solutions through modeling nanonetworks. Another reason is that nanonetworks can be built upon such naturally occurring phenomena with appropriate tools, thus ensuring feasible engineering solutions.

To realize molecular nanonetworks, the foundations of molecular information theory should be established through identification of the existing molecular communication mechanisms, and architectures and networking techniques for nanomachines should be developed, which demand novel engineering efforts. Fortunately, these engineering skills and technology have been prepared within us by the natural evolution in the last several billions of years.

Indeed, the *human body is a large-scale heterogeneous communication network of nanonetworks* as it is composed of billions of interacting nanomachines, i.e., cells, whose functionalities primarily depend on nanoscale molecular communications. Hence, *the vital conditions of the human body directly depend on the performance, reliability, and continuous functioning of intra-body molecular nanonetworks.* Human biological systems are connected to each other and communicate primarily through molecular transactions. For example, nervous system is an ultra-large scale communication network of nerve cells, i.e., neurons, which communicates the external stimulus to brain and enables communication between different systems by conveying information with molecular impulse signal known as *spike*. The heart is a nanonetwork of muscle cells, i.e., cardiomyocytes, communicating via cardiac electrical impulses, i.e., *action potentials*, over molecular communication channels through the gap-junctions for continuous circulation of blood. Endocrine system, a network of glands, provides the communication among cells through specific *molecular information carriers*, i.e., hormones, and regulates concentrations of molecules inside the body.

Biological systems communicate to fulfill the needs of human body, to ensure its continuity and detect the problems to meet the solution mechanisms to heal the body. The network of intra-body molecular nanonetworks operates to preserve the equilibrium state, i.e., homeostasis, inside the human body. Any communication failure and impairment that are beyond the recovery capabilities of this network leads to diseases; e.g., impairment of communication skill of neurons results in *multiple sclerosis (MS)* disease, excessive generation and transmission of action potentials yields *tachycardia*, i.e., excessive heart rhythm, and insufficient amount of insulin secretion and transmission, or irresponsive cells to endocrine molecular information (insuline) leads to *diabetes*.

Although medicine has developed treatment strategies depending on the severity of the diseases and immensely gained ground, it is not yet sufficient to discover the underlying reasons for many crucial health problems. One of the significant directions for completely understand-

ing the nature of the diseases and the complete picture of biological systems' interaction, and healing terminal illnesses is to investigate the issues dealt with medicine community with the perspective of communication theory thoroughly supported with medical background. This brings two major fields together to propose fast and unified solutions to diseases from both medicine and communication theory perspectives.

Sustaining effective communication capabilities in the intra-body molecular nanonetworks is detrimental for the functional and metabolic efficiency of human body. Furthermore, understanding potential disorders caused by communication failures paves the way for the possible development of a new generation of ICT-inspired treatment techniques. In addition, identification of the existing intra-body molecular communication mechanisms, establishment of the information theoretical foundations of these channels, will be a significant step towards the development of real implementable architectures and communication techniques for emerging applications of nanonetworks. *Therefore, introducing the basics of potential models for the molecular communication channels, identifying the intra-body molecular nanonetworks, understanding its communication, network, and information theoretical capabilities and shortcomings, and ultimately contributing to the* ***development of ICT-inspired solutions for certain diseases*** *and* ***bio-inspired solutions for nanonetworks*** *are the main objectives of this chapter.*

Thus, in this chapter, we investigate the molecular information transduction gateways for: *1) nanoscale neuro-spike communication channel, 2) action potential-based cardiomyocyte molecular communication channel, 3) hormonal molecular communication channel,* which are the main molecular communication paradigms of nervous, cardiovascular, and endocrine nanonetworks, and capture potential communication failures in each of these nanonetworks leading to diseases in order to pave the way for the design of ICT-inspired diagnosis and treatment techniques. What these systems have in common is the underlying basic principle of molecular communication. It comprises molecule or signal generation, transduction and reception processes that are the basic constituents of a classical communication system.

From molecule transduction among the organelles of a single cell to the feedback compensation pathways or channels between biological systems, each vital activity inside the human body involves in the course of molecular communication. In addition to the vastly explored field of neural networks, which is an excellent artifact of communications within the hu-

man body, some other communication processes, such as cellular signaling pathways [100], protein interaction networks [166], gene regulatory networks [68], and DNA processing approaches [51], have been identified and studied mostly from the perspectives of medical and computational biology. Cellular signaling concept has been studied in [8], where rate distortion theory is utilized for analyzing performance-cost tradeoffs in cellular decision making. In [100], to understand the signaling mechanism of the molecular communication medium, an information theoretical model is proposed.

The calcium signaling concept and the design of a molecular communication system based on intercellular calcium signaling networks are described in [3] and [119], respectively. The work in [119] also describes possible functionalities, e.g., signal switching and aggregation, that may be achieved in such networks. There is also some current work focusing on communication with biological molecular motors [3, 112], intra-cellular aqueous nanobubbles [114], and artificial cells [148]. Several kind of protein interfaces are listed according to their functionalities, receptor-ligand interactions, e.g., activation or blocking due to therapeutic drugs, and methods for detecting protein interactions are suggested in [24]. In [71], several novel nonviral delivery systems for gene therapy application are reviewed. In [172], an artificial cell-to-cell communication system for mammalian cells using nitric oxide signaling is developed as a building block for complex artificial gene regulatory networks.

Although there is a limited amount of work on nanoscale and molecular communications, the intra-body molecular nanonetworks have not been investigated from the information and communication theoretical point of view. The current literature mostly contains very preliminary results on modeling and analysis of general molecular communication channels based on a set of simplifying assumptions [3]. In [128], a physical channel for molecular communication is modeled by an LTI system, and the channel transfer function is derived. Clearly, molecular mobility and diffusion dynamics are not linear, and may well exhibit time-varying characteristics. The noise in molecular communication channel is modeled in [113]. A molecular communication channel as a binary symmetric channel is modeled and its mutual information and capacity is analyzed in [11, 12]. Similarly, the single, multiple access, broadcast, and relay channel capacities are investigated in [13, 14]. The common fundamental drawback in these studies is that they simply present idealized results based on simplifying models, e.g., LTI channel model in [128], Gaussian channel noise in [13, 14]. The actual information theoretical analysis of molecular nanonetworks of biological nanomachines is still an unknown.

Our research starts with the fundamental pursuit of bringing groundbreaking molecular communication solutions out by observing and understanding the intra-body biological processes we inherently have. One principle objective of this chapter is to point out the essentials in developing solution strategies for intra-body failures and potential problems. The other goal is to pave the way for the *development of ICT-inspired revolutionary diagnosis and treatment techniques*. These objectives can be realized through identification of elementary models for molecular communication mechanisms inside the human body. With this motivation, we identify the blocks for molecular communication channels, reveal the pathways for specifying and analyzing the molecular nanonetworks, and discuss the possible outcomes of analyses for intra-body molecular networks. Furthermore, we investigate the fundamental relations between health problems and various communication channel failures and networking problems, and illustrate the underlying link, message delivery problems or deficiencies due to inefficient communication mechanisms within and among nervous, cardiovascular and endocrine nanonetworks resulted from the breakdowns in physiological operations or malfunctioning of tissues.

The remainder of this chapter is organized as follows. First, in Section 2.2, a general framework for intra-body molecular communication channels are introduced, and nanoscale neurospike communication channel, action potential-based cardiomyocyte molecular communication channel and hormonal molecular communication channel are investigated. Next, in Section 2.3, molecular nanonetworks for nervous, cardiovascular and endocrine systems inside the human body are introduced. Furthermore, in Section 2.4, communication pathways among the tremendous network of these nanonetworks are given. Moreover, in Section 2.5, future research issues and communication theoretic challenges are outlined together with the understanding of underlying pathology of intra-body systems from communication theory perspective to leverage the contribution of medicine and pave the way for future nanomedicine applications.

2.2 Intra-body Molecular Communication Channels

Intra-body biological systems operate in conjunction with each other to realize complex vital activities. Apart from the coexistence of these systems, basically each is composed of a communicating mass of molecular cellular structures to aggregate for implementing certain

biological tasks. What they have in common is the principle communication mechanism for implementing certain tasks, which might be through *molecular information transfer* by way of molecular ion channels, or simply *action potential transduction* to signal the target cells. Although the stimulation mechanisms behind the communication might differ even in distinct substructures, the building principles of molecular communication for biological systems can be realized within a general framework of intra-body molecular communication channels.

2.2.1 A General Framework for Molecular Communication Channels

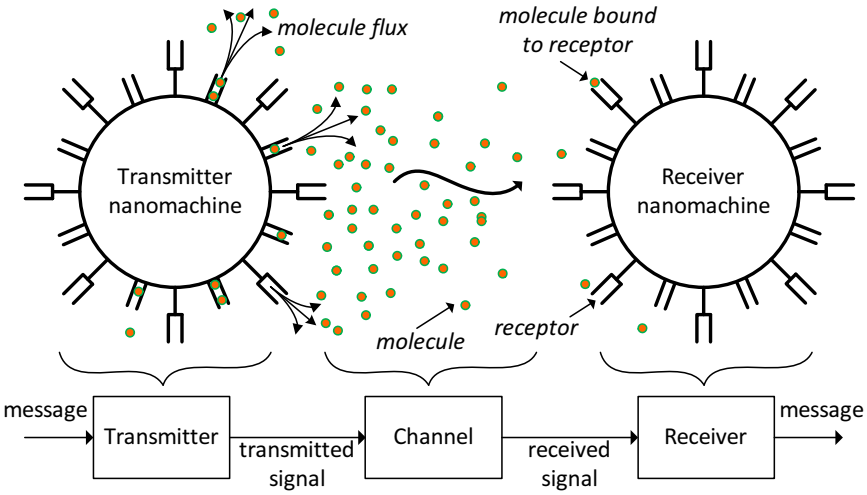

Figure 2.1: General molecular communication system with two nodes.

In general, a molecular *nanonetwork* is simply composed of *nanomachines* or *nanonodes*. A general molecular nanonetwork with two nanomachines or nanonodes is composed of three main functional blocks comprising the molecular communication system, namely, (i) the transmitter, (ii) the channel, and (iii) the receiver, accounting for the emission, propagation and reception processes, respectively, as illustrated in Fig. 2.1.

The transmitter generates a signal, i.e., transmitted signal, which encodes the information message to be exchanged. The molecule emission process provides an output signal by the emission of molecules in the space according to a given input and used molecular information encoding mechanism, e.g., molecular concentration and molecule type in action potential-based molecular communication channel, amplitude and rate of electro-chemical impulses (spikes) in neuro-spike communication channel. The propagation process provides the trans-

port of the modulated signal by means of a molecule diffusion process, which is defined as the movement of molecules in a fluid from an area of higher concentration to an area of lower concentration. In some cases, e.g., hormonal molecular communication in endocrine nanonetworks, the propagation process is governed by both diffusion and drift due to external active mobility, e.g., bloodstream carrying hormone molecules. The receiver collects the incoming information from the received signal and recovers the transmitted message. A typical reception mechanism observed among living cells is based on ligand-receptor binding process [16], in which, arriving molecules at the receiver nanomachine collide and bind to the unbound receptor of the receiver.

In fact, molecular nanonetworks are directly inspired by communication networks among living entities already present in nature. We will first explore the basic foundations for molecular information gateways of single-input single-output molecular nanoscale communication channels, i.e., (a) nanoscale neuro-spike communication channel, (b) action potential-based cardiomyocyte molecular communication channel, and (c) hormonal molecular communication channel. All these three specific molecular communication channels are captured by the model in Fig. 2.1, whose functional blocks vary and will be specialized in the following subsections.

We study the constituents for three specific intra-body molecular channels in terms of their respective functionalities in molecular communication. Therefore, we combine the principles of human physiology and physical laws governing the molecular and signal transduction pathways and mechanisms with the perspectives of communication and network theories.

Considering the complete set of the physiological processes inside the human body, from the tiniest functioning molecular unit to largest scale systems cooperating for sustainment of *homeostasis*, it is unfeasible to study whole communication processes within cellular, organic, systemic structures inside the human body, to which the efforts in medical science have been devoted for centuries. Hence, we mainly concentrate on the fundamental communication principles of three main intra-body molecular nanoscale communication channels, i.e., *(a) nanoscale neuro-spike communication channel, (b) action potential-based cardiomyocyte molecular communication channel,* and *(c) hormonal molecular communication channel.*

2.2.2 Nanoscale Neuro-spike Communication Channel

Nervous nanonetwork, composed of ganglions, i.e., mass of nerve cell bodies as the network nodes, is responsible for gathering information from different parts of the body, and processing it and generating the required response for the body. It is a distributed network overall the body and it extends up to extremities [124].

Neurons, electrically excitable *nerve cells* capable of storing, processing and transmitting information through *chemical* and *electrical signaling mechanisms*, are considered as *nanotransceivers* of the *nervous nanonetwork*. They receive signals from other neurons or sensory cells, which changes the *membrane electrical polarization*. Electrical potential is spread along the cell body and combined at the base of axon, causing the generation of *action potentials*, which are then transmitted through the axon and arrive to its branches, where the neuron makes an interface with other neurons through *synapses*, i.e., the conductive links between postsynaptic and presynaptic cells [124], where cell-to-cell signals are produced [67]. Action potentials, i.e., *spikes or impulses*, are used to carry information from one neuron to the other. Hence, we call the communication among neurons as *neuro-spike communication* [19].

In the literature, there are some studies concentrating on neuro-spike communication. In [65], molecular neuro-spike communication is introduced. Then, its channel capacity and error probability are analytically investigated. In [21], nanoscale neuro-spike communication characteristics through developing a realistic physical channel model between two terminals is investigated. The neuro-spike communication channel is analyzed based on the probability of error in spike detection at the output, and the channel delay is characterized. In [20], synaptic gaussian interference channel is investigated. Furthermore, the *achievable rate region* for the channel is characterized in terms of power or firing rate.

Performance of neuro-spike communication depends on the physical features of neurons, which affect the action potential transmission characteristics through neurons. Although areas of the axon covered with a *myelin sheath* cannot regenerate *action potentials*, they can rapidly conduct an electrical field to the next node of *Ranvier*, where the *action potential* is regenerated and transmitted further along the axon [124]. Another way to increase conduction velocity is to increase the diameter of an axon, through which axons with *myelin sheaths* can transmit action potentials extremely fast [124].

There are mainly two different types of synapses, *electrical* and *chemical synapses* [136]. *Electrical synapse* is a *mechanical* and *electrically conductive link* that is formed in a narrow gap between two neurons, i.e., the *presynaptic and postsynaptic neurons*. Despite causing amplitude loss in signal transmitted, it conducts nerve impulses faster compared to *chemical synapse*. Mostly, the electrical impulses can be transmitted in either direction [136].

Different from electrical synapses, chemical synapses are specialized links through which signals are transmitted from neurons to other neurons and non-neuronal cells. Chemical synapses allow neurons to form communication paths within the *CNN*, enable the nervous nanonetwork to communicate with and control other networks within the body, and they are crucial to the biological computations that underlie perception and thought.

The essential components of neural signaling include presynaptic terminal, action potential generation, neural firing, vesicle release processes and the postsynaptic terminal and the postsynaptic potential.

Presynaptic terminal is an area within the axon of the presynaptic cell that contains neurotransmitters enclosed in small spheres called synaptic vesicles bounded to the membrane. ***Action potential*** is a short-lasting event in which the electrical membrane potential of a cell rapidly rises and falls, following a consistent trajectory [21]. During the action potential, part of the neural membrane opens to allow positively charged ions inside the cell and negatively charged ions out. This process causes a rapid increase in the positive charge of the nerve fiber. When the charge reaches +40mV, the impulse is propagated down the nerve fiber. This electrical impulse is carried down the nerve through a series of action potentials. ***Neural firing*** is the response of a neuron when it is stimulated. A neuron that emits an action potential is often said to fire. Synaptic vesicles store neurotransmitters to be released at synapses and constantly reproduced by the cells. These vesicles are essential for conduction of nerve impulses among neurons. Action potentials trigger the complete fusion of the synaptic vesicle with the cellular membrane, and then, the excretion from the cell through exocytosis, which is called ***vesicle release*** [110]. ***Postsynaptic terminal*** is the receiving part of the synapse between two neurons, and the ***postsynaptic potential*** is the membrane potential at the postsynaptic terminal of a chemical synapse. In neuroscience, an EPSP is the temporary increase in the postsynaptic membrane potential caused by the flow of positively charged ions into the postsynaptic cell due to the vesicle release [22]. An Inhibitory PostSynaptic Potential (IPSP), which is the op-

posite of an EPSP, is a kind of synaptic potential that makes a postsynaptic neuron less likely to generate an action potential.

An arriving spike yields an influx of calcium ions through voltage-dependent calcium ion channels. Calcium ions then bind to the proteins found within the membranes of the synaptic vesicles. The vesicles then release their contents, *neurotransmitters*, i.e., *information molecules*, to the synaptic cleft [103]. The release of a *neurotransmitter* is triggered by the arrival of a nerve impulse, i.e., action potential, and occurs through an unusually *rapid process of cellular secretion*. Therefore, we consider *neuro-spike communication channel* as series of electrical and molecular channels and model it accordingly.

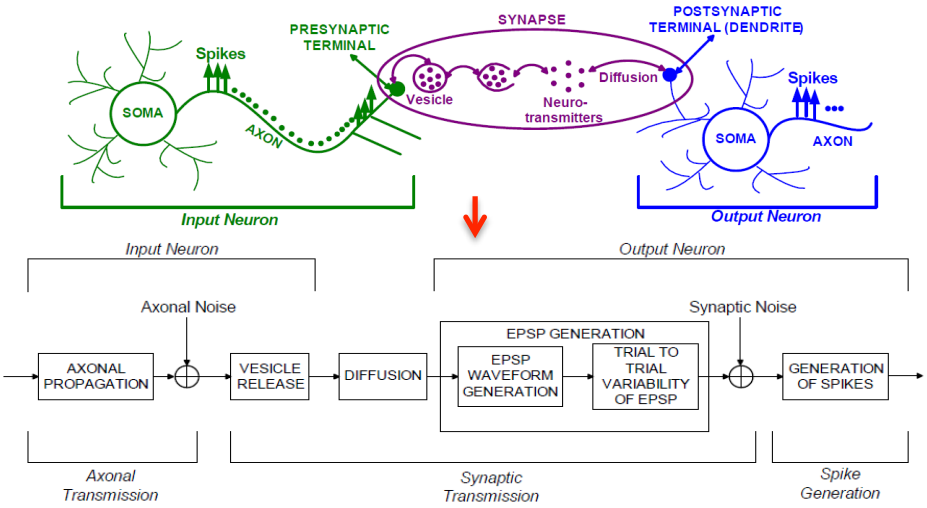

Figure 2.2: Realistic channel model for nanoscale neuro-spike communication.

The neuro-spike communication between single presynaptic neuron and single postsynaptic neuron includes the *axonal, synaptic* and *spike generation phases* [19]. Synaptic transmission is composed of vesicle release, diffusion, and generation and trial-to-trial variability of *excitatory postsynaptic potential (EPSP)*, i.e., the excitation due to the vesicle release. There are two major sources of noise in neuro-spike communication, axonal and synaptic noises. Hence, the overall model of single-input single-output neuro-spike communication channel for *action potential generation and propagation phases* between two neurons is illustrated in Fig. 2.2.

2.2.3 Action Potential-based Cardiomyocyte Molecular Communication Channel

The heart, as both serving as the source, i.e., *transmitter*, and the destination, i.e., *receiver*, for the *cardiovascular network*, can be modeled as a *transceiver* of the communication system of the overall body. It has an inherent signal generating and transmission mechanism, which is of great importance, and needs to be given a special attention to understand the characteristics of transmission of blood to every single cell, i.e., *destination* inside human body.

Various mathematical and circuit models for cardiac action potentials and ion channels are developed in the literature. The Hodgkin-Huxley model is a electrical circuit model of cardiomyocyte surface membrane describing how action potentials in neurons are initiated and propagated [70]. In [154], a safety factor for conduction was formulated and computed for reduced membrane excitability and reduced gap junction coupling conditions. A multicellular ventricular fiber model is used to determine mechanisms of conduction failure during acute ischemia in [155]. In [143], it is shown that fibroblasts establish successful conduction between sheets of cardiomyocytes over long distances, explaining electrical synchronization of heart transplants. Furthermore, computer simulations show the feasibility of conduction in the absence of gap junctional coupling in [143]. Despite the current effort is on the physiological operational principles and physical channel models, to the best of our knowledge, there is no work focusing on the information theoretical foundations and principles of communication between cardiomyocytes and within the overall cardiovascular system.

The gap junction coupling is important for the organization of the heart tissue as a mass of electrically connected communicating cells through specialized membrane proteins. A generic model for molecular communication through gap junction channels is implemented in [120]. Furthermore, there exists some preliminary research on molecular channel of heart muscle cells, i.e., *cardiomyocytes*. The role of gap junctions in the cardiac electrical impulse, i.e., *cardiac action potential*, propagation is investigated in [143]. Changes in gap junction channels for various cardiovascular diseases are investigated in [76]. A review of the features of cardiac electrical function and discussion of underlying ionic bases are provided in [152]. A model for the electrical activity of the heart is presented and a solution approach for electrical potential distribution based on the bidomain model is suggested [99]. In [77], authors conduct numerical simulations of electrically coupled cells to understand how an action potential is initiated in the atrial cells. Although electrical activity and ionic properties of heart are studied

in different works, none of them concentrates on the mechanism of cardiomyocytes from molecular communication perspective.

We consider and model heart as a *molecular nanonetwork of cardiomyocytes*. Cardiomyocytes communicate through the transmission of the cardiac action potential, which we consider as the main information carrier. Cardiac cells, different from the muscle cells, are very convenient for the transmission of the *cardiac action potential*, which is crucial for the *electrical conduction system of the heart* [85]. *Cardiac muscle cells* have a contraction rate determined by the *sinoatrial (SA) node* known as *pacemaker*. *SA node* generates electrical impulses, i.e., *action potentials*, similar to neuro-spikes produced by nerve cells, i.e., neurons. Hence, we model the *SA node* as the primary transmitter in this molecular communication. Since the *cardiac muscle cells* are *electrically coupled*, impulses from *SA node* spread rapidly through the walls of the atria, causing both atria to contract together.

There is another specialized cardiac muscle tissue, *atrioventricular (AV) node*, located in the wall between the right atrium and the right ventricle. *AV node* causes a *delay* before the electrical impulses are broadcast to the walls of the ventricle, ensuring that atria empty completely before ventricles contract.

At the same time, specialized muscle fibers called *purkinje fibers* conduct the electrical signals, i.e., the *action potential signals* throughout the ventricular walls. This entire cycle, a single heartbeat, is a result of *successful molecular communication of action potential* over the nanonetwork of cardiomyocytes and lasts about 0.8 seconds [64, 27].

The channel we outlined in Fig. 2.3 is, in fact, molecular ion channel. In the conduction system of heart, molecular ion channels play a crucial role. They create the pathways from extracellular medium to intracellular medium, or vice versa, for certain ions, and contribute the contraction process of the *cardiac muscle cells* according to the concentration levels of potassium (K^+), sodium (Na^+), calcium (Ca^{++}) ions, which determine the existence and direction of ion flows generating *action potential signals*. Hence, ion channels enable the creation and propagation of *action potentials* [85]. As a result of *action potential generation*, i.e., inflow of Ca^{++} ions to cardiac muscle cells, the intracellular concentration of calcium increases, and calcium ions bind to the protein troponin, a protein that is found on the actin filament, causing the *cardiomyocytes* to start to contract [49].

Heart can be described by a circuit model, similar to Hodgkin-Huxley model [70], in which K^+, Na^+ and Ca^+ channels are considered as molecular current sources. In our circuit model for a single cardiomyocyte, there is a parallel capacitance (C_i) to the voltage-dependent current source due to charge difference of intra and extra media, as the voltage difference determines whether the specific ion channels will be open or closed, i.e., whether or not there is current inflowing. The current is the sum of bidirectional K^+, Na^+ and Ca^+ ion currents, $I_i = I_K + I_{Na} + I_{Ca}$. The circuit model is incorporated into the cardiomyocyte molecular communication channel model of the heart in Fig. 2.3.

There is a potential difference between the intracellular and extracellular media of *cardiac muscle cells* (V_i). Due to the potential difference, K^+, Na^+ and Ca^+ molecules are diffused through these channels in the opposite direction of voltage gradient. Therefore, the voltage gradient is the determining factor for the molecule currents.

To construct the overall communication model of heart, the ion channels, their diffusion process through the cardiac muscle cells, *action potential* generation and transmission through the cardiac cells and the autonomic structure of cardiac muscle cells should be combined carefully. Although in [77], the propagation of *action potentials* is modeled using circular symmetry approximation, it is so hard to construct the overall communication models for human heart and cardiovascular system. The pacemaking cells in *SA node* is controlled by *autonomic nervous system*. Therefore, when stimulated by *sympathetic* and *parasympathetic nervous systems*, the *action potentials* are enhanced and degraded, respectively. The capacity of blood flow through coroners also controls the ion diffusion into/off the cardiac cells, which reshapes the *action potential* and its duration, hence the pumping rate of ventricles. In addition to the contribution of ion channels to *action potential generation*, other factors, such as O_2 molecule and nutrients, also affect the *action potential generation process*, as energy, i.e., ATP, should be provided for muscular contraction.

The *action potential* generated by the *SA node* passes down the cardiac conduction system, and arrives before the other cells have had a chance to generate their own spontaneous *action potential*. This is the electrical conduction system of the heart (normal conduction of electrical activity within the heart). If the *SA node* does not function, a group of cells further down the heart will become the heart's pacemaker, which is known as an ectopic pacemaker. These cells form the *atrioventricular (AV) node*, which is an area between the left atria and the right

ventricles, within the atrial septum.

While constructing the overall information theoretical and communication model for heart, we consider the effects of *noise* on *SA* (N_1) and *AV nodes* (N_2), and *external disturbance factors* on *SA* (D_1) and *AV nodes* (D_2). Opening and closing of ion channels, atrial fibrillation, which is some sort of heart rhythm disorder caused by the inability of ventricles to pump efficiently when the *action potential* cannot be transmitted from atria to ventricles due to irregular and rapid rhythm of the heart's atrial chambers, and the cardiac output itself are the main sources for noise generation in heart. Furthermore, some drugs, CO_2 and CO are the main disturbance factors for the heart. Intrinsic noise and disturbance filters used by *SA* and *AV nodes*, i.e., $n_1(t)$ and $h_1(t)$, and $h_2(t)$, respectively, are incorporated into the communication model for heart. Overall communication model for heart is illustrated in Fig. 2.3 with the fundamental blocks of the molecular communication system.

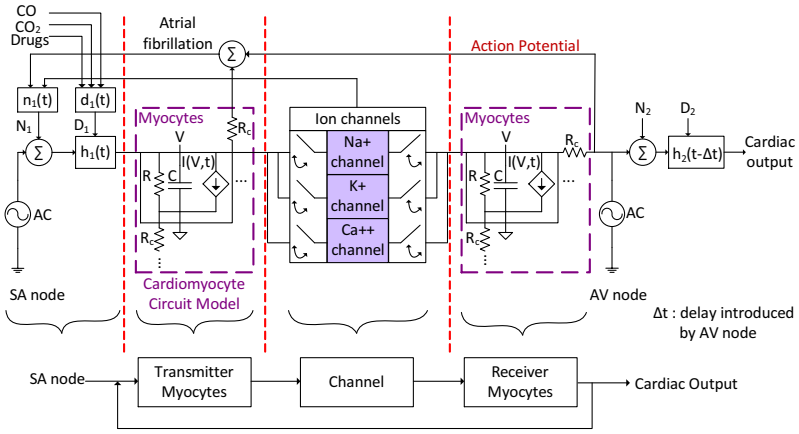

Figure 2.3: Cardiomyocyte molecular communication channel.

2.2.4 Hormonal Molecular Communication Channel

Endocrine system, which is a nanonetwork of glands, provides communication among cells, senses the molecule concentration changes in tissues and secretes hormones for the regulation of body. It has a crucial role in *homeostasis*, i.e., *regulation of internal environment and maintaining a stable, constant condition*. Hence, it acts like *a molecular sensor and actor network*, to maintain the homeostasis. In our model, we consider hormones as *modulated molecular endocrine network information carriers*.

Endocrine glands are controlled by the *nervous nanonetwork*. When the cell receptors are signaled, glands secrete certain hormones, i.e., *chemical messengers*, directly to blood vessels since endocrine glands are ductless. The secreted hormone targets a specific tissue and instructs the tissue to produce a particular substance [79].

Hormones have different biochemistries. They can be divided into two groups according to the ability to diffuse through the cell membrane of the receiver, i.e., target cell. *Lipid-soluble hormones*, e.g., steroids, are carried by the cardiovascular nanonetwork as in Fig. 2.4 and can diffuse through the membrane and directly deliver the message, i.e., stimulate or inhibit certain regions of DNA. On the other hand, *lipid-insoluble hormones* cannot penetrate through the cell membrane by themselves and need extra messengers to translate the message to the cytoplasm of the target cell. Due to its outweighing number [126], *we consider lipid-soluble hormones in our channel model*. *Lipid-soluble hormones* can diffuse through the cell membrane and target the receptors in the cytoplasm. The cytoplasmic receptors diffuse into the nucleus to act on DNA by stimulating certain regions. Therefore, *lipid-soluble hormone* activity is long durational. Steroids and thyroid hormones are main *lipid-soluble hormones* having direct effect on DNA [126].

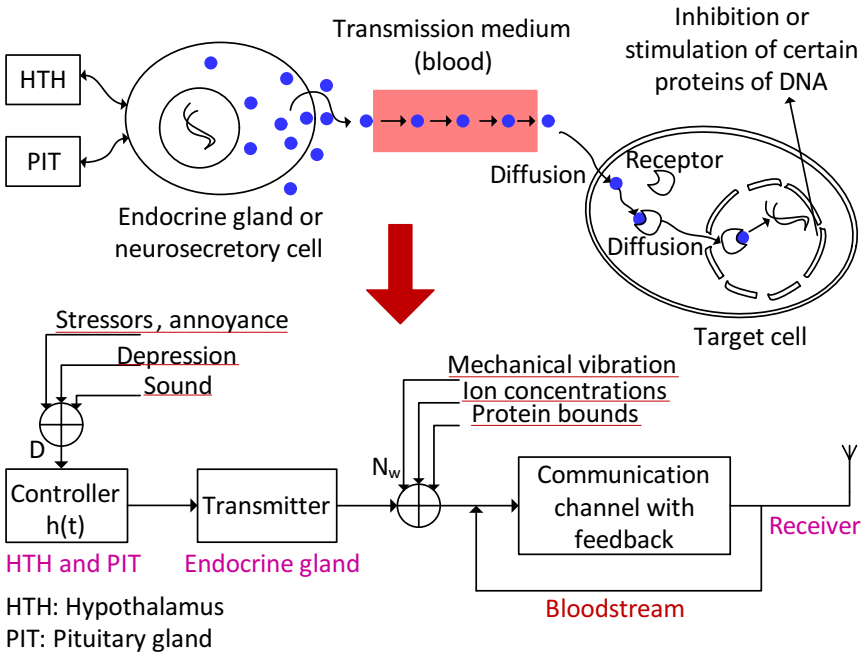

Figure 2.4: Hormonal molecular communication channel.

Successful delivery rate of hormones within the human body network directly depends on

at what concentration they are transmitted (secreted) to the blood (affected by the nervous nanonetwork), at what concentration they are being circulated within the blood stream (controlled by *cardiovascular nanonetwork*), and the rate of removal of the hormone from the blood plasma, i.e., *metabolic clearance rate* [67].

The propagation of the hormones is due to the combination of the blood circulation rate that stimulates a net hormone movement on top of their free diffusion, i.e., *diffusion with drift*. Molecules diffuse with drift when the *Brownian motion* is coupled with a drifting contribution to the molecule velocity. At the same time, the *clearance rate* depends the concentration of hormone in the plasma, and its rate of disappearance from the plasma per unit time.

Reception process of the channel is selective due to the incompatible chemical structure of hormones to any other receptor type except for the target cells' receptors. In fact, once these molecular information carriers (hormones) are broadcast (secreted) into the communication medium (blood), only one type of nanoreceiver, i.e., cells of the target receiver tissue, responds. Furthermore, *endocrine nanonetwork* have different response times to the stimuli, and concentration of the molecular hormone substances is incredibly small. Moreover, target cells may be promoted or inhibited depending on the stimulation type. Hence, the *reception process should be modeled considering its highly time-sensitive and input-dependent nature*.

Diffusion in cytoplasm is the fourth step for the successful diffusion of the molecular endocrine information towards the ultimate nanoreceivers, i.e., receptors inside the cell, e.g., DNA, and binding to it. The capacity of diffusion-based molecular communication channels with ligand-receptor binding have been information theoretically modeled and analyzed [11, 12, 13, 14].

The endocrine cell responds to changes in the concentration of a substance in the extracellular fluid, and provides homeostatic regulation of concentration of substances inside it through *negative feedback mechanism*. After a hormone is released, its further release is suppressed by its products and activity of the target cells. *Feedback regulation of hormones* can occur at all levels, including in the synthesis and processing of hormones and releasing stored hormones [67]. Consider hormone secretion as a *negative feedback regulatory system*. Note that the endocrine cell acts as a *sensor*. For example, any increase in blood glucose level triggers pancreas secretory glands to increase the hormonal information, i.e., insulin, emission rate into transmission channel, i.e., bloodstream, for further transduction of hormonal molecular

information to target cells, i.e., receptors. After signaled, targets of the molecular information start glucose uptake and utilization. Hence, the glucose level of the blood is decreased by molecular feedback regulation between the transmission channel and hormonal molecular information source [52].

Overall *hormonal molecular communication channel* is constructed by considering endocrine glands as *transmitter* and the target cells are the *receiver* as in Fig. 2.4. The bloodstream is the communication channel between the *transmitter* and the *receiver*. Channel is a *feedback channel*, which regulates the overall system using the *negative feedback* given by the target cell concentration. Furthermore, the system is under the control, *h(t)*, of nervous network nodes, i.e., *hypothalamus* and *pituitary gland*, regulating the hormonal activities inside the body. On the other hand, the channel is susceptible to some *disturbance factors (D)*, such as stressors, annoyance, antipsychotic agents, depression, fat gain and sound [169, 109]. In addition to that, the *transmitter side* is exposed to noise (N_w) due to the extracellular ion concentrations and mechanical vibrations during secretion, and protein bounds during hormone transmission through the *feedback channel, i.e., bloodstream* [133].

2.3 Intra-body Molecular Nanonetworks

We explore the basic communication interactions among the main functional subunits of multi-terminal molecular structures inside the human. In fact, we mainly concentrate on intra-body molecular nanonetworks, i.e., nervous, cardiovascular, endocrine nanonetworks.

2.3.1 Nervous Nanonetwork

The *nervous nanonetwork* is intrinsically a large-scale network of nanotransceivers, i.e., neurons, spanning the overall body. It is divided into two main subnetworks, namely *central nervous network (CNN)* and *peripheral nervous network (PNN)*. *CNN* integrates the sensory input information and provides the motor output to the effector cells, i.e., muscle cells, gland cells [79, 124]. It is the main processor of the body. *PNN* is grouped into two parts, which are *somatic nervous subnetwork (SoNS)* and *autonomic nervous subnetwork (ANS)*. *SoNS* collects information from the receptors of five-senses and heads through sensory neurons to convey to *CNN*. *ANS* transports the motor outputs generated by *CNN* to muscles and glands through

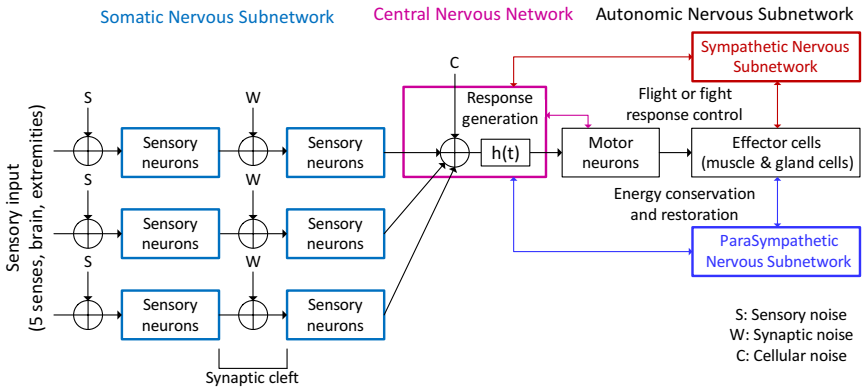

Figure 2.5: Communication architecture for overall nervous network.

motor neurons. The main function of the *PNN* is to connect the *CNN* to the systems. *ANS* carries information from *CNN* through motor neurons to smooth muscles, cardiac muscles and glands [124]. Hence, we consider *PNN* as the gateway network for *CNN* to reach the rest of the Internet in human body.

ANS is composed of two subnetworks, i.e., *sympathetic nervous subnetwork (SNS)* and *parasympathetic nervous subnetwork (PSNS)*. *SNS* controls most of the internal organs, neural and hormonal stress, i.e., *flight-or-fight responses*.

Hence, *SNS* directly communicates with the *cardiovascular* and *endocrine networks*. *PSNS* is responsible for regulation of internal organs and glands, which occurs unconsciously. Its action is basically complementary to that of the *SNS*. *PSNS* is the *energy conservation and restoration center* of the body unlike the *flight-or-fight response* of *SNS* [124]. Naturally, rather than functioning in opposition to each other, sympathetic and parasympathetic divisions complement each other's operation. The sympathetic division typically functions in actions requiring quick responses. The parasympathetic division functions with actions that do not require immediate reaction.

Finally, the brain, built by complex synaptic connections of interacting neurons in *CNN*, is also a nervous communication network itself as the main processor and memory for the information coming from all other networks inside the human body and controlling their activity. It acts like *a large-scale ultrafast network switch* among the other networks inside us, and by collecting the sensory inputs for further processing in *CNN*, and delivering motor outputs

through the spinal cord, it achieves the communication with the rest of the *internel Internet*.

Hence, the complete architecture for the nervous nanonetwork can be established using the connections and communication relations among its subnetworks, i.e., *SoNS*, *CNN* and *ANS*. Furthermore, *nervous nanonetwork* is susceptible to various major noise sources, which are *sensory* and *cellular noises* apart from *axonal* and *synaptic noises* described in the model for *nanoscale neuro-spike communication channel*. *Sensory noise (S)* is noise in sensory signals and sensory receptors. It limits the amount of information that is available to other areas of the *CNN*. *Cellular noise (C)* is an underestimated contributor to neuronal variability. The stochastic nature of neuronal mechanisms becomes critical in the many small structures of the *CNN*. Finally, *synaptic noise (W)* results from the noisy biochemical processes that underlie synaptic transmission. Adding up these noise sources can account for the observed postsynaptic-response variability. Incorporating the noise sources into the network model, *communication architecture for overall nervous network* is established, as depicted in Fig. 2.5. Despite excluded in *nervous network model*, there is another noise type, due to the random opening and closing of ion channels, which is I_w. It is the electrical noise in neurons, especially channel noise from voltage-gated ion channels, limits neuronal reliability and cell size, producing millisecond variability in action-potential initiation and propagation [50].

2.3.2 Cardiovascular Molecular Nanonetwork

Cardiovascular system, a broad network reaching to every single cell inside the body, is basically a large-scale molecular communication network. It transports amino acids, electrolytes, gases, hormones, and blood cells from or to the cells. Hence, we consider *cardiovascular system*, i.e., the system of blood, heart and blood vessels, as a huge dynamical communication network distributed over the body, i.e., *cardiovascular molecular nanonetwork*.

Understanding the multi-molecule transmission scheme helps determine the transmission characteristics of *systemic blood circulation*.

Plasma communicates with interstitial fluid, a solution surrounding the cells, through pores and inter-cellular clefts to provide the cells with nutrients and helps waste removal [78]. This molecular communication process is guided by hydrostatic and osmotic pressures of plasma and interstitial fluid, determining the rate and direction of the transmission for each granule

of molecular information.

To construct the overall communication model of heart as a nanonetwork of cardiomyocytes, we need to carefully investigate not only individual communication channels, but also the interactions with other specific nodes in the *cardiovascular* and *nervous nanonetworks*. For example, the pacemaking cells in *SA node* are controlled by *ANS*. Thus, when stimulated by *SNS* and *PSNS*, action potentials are enhanced and degraded, respectively. The capacity of blood flow through coroners also controls the molecular communication channels among cardiomyocytes by varying the ion diffusion, and hence, the action potential and its duration, which, in turn, affects the pumping rate of ventricles.

2.3.3 Endocrine Nanonetwork

Endocrine system, which is a network of glands, provides the communication among cells, senses the molecule concentration changes in the tissues and initiates the hormonal secretion process for the regulation of the molecular stability inside body. Hence, it acts like *a sensor and actor network*, to maintain the homeostasis.

In analyzing the overall communication model of *endocrine nanonetwork*, a network model with the source nodes, where hormone is generated, and the end-to-end path composed of links, through which the hormones are transmitted to destinations, should be defined. The *endocrine nanonetwork nodes* should be modeled as broadcast stations providing unidirectional transmission of hormone molecules from glands to target destinations in a broadcast medium, and bloodstream as the communication link of hormonal molecular communication, which will finally pave the way for analyzing the *information generation and delivery capacity of the overall endocrine nanonetwork* with network information theory.

2.4 Network of Intra-body Molecular Nanonetworks

To understand the molecular communication among different intra-body nanonetworks, we need to consider the relation between *nervous, cardiovascular* and *endocrine nanonetworks*, and intra-body molecular nanosensor networks.

Five senses, i.e., audition (hearing), vision (sight), tactition (touch), olfaction (smell) and gus-

tation (taste), along with the nervous nanonetwork and brain construct a large-scale nanosensor network within human body. The external stimuli signal, e.g., acoustic, visual, pressure signal, detected by these sensors are converted into neuro-spike signals by sensory neurons, which act as signal converters, and carried by the nervous nanonetwork to the brain. Depending on the nature of the external stimuli, e.g., a loud scream, a frightening scene, pressure sense, communication paths emanate from nervous nanonetwork and extend to special nodes of endocrine and cardiovascular nanonetworks.

2.4.1 Communication among Nervous, Cardiovascular Molecular, and Endocrine Nanonetworks

In the communication between sympathetic nervous subnetwork and cardiovascular molecular nanonetwork, the vasomotor centre, a special portion of medulla in nervous nanonetwork, has a substantial role. It transmits excitatory impulses through the sympathetic nerve fibers to the heart when there is need to increase heart rate and contractility, such as muscle exercise and under other types of stress. Conversely, it sends signals to the vagus nerves, which, in turn, transmit parasympathetic impulses to the heart to decrease the rate and contractility and hence, heart pumping when needed. The neurons of the *sensory area* receive sensory nerve signals from the *cardiovascular molecular nanonetwork*. Output signals emanating from the sensory area, then help control activities of both the *vasoconstrictor* and *vasodilator areas* of the *vasomotor center*, thus providing “reflex" control of many *cardiovascular functions* [67]. *Hypothalamus* and many parts of the *cerebral cortex* can also excite or inhibit the *vasomotor center* [67]. Thus, widespread basal areas of the brain can have profound effects on *cardiovascular nanonetwork functions*.

Nervous nanonetwork causes rapid increases or decreases in the amount of *action potential traffic flow* in *cardiomyocyte nanonetwork*, which is detected by way of receptors. Activation of receptors stimulate related hormonal molecular information emission, causing vasodilation or vasoconstriction, i.e., changes in the blood pressure. The best known of the nervous network arterial pressure control mechanisms is the baroreceptor reflex, which is based on special neurons, baroreceptors [78]. They reside mainly in the aorta and function as a molecular nanonetwork by sensing the drastic changes in blood pressure and communicating this information to the brain.

Hormonal changes and molecular concentrations inside the body are detected by endocrine and nervous nanonetworks, and these nanonetworks complement each other in order to maintain *homeostasis*. Chemically, both nervous and endocrine nanonetworks utilize hormonal molecular information in signaling and communication, but in different ways. As an example, norepineprine functions as a neurotransmitter and as an adrenal hormone in the *nervous* and *endocrine nanonetworks*, respectively [79]. Endocrine nanonetwork nodes, i.e., glands, are responsible for hormonal molecular emission process. The hormonal molecular information is directly secreted, i.e., transmitted, into cardiovascular nanonetwork. Nervous nanonetwork nodes, i.e., neurons, collect the molecular information from cardiovascular nanonetwork by sympathetic and parasympathetic fiber connections, and transmit the information to *CNN* regions. The hypothalamus controls the communication between the nervous and the endocrine nanonetworks, and regulates the hormonal emission process by signaling the endocrine nodes [79]. When it signals, the specific endocrine node, i.e., pituitary gland, releases hormones that control many of the *endocrine system's functions*.

2.4.2 Communication between Nanosensor Networks and Nervous Nanonetwork

2.4.2.1 Audio Molecular Nanosensor Network

The nerve impulses travel from the left and right ears to both sides of the brain stem and up to the portion of the cerebral cortex dedicated to sound, which is in the temporal lobe [67]. Human localize sound within the *CNN*, by comparing arrival-time differences and loudness, i.e., signal powers, in brain circuits that are connected to both ears, which is commonly referred to as *Echo Positioning (EPS)* [78]. The *outer ear* helps get sound and imposes low-pass filtering to the sound signal and transmitting it to the middle ear. The *middle ear* includes the ear bones, i.e., ossicles [67]. Besides their role in the transmission of sound, these bones help protect the ear from damage by constricting and limiting sound transmission when sound is too loud [151]. Therefore, the middle ear should be modeled as an adaptive communication channel, in which the bones attenuate the carrier when sound level is too high. The *inner ear* has a crucial role in hearing by the cochlea. After sound strikes the ear drum, the movement is transferred to the ear bones, which press it into one of its fluid-filled ducts through the oval window of cochlea. Therefore, inner ear should be analyzed considering and modeling it as an *acoustic-to-molecular nanoscale communication gateway*. The fluid inside this duct

is moved, flowing against the receptor cells, and stimulating the nerve cells, which then send information through the auditory nerve to the center of the *nervous nanonetwork*, i.e., the brain [67].

Different methods are developed for identification and modeling of the *audio molecular nanosensor network*. For example, in [97], benefiting from artificial neural networks, authors investigate an extended ear type system for multiple inputs and outputs. Measurement of *auditory evoked potential responses* for the extended system enables the characterization of auditory disorders. Furthermore, in [32], authors develop a computer processing method to evaluate audition using analytical technology of speech signal.

2.4.2.2 Visual Nanosensor Network

Our *visual nanonetwork* perceives the objects by *distinguishing their energy levels*. Here, the important issue about how to detect and store the information arises. Information, i.e. photons coming from source, enters the eye through an opening in the center of iris, i.e., pupil. Eye has the ability to focus on the information using its inherent adjustable lens. After gathering the information, the lens output is transmitted to the retina, the inner part of the eye containing visual receptors, i.e., rods and cones. Basically, the information is detected in the *visual nanonetwork* by rods and cones responding to faint and bright light information, respectively. When light stroke the receptors, the strength of the stimulus specified by the number of photons and their frequency determines the amount of depolarization of a receptor cell. In the visual nanosensor network, retinal, a light-sensitive form of vitamin A, is an essential signaling molecule in the rods and cones. In the presence of light, the chemical structure of retinal molecule is altered for nerve impulse, i.e., action potential, generation [28]. The amplitude of the receptor's response determines the number of *action potential generating neurons* extending from the retina through the visual nerves for further processing in the *CNN* [78, 67]. Which neurons have responded to the stimuli and how much they respond give a way to interpret how efficiently the cells are processing the information coming from light. Moreover, the timing of the responses gives an idea about the sustainability of the information during processing. Information storage in the *visual nanonetwork* is managed by the variability of the responses of the neurons.

Visual nanosensors have applications in optical industry, optical communications and pat-

tern recognition. Appropriate design of nanosensors for optically selective, sensitive sensing systems is needed for naked-eye detection of pollutants for environmental cleanup of toxic heavy-metal ions [48]. In [175], authors present an automatic speech recognition (ASR) technique integrating audio-visual sensory information, which makes ASR more robust against speaker's distance, interference and environmental noises.

2.4.2.3 Somatosensory Network

The somatosensory receptors are distributed over the skin, muscles, internal organs and the *cardiovascular nanonetwork*. The body can react many different stimuli, such as temperature, pressure, texture and chemical properties of the objects, through specialized receptors. After the stimulus is detected by sensory cells, nerve endings are depolarized and then an *action potential* is initiated, which is then transmitted to *CNN* for further processing. This *action potential* usually travels towards the spinal cord [53].

Somatosensory networks have clinical and neurological applications. *Somatosensory evoked potential (SEP)* is widely used for detecting the abnormal nerve conduction in various diseases [55]. Authors in [10] propose a new signal processing method in order to predict externally applied forces to human hands by deriving a relationship between the surface electromyographic (SEMG) signals, i.e., the electrical potential generated by muscle cells when activated, and experimentally known forces. Furthermore, in [90], the relation between the objects weight and the motor outputs during the grasping motion is investigated [91].

2.4.2.4 Olfactory Nanosensor Network

The receptor neurons in the nose are particularly interesting because they are the only direct recipient of stimuli among the nanosensory networks. When the molecules of odorant are detected by the receptors, an *action potential* in the receptor neuron is generated by the activation of ion channels, causing Ca^{++} inflow into the cells. Olfactory sensory neurons project axons within the olfactory nerve to the brain. These axons pass to the olfactory bulb, which, in turn, projects *olfactory information* to the olfactory cortex and other areas. Odor information is stored in long-term memory and has strong connections to emotional memory, possibly due to the *olfactory nanonetwork's* close anatomical ties to the limbic system and hippocampus,

areas of the brain that have long been known to be involved in emotion and placing memory, respectively [134]. Different from other nanosensor networks, olfaction, i.e., smell, is an adaptive sense. Olfactory adaptation, which is the normal inability to distinguish a particular odor after exposed to the specific odorant, is the adaptation mechanism of the neurons to protect themselves from being overloaded. Therefore, if the particular odor information does not change, the system ignores that information until a different information, i.e., odorant, is sensed and system starts to respond to this new information [39], i.e., olfactory nanosensory network responds primarily to changes in stimulation.

Nanosensor systems for the rapid detection of specific odorants have applications in biotechnology, medicine, and food safety. In [84], authors explore the real time detection of odorant molecules with single atomic resolution and high sensitivity using a 'bioelectronic nose' inspired from human olfactory receptor. In [72], authors introduce a gas discrimination system that integrates a cross-reactive array of chemiresistive nanosensors to accurately and efficiently identify the gas (odor) to which the system is exposed.

2.4.2.5 Gustatory Molecular Nanosensor Network

Taste is detected through the taste receptors, i.e., the ion channels and G-protein coupled receptors, which are capable of detecting bitterness, sweetness, saltiness, sourness and umaminess [18]. Tongue has taste pores top of the taste receptors, where the food is dissolved to contact with the receptors and ion channels. After detection, the taste information is simply sent to the brain via nerves.

Gustatory molecular nanosensors have applications in many fields ranging from medicine and food industry to military defence and national safety. In [88], authors describe the development of the biosensor intelligent system with software on electronic tongue and electronic nose for rapid analysis of gaseous, liquid and heterogeneous matters.

Nanosensor networks, in brief, build our connection with external sensible stimuli, e.g., sound, light, temperature, pressure, texture, smell, taste and so on. The response of these networks are directly communicated through *nervous nanonetwork* for further processing in special lobes of brain. Besides, *nanosensory networks* prepare the body responses, i.e., actions and reactions, to various stimuli through elaborated communication relations among

molecular nanonetworks. In fact, even a simple special case, e.g., intra-body audio molecular nanosensor network, is a very complex process in terms of communication and information theory perspectives. It involves audition sense, nervous, cardiovascular and endocrine nanonetworks. External acoustic wave initiates a series of communication processes in the network. First, it is transduced into neuro-spike communication signal. Next, the molecular communication within the endocrine nanonetwork as a response to this stimulus amplifies the traffic load in the cardiovascular molecular nanonetwork. Therefore, investigation of the communication principles, end-to-end rate and delay characteristics, flow control, bottlenecks and potential communication failures, even for *a nanosensory network to single stimulus* from the perspectives of communication, information, and network theories needs lots of effort and devotion.

Akyildiz et al. describe nanosensor technology and electromagnetic communication among nanosensors [5]. The state of the art in nanosensor technology is surveyed. Furthermore, some applications of wireless nanosensor networks are highlighted to emphasize the need for communication among nanosensor devices. A new network architecture for the interconnection of nanosensor devices with existing communication networks is provided. The communication challenges in terms of terahertz channel modeling, information encoding and protocols for nanosensor networks are highlighted, defining a roadmap for the development of this new networking paradigm.

2.5 Future Research Avenues

The biological systems provide the cooperation of human body as a whole even in abnormal conditions. However, in some diseases, biological systems cannot overcome the problems related to peripheral factors or originating from body itself. In this section, we focus on the unsolved or partially diagnosed problems of human health, related to the improper or inadequate operation of *cardiovascular, endocrine, nervous nanonetworks* and *nanosensory networks*.

Medicine has been mainly concentrating on the recruitments of the physiologically indispensable organ systems in human body. As a matter of fact, urgent treatment of cardiac and brain diseases are crucial as these organs are strategically much more important for survival and

they have control mechanisms over the other vital organ systems in human body. Thus, crucial effort is attached on cardiovascular surgery, neurosurgery, endocrinology and metabolic diseases, etc. Major advances in medicine has enabled the treatment many illnesses, such as diabetes, heart failure, cardiac arrhythmias, renal failure, and many cancer types [122]. However, especially for some nervous system related illnesses, such as multiple sclerosis (MS), epilepsy, meningitis, medicine has been inadequate, as main reasons for these illnesses have been still not understood [31]. Moreover, for the remaining physiological illnesses, the remedies that medicine provided can be strengthened by understanding the underlying causes for illnesses by investigation of molecular communication principles and relations among biological systems. In this section, we aim to open the way for extracting the communication relations and channels for molecular nanonetworks, and analyzing the problems in molecular and signal transmission paths that cause burdens to harmonic operation of molecular communication of nanonetworks independently, or as a whole.

To realize the communication links and failures among intra-body nanonetworks, we need to concentrate on the foundations of communication structures and tasks inside the biological systems from the perspectives of molecular communications and network theory. Open research issues, hence, include the modeling and analyses for *molecular communication channels*, *intra-body molecular nanonetworks*, and finally, *investigation of operational principles and diseases arisen from improper processing of molecular nanonetworks inside the body from the perspective of communication and networking theories*.

2.5.1 Molecular Communication Channels

Molecular communications has been widely investigated in the literature, most particularly from the perspectives of propagation media, diffusion and the noise sources employed in the diffusion process. In [125], several bio-inspired techniques are discussed according to whether a fixed physical link is required for signal propagation or not, i.e., either wired or wireless communication. Pheromones, spores, pollen and light transduction are discussed. In the second group, neuron-based communication techniques and capillaries flow circuit are explored. In [4], nano-electromagnetic communication and molecular communication are envisioned, and propagation models are discussed. In [129], a new physical end-to-end communication model for molecular communication is introduced, and numerical results are provided.

In [132], authors provide a mathematical study of the noise at the reception of the molecular information in a diffusion-based molecular communication system when the ligand-binding reception is employed. The reception noise is modeled by following the ligand-receptor kinetics and the stochastic chemical kinetics. In [59], diffusion-based molecular communication is studied through N3Sim, a physical simulation framework for molecular communication. In [102], the diffusion-based molecular communication, whose physical channel is governed by Fick's laws of diffusion, is focused on. In [131], the noise sources in diffusion-based molecular communication are analyzed using signal processing, statistics and communication engineering instruments. Important diffusion-based noise sources, i.e., the particle sampling and counting noise, are investigated.

Although there exists preliminary research on diffusion-based molecular communication commonly for generic frameworks, the main molecular communication directions for biological systems and specifically, communication pathways inside the human body are not explored yet. Hence, future research issues include the communication models and extensive performance analyses for intra-body molecular communication channels. More specifically:

2.5.1.1 *Nanoscale Neuro-spike Communication Channel*

- Based on the neuro-spike communication channel model in [21], the neuro-spike synaptic multiple-access, relay, and broadcast channels should be defined, derived, and analyzed from communication theoretical perspective.
- Fundamental communication parameters and metrics, such as interference, channel access, and collision probability over multi-neuron connections, should be investigated.
- Network information theoretical analysis of the realistic multi-terminal neuronal communication channels should also be performed to find the corresponding achievable rate regions. Furthermore, the results in [20], can be extended to multi-output case for achieving automatic gain control.

2.5.1.2 *Action Potential-based Cardiomyocyte Molecular Communication Channel*

- The information theoretical foundations of molecular communication between two cardiomyocytes should be investigated. The reception of an action potential by the receiver

cardiomyocyte should be modeled by molecular detection and counting process under the light of detection and estimation theory.

- Based on the *cardiomyocyte molecular communication channel model* given in Section 2.2.3, the investigation of the realistic multi-terminal channel models for multiple-access, broadcast, and relay channels and analysis of their information theoretical capacities to find the required molecular communication rates for sustainability of heart functions should be implemented.

- The statistical properties of all noise and disturbance sources should be mathematically investigated and modeled through stochastic modeling of the potential sources for *interference* and *fading* of the communication signal in the channel. The *information capacity of cardiomyocyte molecular communication channel should be derived.*

2.5.1.3 *Hormonal Molecular Communication Channel*

- Ligand-receptor binding models could be benefited to mathematically model and analyze the molecular diffusive communication channel, in which hormones propagate and bind to the receptors [24, 11, 12, 13, 14, 16].

- The noise sources of the communication system should be defined and mathematically modeled, and the rate and delay performance of hormonal molecular communication channel should be analyzed.

2.5.2 Intra-body Molecular Nanonetworks

Realization of molecular nanonetworks stem from the development of nanomachines. In [6], the state-of-the-art in nanomachines are explained for a better understanding of the nanonetwork scenarios. Furthermore, nanonetworks and components are described and compared with traditional communication networks. In [62], molecular transmission between nano-scale devices over medium distances, is studied, and a molecular network architecture is proposed to realize the communication between nano-machines that can be deployed over different distances. In addition, flagellated bacteria and catalytic nanomotor techniques are proposed to cover the medium-range. Both techniques are based on the transport of DNA encoded information between emitters and receivers by means of a physical carrier. In [130], a

mathematical expression for the capacity of diffusion-based molecular communication nanonetworks is provided. In [89], *Concentration Shift Keying* and *Molecule Shift Keying* modulations are proposed for coding and decoding information in nanonetworks. In [34], a bacteria-based nanonetwork for communication between nanoscale devices is described. The communication is achieved by switching of DNA molecules by chemotaxis. Furthermore, an analytical model is developed to assess the communication range, capacity, end-to-end delay and throughput by considering the available information about the biological mechanisms used. In [1], authors propose *Quorum Sensing*, a mechanism used by bacteria to sense their own population and coordinate their actions, through the emission and sensing of molecules called autoinducers, as a novel way to achieve synchronization between nodes of a nanonetwork. Molecular nanonetworks have been explored with different perspectives. Many studies concentrate on developing new modulation scenarios and molecular sensing mechanisms without considering intra-body molecular pathways. However, understanding of molecular channel foundations inside human body will contribute to extension of *single-input single-output (SISO)* channel models to *multi-input multi-output (MIMO)* cases, i.e., intra-body molecular nanonetworks: *nervous, cardiovascular, endocrine nanonetworks*, and then, the overall network of multi-terminal molecular communication nanonetworks will be concentrated on.

2.5.2.1 *Nervous Nanonetwork*

Extension of the results in the modeling and analysis of neuro-spike communication channels to the study of the overall nervous nanonetwork composed of ultra-large scale and heterogeneous connections of various types of neurons should be implemented as illustrated in Fig. 2.5. Therefore, this architecture should correspond to combination of multiple-access, relay and broadcast channels. The network information theoretical analysis of the entire nervous network should be performed to reveal its network information capacity.

2.5.2.2 *Cardiovascular Molecular Nanonetwork*

To construct the overall communication model of heart as a nanonetwork of cardiomyocytes, not only individual communication channels, but also the interactions with other specific nodes in the *cardiovascular* and *nervous nanonetworks* should be carefully investigated. Hence, all these factors should be incorporated into the model of *cardiovascular nanonet-*

work, and the overall model should be analyzed using information, communication and network theoretical tools.

2.5.2.3 *Endocrine Nanonetwork*

Overall communication model of *endocrine nanonetwork* with the source nodes, where hormone is generated, and the end-to-end path composed of links, through which the hormones are transmitted to destinations, should be defined. The *endocrine nanonetwork nodes* as broadcast stations providing unidirectional transmission of hormone molecules from glands to target destinations in a broadcast medium should be considered and mathematically modeled. The *information generation and delivery capacity of the overall endocrine nanonetwork* should be analyzed.

2.5.2.4 *Multi-terminal Molecular Communication inside Us*

- The noise, potential communication failures, and the information capacity should be analyzed in order to reveal the fundamental limits for intra-body molecular channels.

- The principle communication relations among the nervous, cardiovascular and endocrine nanonetworks should be investigated. Basically, nanosensor networks, which collect the information through various receptors, are the communication links between the intra-body networks and the outside world. The output signals of nanosensory networks are transduced into neuro-spike communication channels. Nervous network, is then stimulated and hormonal molecular information, depending on the type of the stimulation, is secreted into the bloodstream. To understand the communication between the nervous and endocrine nanonetworks, a detailed communication theoretical analysis on the neuro-secretion process should be performed. Finally, the traffic load in the cardiovascular molecular nanonetwork is altered, which is to be sensed by nervous nanonetwork. Thus, the overall network of intra-body nanonetworks communicate through feedback regulation mechanisms, and each response emanating from a nanonetwork is transported to another nanonetwork for the generation of required response. Thus, intra-body multi-terminal molecular communication nanonetworks should be analyzed from the perspectives of communication, information, and network theories, by proper

understanding of the physiology, and mathematical modeling of these interactions, investigating the theoretical limitations, and identifying the potential communication failures.

- To the best of our knowledge, there is no unified network simulator for intra-body molecular nanonetworks although there are some web-based neural network simulators implemented by modeling of motor neurons [33], and a cardiovascular simulator to complement research with the medical experimental data [116], and a diffusion-based molecular communication simulator, NanoNS, developed based on the commonly used network simulator (NS-2) [63]. A molecular nanonetworks simulator should be developed to evaluate the theoretical results, capture potential communication failures in each of these nanonetworks leading to diseases, and pave the way for the design of ICT-inspired diagnosis and treatment techniques.

2.5.3 Physiology and Underlying Pathology of Intra-body Systems from Communication Theory Perspective

Biological operation principles and most particularly, diseases of intra-body systems should be investigated from the perspectives of communication and network theories.

2.5.3.1 *Nervous Nanonetwork:*

- Multiple sclerosis (MS), the illness resulted from destruction of myelin, affects the ability of nerve cells in the brain and spinal cord to communicate with each other [82]. In MS, the human immune system attacks and damages the myelin. When myelin is lost, the axons can no longer effectively conduct signals. Therefore, analyzing the symptoms of MS could enable us to discover the role of myelin in nervous system.

- Epilepsy, a demyelinating disease, is the damage of myelin sheath of neurons. One of the reasons for epilepsy is neuroleptics [107]. Hence, understanding the role of neuroleptics on myelin tissue loss helps nanomedicine improve treatment opportunities, such as enhancing the effectiveness of communications between neurons by enabling the myelin sheath to be more resistant to this type of drugs.

- Meningitis, which is the inflammation of the meninges covering the brain and spinal

cord, can lead to serious long-term consequences, such as deafness, epilepsy, hydrocephalus and cognitive deficits [123]. Symptoms of meningitis, such as the decrease of sodium amount in blood and dehydration, can give a path to analyze the reasons behind signal transmission failures and molecular communication ion channel nonfunctionalities.

- Destruction of occipital lobe causes cortical blindness. Hence, communication relations of occipital lobe with visual nanosensor network, and role of this brain portion especially in visual perception should be investigated, and thus, the main causes for visual deficits could be analyzed.

- Damage of temporal lobe can result in fear to display normal fear and anxieties. Therefore, operation of temporal lobe in controlling this kind of actions should be analyzed and

  alternative treatment methods for enabling effective communication inside nervous nanonetwork should be developed, suppressing such damages caused by deterioration of signaling pathways.

2.5.3.2 *Cardiovascular Nanonetwork:*

- Reasons for sudden cessation of normal cardiac rhythm, i.e., cardiac arrest, tachycardia, i.e., extremely rapid heart beat, and asystole, i.e., losing the ability of contraction, could be analyzed from the perspectives of communication and information theories by studying the cardiac action potential waveform texture.

- Cardiac tamponade, which is the condition that the tissue surrounding the heart fills with excess fluid or blood [153], blocking the proper heartbeat rate, could also be studied to find the relation between the permeability of this tissue and the extracellular fluid molecules, which will help extract the characteristics of heart tissue.

- The partial pressure of oxygen in blood, and its effect on suppressing other molecules in vessels could also be analyzed to investigate the effect of oxygen amount in *pressure regulation mechanism of cardiovascular nanonetwork*.

- Cardiovascular transmission problems due to overactivity of daily living, such as varsity, due to long periods of standing on feet and over walking should be analyzed, and

ICT solutions for regulation of the blood circulation should be proposed.

- High blood pressure, i.e., hypertension, should be studied to understand the reaction of body to external stimuli. Studying the molecular communication principles and signaling interactions among nervous, cardiovascular and endocrine nanonetworks provides a mathematical model for the response of body to environment, and hence, treatment of hypertension could be succeeded through joint contribution of medicine and ICT fields.

2.5.3.3 *Endocrine Nanonetwork:*

- The role of *endocrine nanonetwork* in regulating the amounts of blood molecules, i.e., the fundamentals of communication between endocrine and cardiovascular nanonetworks should be understood. Especially for glucose and lipid molecules, in order to understand the role of liver in adjusting blood cholesterol level and model insulin and glucagon secretion processes, hormonal signaling mechanisms and models should be investigated and molecular emission, propagation and reception processes should be incorporated into them.

- Circadian rhythm, which is important in adjusting the body to environmental alterations, such as seasonal changes, variation in the amount of light during the day and night, and temperature variations, should be investigated and solutions for how the human body establishes the communication with outside world through nanosensory networks should be quested.

- Neurotransmitters should be analyzed to understand the relation between *endocrine* and *nervous nanonetworks*, and to provide the reasons behind *spike transmission capability of neurons*.

2.5.3.4 *Nanosensor networks:*

- The communication theoretical behavior of inner ear should be analyzed considering and modeling it as an acoustic-to-molecular nanoscale communication gateway.

- The human eye is a complex nanosensor collecting light, i.e., *photonic molecular information*, and conveying through the network of light sensors, i.e., rods and cones, where they convert the light input to neural signals to be finally transmitted to brain. However,

the human eye is disturbed by the nerves and blood vessels in front of the visual sensors, which leads to imperfections in vision. Therefore, visual sensing mechanism should be analyzed by incorporating the effect of visual nerves and vessels on the ability to see, and a communication model for human eye can be developed to pave the way for future diagnosis and enhanced treatment opportunities.

- Tactition is an important sense to be studied in detail. The conditions under which the human cannot sense and respond to various stimuli should be investigated and communication models to overcome inability to sense pain, chemical stimuli and pressure could be developed.
- Neural adaptation mechanisms underlying olfactory fatigue should be investigated to understand how the human body responds to over stimuli.
- Common gustation disorders, such as ageusia and dysgeusia (which may be resulted from chemotherapy) [35] that prevent the detection of taste, could be studied and solution approaches could be developed.

CHAPTER 3

A COMMUNICATION THEORETICAL ANALYSIS OF SYNAPTIC MULTIPLE-ACCESS CHANNEL IN HIPPOCAMPAL-CORTICAL NEURONS

Communication between neurons occurs via transmission of neural spike trains through junctional structures, either electrical or chemical synapses, providing connections among nerve terminals. Since neural communication is achieved at synapses, the process of neurotransmission is called synaptic communication. Learning and memory processes are based on the changes in strength and connectivity of neural networks which usually contain multiple synaptic connections. In this chapter, we investigate multiple-access neuro-spike communication channel, in which the neural signal, i.e., the action potential, is transmitted through multiple synaptic paths directed to a common postsynaptic neuron terminal. Synaptic transmission is initiated with random vesicle release process from presynaptic neurons to synaptic paths. Each synaptic channel is characterized by its impulse response and the number of available postsynaptic receptors. Here, we model the multiple-access synaptic communication channel, and investigate the information rate per spike at the postsynaptic neuron, and how postsynaptic rate is enhanced compared to single terminal synaptic communication channel. Furthermore, we analyze the synaptic transmission performance by incorporating the role of correlation among presynaptic terminals, and point out the performance improvement in terms of postsynaptic rate. Finally, we concentrate on the disorders characterized by abnormalities in pre- and postsynaptic terminals and synaptic connections, and establish relations between neural diseases and synaptic communication problems.

3.1 Introduction

Molecular communication is a new communication paradigm in which molecules are the information carriers [3], [69]. Some examples of molecular communication mechanisms are calcium signaling [119], molecular motors, pheromones, neurotransmitters [3].

The calcium signaling concept is described in [3]. In [119], the authors describe the design of a molecular communication system based on intercellular calcium signaling networks. There is also some current work focusing on communication with biological molecular motors [3], intra-cellular aqueous nanobubbles [114], and artificial cell-to-cell communication systems [172].

In the literature, different molecular network architectures are proposed to realize the communication between nanomachines that can be deployed over different distances. In [62], flagellated bacteria and catalytic nanomotor techniques are proposed to cover the medium-range. In addition, there are various molecular communications options for short range [92], and long range [125]. Although, neural signaling has a long history initiated from the Hodgkin's pioneering work [70], among all molecular communication paradigms, neuro-spike communication that uses the neurotransmitters as information carriers has not been studied to the fullest extent [21].

There are several studies about the physiological principles of the neuron. The axonal propagation in the hippocampal neurons and the reliability of this transmission are investigated in [111] and [137]. The vesicle release process, which initiates the synaptic transmission in hippocampal neurons is described [42, 159]. Trial-to-trial variability in synapses is explained in [108]. These contributions mediate the analysis of neurons from the perspective of communication theory.

Neuro-spike communication is an interdisciplinary research area, which combines the fields of neuroscience, communications and nanotechnology. The transferred amount of information through a synaptic connection has an important role in learning and memory processes. There has been some research concentrating on the limits on information transmission over synaptic terminals [106]. In [21], authors investigate the communication behavior of neurons as a new nanoscale communication paradigm and model the end-to-end neural communication channel. A synaptic communication model is suggested in [106]. It involves the funda-

mental events during the synaptic transmission as different blocks, namely the vesicle release in response to a spike, Excitatory PostSynaptic Potential (EPSP), which is the temporary increase in the postsynaptic membrane potential caused by the flow of positively charged ions into the postsynaptic cell due to the vesicle release [22], and trial-to-trial variability of this potential. The authors derive the theoretical lower bounds on the capacity of a simple model of a cortical synapse by signal estimation and signal detection paradigms. However, the model is based on point-to-point synaptic connections. Furthermore, authors employ univesicular release in their model, and do not take into account the variability in vesicle fusion rate on different sites of the presynaptic terminal.

In this chapter, we investigate the multiple-access communication among hippocampal-cortical neurons occuring via exchange of molecules through chemical synapses, which involve neurotransmitters and are far more common and modifiable compared to electrical synapses that do not involve neurotransmitters [36]. We perform analysis to observe how the postsynaptic rate improves with increasing number of users, i.e., presynaptic terminals. Our main motivation in this work is that learning and memory processes are based on the changes in strength and connectivity of neural networks, which usually contain multiple synaptic connections. Therefore, we specifically focus on the multi-input single-output neuro-spike communication channel characteristics to observe the tradeoff between multiple users and total rate at the output. Synaptic plasticity, i.e., the changes in the synaptic connection strengths depending on the presynaptic input strengths and channel parameters, is the main mechanism behind learning and memory. Learning occurs through cooperation between synaptic inputs and the plasticity rules select inputs which have a strong correlation with other inputs [146]. Synaptic plasticity contributes to memory storage, and the activity-dependent development of neuronal networks. Therefore, we especially concentrate on the positive influence of correlation among presynaptic neural spike trains on the communication rate at the postsynaptic neuron. For that purpose, after focusing on the transmission capability in neuronal connections when there are multiple presynaptic terminals, we analyze the role of spike train correlations on synaptic performance. We investigate the rate region for two different cases: a) uncorrelated firing of neurons where the neural spike trains generated at each presynaptic terminal are independent, and b) correlated firing of neurons where the neural spike trains have a first order correlation. Our analysis reveals that the information rate at the synaptic communication channel is improved as the number of presynaptic terminals increases. Furthermore, the total commu-

nication rate is reinforced in the same way as of the amount of correlation among the action potentials generated at the input neurons.

In this chapter, we apply existing techniques in communications to analyze the performance of the neuronal channels. However, we provide a comprehensive mathematical model of the communication channel including the stochastic behavior of the input, the action potential generation, dynamic and stochastic nature of vesicle release process, stochastic nature of the communication channel. Although the point-to-point synaptic channel performance is studied in the literature widely as in [74], [66] and [21], we provide a more comprehensive neuro-spike communication channel model in Section 3.2. Our contributions range from incorporation of the stochastic nature of all the parameters along the communication line into the dynamic nature of processes, including the random nature of the input, the communication channel, the quantal variability, multivesicular release process, pool-based synapse model. Furthermore, the multiple-access neuronal communication channel model we develop in this chapter is completely new. Multiple-access extension is not simply the addition of the input signals. To the best of our knowledge, the effect of the correlation among the presynaptic terminals has not been studied yet in the literature. In this chapter, we develop a rate region analysis for the multiple-access communication channel, and show the boosting effect of the correlation on the sum rate at the channel output. In addition, incorporation of the effect of correlation among presynaptic terminals on the postsynaptic rate is also provided for the first time in the literature. We analytically show that as the correlation between presynaptic terminals increase, the postsynaptic rate is enhanced.

The remainder of this chapter is organized as follows. In Section 3.2, we provide the linear-nonlinear-Poisson (LNP) model of spike generation, vesicle release and postsynaptic response variability in a link-to-link synaptic communication channel. In Section 3.3, we extend the single-input single-output channel model to a multiple-access synaptic communication channel and obtain the analytical expression for multiuser channel rate regions. In Section 3.4, we evaluate the performance of the multiple-access synaptic communication channel, quantitatively investigate the total information rate per spike at the postsynaptic neuron for the multiuser communication system, and compare it to a single terminal synaptic channel. In Section 3.5, we concentrate on the disorders characterized by abnormalities in pre- and postsynaptic terminals and synaptic connections, and establish relations between neural diseases and synaptic communication problems.

3.2 Model Description

In this section, first, we give an overall picture of point-to-point neural communication and biological processes specifically pertinent to the functioning of integrated living cells behind this communication paradigm to provide the reader with the essential background knowledge of neural signaling. Then, stating our objectives and methodology, we concentrate on the fundamental blocks of the single-input single-output (SISO) neuro-spike communication channel.

Neural Signaling Background: we provide the essential components of neural signaling. These include *action potential generation*, *neural firing*, *vesicle release*, *postsynaptic potential* and *postsynaptic response variability*.

Action potential is a short-lasting event in which the electrical membrane potential of a cell rapidly rises and falls, following a consistent trajectory [21]. During the action potential, part of the neural membrane opens to allow positively charged ions inside the cell and negatively charged ions out. This process causes a rapid increase in the positive charge of the nerve fiber. When the charge reaches $+40$mV, the impulse is propagated down the nerve fiber. This electrical impulse is carried down the nerve through a series of action potentials. *Neural firing* is the response of a neuron when it is stimulated. A neuron that emits an action potential is often said to fire.

Synaptic vesicles store neurotransmitters to be released at synapses and constantly reproduced by the cells. These vesicles are essential for conduction of nerve impulses among neurons. Action potentials trigger the complete fusion of the synaptic vesicle with the cellular membrane, and then, the excretion from the cell through exocytosis, which is called *vesicle release* [110].

Postsynaptic potential is the membrane potential at the postsynaptic terminal of a chemical synapse. In neuroscience, an EPSP is a temporary depolarization of postsynaptic membrane potential caused by the flow of positively charged ions into the postsynaptic cell as a result of opening of ligand-gated ion channels [22]. An Inhibitory PostSynaptic Potential (IPSP), which is the opposite of an EPSP, makes a postsynaptic neuron less likely to generate an action potential. *Postsynaptic response variability* is the trial-to-trial variability in the amplitude of the postsynaptic response to a vesicular release.

Objectives and Methodology: we aim to analyze the rate region at the postsynaptic terminal when there are multiple presynaptic terminals. Hence, as the initial step to the rate region analysis, in this section, we focus on the SISO synaptic channel characteristics. Therefore, we first explain the firing and spike generation mechanisms. Then, we provide a model for vesicle release from presynaptic terminals, and the model of channel response depending on the trial-to-trial variability in vesicle release process. To characterize the rate region, we need to find the power spectral densities (PSDs) of the signal and noise components at the postsynaptic terminal by incorporating the stochastic characteristics of presynaptic input, neuron terminal, and the synaptic channel parameters. Therefore, in this section, we provide the main blocks and steps for analytically obtaining the PSD at the postsynaptic terminal for the SISO synaptic communication channel, and calculate the statistical parameters, i.e., the means and variances of the random variables denoting the action potential rate, vesicle release processes, quantal variability, which play fundamental roles on the performance of neuro-spike communication.

3.2.1 Neuronal Firing: The Soma Channel

In a SISO neuron channel model, when a random stimulus, $m(t)$, is applied to the presynaptic terminal, a spike train, $S(t)$, is generated at its axon which has a time varying neuronal firing rate $\lambda(t)$. In our model, $m(t)$ and $S(t)$ are jointly wide-sense stationary (jointly WSS), implying that both $m(t)$ and $S(t)$ are WSS processes, and the cross correlation function $R_{m,S}(\tau) = \mathrm{E}[m(t)S(t+\tau)]$ is independent of t for all τ.

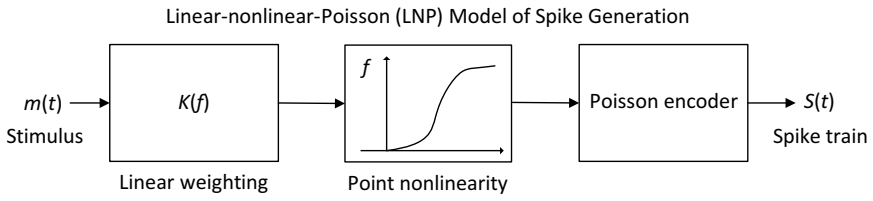

Figure 3.1: A simplified functional model of neural spike responses [156]. In [156], a Linear-Nonlinear-Poisson (LNP) model for neural responses is proposed, which has been successfully used to describe the neuronal response characteristics.

3.2.1.1 Low Pass Filtering

Consider that the stimulus $m(t)$, which is a wide sense stationary (WSS) process, with bandwidth B_m, and autocorrelation function (ACF) $R_m(t+\tau,t) = R_m(\tau)$ enters the hypothetical $k(t)$ filter, which simulates the empirical characteristics of axonal filtering process. We ignore axonal noise for simplicity. Hence, the filter response, i.e., $v(t)$ is

$$v(t) = m(t) * k(t),\ k(t) = \frac{1}{C}\exp\left(-\frac{t}{RC}\right)U(t). \tag{3.1}$$

$k(t)$ is a low-pass filter denoting axonal response. Hence, $k(t)$ corresponds to the first block of LNP model shown in Fig. 3.1. The absolute square of the frequency response of $k(t)$ filter is $|K(f)|^2 = \frac{R^2}{1+(2\pi fRC)^2}$, which is later utilized in the calculation of the PSD of the generated spike train. Hence, the ACF of $v(t)$, i.e., $R_v(t+\tau,t) = R_v(\tau)$, is obtained as

$$R_v(\tau) = \int_0^\infty \int_0^\infty R_m(\tau-\alpha+\beta)\frac{1}{C^2}\exp\left(-\frac{\alpha+\beta}{RC}\right)\mathrm{d}\alpha\mathrm{d}\beta, \tag{3.2}$$

which is also a WSS random process since it is obtained by low-pass (linear) filtering of the stimulus $m(t)$, which is a zero mean random process. Hence, the PSD of $v(t)$ is obtained as

$$S_v(f) = |K(f)|^2 S_m(f) = \frac{R^2}{1+(2\pi fRC)^2} S_m(f). \tag{3.3}$$

3.2.1.2 Point (Sigmoidal) Nonlinearity

Point nonlinearity block, the second stage of the LNP model, transforms the linearly weighted input into an inhomogenous spike rate function, which is later utilized in Poisson encoder, the third stage of the LNP model, to generate Poisson impulses [156]. The inhomogeneous spike rate can be determined as $\lambda(t) = f(m(t) * k(t))$, where f is a sigmoidal nonlinearity, and is a scalar and continuous function with nonnegative outputs. In the limit of small time bins, the probability of spike generation becomes $P(\text{Spike}) \propto f(m(t) * k(t))$. Considering the number of arrivals in the time interval Δt, given as k, which follows a Poisson distribution with associated parameter $\lambda_{\Delta t} = \int_{\Delta t} \lambda(t)\,\mathrm{d}t$, $Prob(k) = e^{-\lambda_{\Delta t}}\lambda_{\Delta t}^k/k!$. In the limit of very small Δt, $Prob(0) = 1-\lambda(t)\Delta t$. Hence, the spike generation probability is given as $P(\text{Spike}) = \lambda(t)\Delta t$, which is proportional to $\lambda(t)$.

The sigmoidal nonlinearity function is given as

$$f(v(t)) = \frac{1}{1+\exp\left(-a\left(v(t)-v_{1/2}\right)\right)}, \tag{3.4}$$

which is a mapping on $v(t)$ and depends on the constant parameters a and $v_{1/2}$. In [41], authors model the spike rate for cortical neurons of a monkey, and the sigmoidal nonlinearity curve is fitted with the parameters $a = \frac{1}{0.029^\circ}$ and $v_{1/2} = 0.036^\circ$ and scaled with $\lambda_{\max} = 36.03$ Hz. These parameters are also applicable to our analysis.

The sigmoidal nonlinearity is a result of the saturation of presynaptic neurons. As the firing rate increases, the synaptic channel is saturated with available vesicles in the docked pool. Hence, the number of available vesicles in the docked pool decreases. In this section, the neuronal firing rate should be high enough to avoid zero throughput. Furthermore, we assume that the synaptic channel could be saturated. However, to simplify the analysis, we approximate the nonlinear model about the non-saturated region of the sigmoidal curve by linearizing the sigmoidal function around $f(v(t)) = 0.5\lambda_{\max}$, where $v(t) = v_{1/2}$. Hence, we can approximate $f(v(t))$ as

$$f(v) = \begin{cases} 0 & \text{if } v(t) \leq v_{1/2} - \frac{2}{a} \\ \lambda_{\max}\left(\frac{1}{2} + \frac{a\left(v - v_{1/2}\right)}{4}\right) & \text{if } \left|v(t) - v_{1/2}\right| \leq \frac{2}{a}, \\ \lambda_{\max} & \text{if } v(t) \geq v_{1/2} + \frac{2}{a} \end{cases} \tag{3.5}$$

where $f(v_{1/2} - \frac{2}{a}) \approx 0.12\lambda_{\max}$, and $f(v_{1/2} + \frac{2}{a}) \approx 0.88\lambda_{\max}$. Therefore, linearizing the output of the sigmoidal nonlinearity block, we obtain

$$\lambda(t) = \lambda_{\max}\left(\frac{2 - av_{1/2}}{4} + \frac{av(t)}{4}\right)P\left(|v(t) - v_{1/2}| \leq \frac{2}{a}\right) + \lambda_{\max}P\left(v(t) - v_{1/2} \geq \frac{2}{a}\right), \tag{3.6}$$

where the rate of the Poisson spike generation process changes linearly, provided that $v_{1/2} - \frac{2}{a} \leq v(t) \leq v_{1/2} + \frac{2}{a}$ is satisfied. When $v(t) \geq v_{1/2} + \frac{2}{a}$, the neuron is saturated and $\lambda(t) = \lambda_{\max}$. Hence, the mean firing rate can be determined as

$$\bar{\lambda} = \mathrm{E}[\lambda] \quad = \quad \lambda_{\max}\left(\frac{2 - av_{1/2}}{4}\right)P\left(|v(t) - v_{1/2}| \leq \frac{2}{a}\right) + \lambda_{\max}P\left(v(t) - v_{1/2} \geq \frac{2}{a}\right) \tag{3.7}$$

We assume that the stimulus to each presynaptic terminal is normal distributed with zero mean and variance σ^2. Hence,

$$\begin{aligned} P\left(|v(t) - v_{1/2}| \leq \frac{2}{a}\right) &= \frac{1}{2}\left[\mathrm{erf}\left(\frac{g^{-1}\left(\frac{2}{a} + v_{1/2}\right)}{\sigma\sqrt{2}}\right) + \mathrm{erf}\left(\frac{g^{-1}\left(\frac{2}{a} - v_{1/2}\right)}{\sigma\sqrt{2}}\right)\right] \quad (3.8) \\ P\left(v(t) - v_{1/2} \geq \frac{2}{a}\right) &= \frac{1}{2}\left[1 - \mathrm{erf}\left(\frac{g^{-1}\left(\frac{2}{a} + v_{1/2}\right)}{\sigma\sqrt{2}}\right)\right], \end{aligned}$$

where $g(m(t)) = m(t) * k(t)$ is a function of the stimulus, and we assume that $g(.)$ is one-to-one. Hence, the inverse of g, denoted by g^{-1}, is the unique function with domain equal

to the range of g that satisfies $g\left(g^{-1}(x)\right) = x$ for all x in the range of g. Furthermore, since we assume that $v(t) \geq v_{1/2} - \frac{2}{a}$ (to prevent firing rate from being zero), we should scale the probabilities in (3.8) so that they add up to 1. From (3.6), (3.7) and (3.8), we obtain

$$\lambda(t) \quad = \quad \bar{\lambda} + \bar{\lambda} b v(t), \tag{3.9}$$

where $b = \frac{a\lambda_{\max}}{4\bar{\lambda}} P\left(|v(t) - v_{1/2}| \leq \frac{2}{a}\right)$. Using (3.9), the ACF of $\lambda(t)$ can be determined as

$$R_\lambda(\tau) = \mathrm{E}\left[\lambda(t+\tau)\lambda(t)\right] = \bar{\lambda}^2 \mathrm{E}\left[\left(1 + bv(t+\tau)\right)\left(1 + bv(t)\right)\right] = \bar{\lambda}^2\left(1 + b^2 R_v(\tau)\right). \tag{3.10}$$

Hence, the autocovariance function of $\lambda(t)$ can be obtained by subtracting $\bar{\lambda}^2$ from $R_\lambda(\tau)$ as $C_\lambda(\tau) = \bar{\lambda}^2 b^2 R_v(\tau)$. The variance of the spike rate, i.e., $\sigma_\lambda^2 = C_\lambda(0)$ can be obtained as

$$\sigma_\lambda^2 = \bar{\lambda}^2 b^2 R_v(0) = \bar{\lambda}^2 b^2 {\sigma_v}^2, \tag{3.11}$$

where ${\sigma_v}^2$ is the variance of $v(t)$, which is a zero mean WSS process. Using (3.7) and (3.11), the coefficient of variation, i.e., the contrast of firing rate, for the spike train could be found as

$$c_\lambda = \sigma_\lambda / \bar{\lambda} = b\sigma_v. \tag{3.12}$$

3.2.1.3 Poisson Encoding

The Poisson spike train at the output of the axon of the presynaptic neuron, denoted as $S(t)$, can be formulated as

$$S(t) \quad = \quad \sum_{i=1}^{N} \delta(t - t_i) = \frac{d}{dt} \sum_{i=1}^{N} u(t - t_i) = \frac{dN(t)}{dt},$$

where $N(t)$ models an inhomogeneous, i.e., non-constant rate, Poisson arrival process characterized with rate parameter $\lambda(t)$, which is the expected number of arrivals that occur per unit time. The mean of this Poisson arrival process is $\mathrm{E}[N(t)] = \int_0^t \lambda(\tau)\,\mathrm{d}\tau$. Hence, the average rate for spike generation at the presynaptic terminal is

$$\lambda(t) \quad = \quad \langle S(t) \rangle = \mathrm{E}[S(t)] = \frac{d\mathrm{E}[N(t)]}{dt}. \tag{3.13}$$

The ACF $R_S(t,s)$ belonging to the spike train, which is an inhomogeneous Poisson process with rate $\lambda(t)$, can be calculated using the ACF of the Poisson spike process, i.e., $R_N(t,s)$, as

$$\begin{aligned} R_S(t,s) \quad &= \quad \frac{\partial}{\partial t}\left[\frac{\partial R_N(t,s)}{\partial s}\right] = \begin{cases} \frac{\partial}{\partial t}\left[\lambda(s)\int_0^t \lambda(\eta)\,\mathrm{d}\eta + \lambda(s)\right] & \text{if } t > s \\ \frac{\partial}{\partial t}\left[\lambda(s)\int_0^t \lambda(\eta)\,\mathrm{d}\eta\right] & \text{if } t < s \end{cases} \\ &= \quad \bar{\lambda}^2 + \bar{\lambda}^2 b(v(t) + v(s)) + (\bar{\lambda} b)^2 v(t)v(s) + (\bar{\lambda} + \bar{\lambda} b v(s))\delta(t-s). \end{aligned} \tag{3.14}$$

However, $R_S(t,s)$ is not a WSS random process. Therefore, it does not make sense to talk about its power spectrum. Hence, we assume that the process is ergodic, and take its expectation. The expectation can be replaced by the limit of a time average. Then, we calculate the autocorrelation of time averaged process using the result (3.14), which we interpret as

$$R_{\bar{S}}(t,s) = \bar{\lambda}^2 + (\bar{\lambda}b)^2 R_v(t-s) + \bar{\lambda}\delta(t-s), \tag{3.15}$$

which is a WSS process, and we can rewrite (3.15) as

$$R_{\bar{S}}(\tau) = \bar{\lambda}^2 + (\bar{\lambda}b)^2 R_v(\tau) + \bar{\lambda}\delta(\tau), \tag{3.16}$$

of which we can talk about the power spectrum. The PSD of $R_{\bar{S}}(\tau)$, thus, can be found as

$$S_{\bar{S}}(f) = \bar{\lambda} + \left(\bar{\lambda}b\right)^2 |K(f)|^2 S_m(f) + \bar{\lambda}^2\delta(f). \tag{3.17}$$

Authors in [106] have shown that, the mean firing rate should be at least three times as large as the standard deviation of firing rate to ensure linear encoding, for which the probability that $\lambda(t)$ is negative is less than 0.01. Hence, the contrast (the coefficient of variation) of firing rate, i.e., the ratio of the standard deviation to the mean of the neural firing process, shoud be less than or equal to 1/3, i.e., $c_\lambda \leq 1/3$ condition should be satisfied. Using (3.12), it is clear that $\sigma_\lambda = \bar{\lambda}b\sigma_v$ as the rate, i.e., $\lambda(t)$ is linearly dependent on $v(t)$, which is a zero mean linear filtered WSS random process. Therefore, $\sigma_v \leq 1/(3b)$ is the required condition for linear encoding. Due to the linear relation between $m(t)$ and $v(t)$, we infer that

$$\sigma_v^2 \;=\; \int S_m(f) \frac{R^2}{1+(2\pi fRC)^2}\,\mathrm{d}f \leq \left(\frac{1}{3b}\right)^2. \tag{3.18}$$

Hence, the variance of the presynaptic stimulus should satisfy the constraint given in (3.18) to ensure linear encoding.

3.2.2 Vesicle Release Model

We use a pool-based synapse model for each presynaptic neuron to study vesicle depletion and recovery. The vesicle release process depends primarily on the vesicle pool size and postsynaptic receptor saturation [110]. In chemical synapses, some vesicles are docked at the membrane waiting to release their content upon the arrival of a trigger signal. Others are stored in the membrane pool, just above the docked vesicles, being more distant to the cell

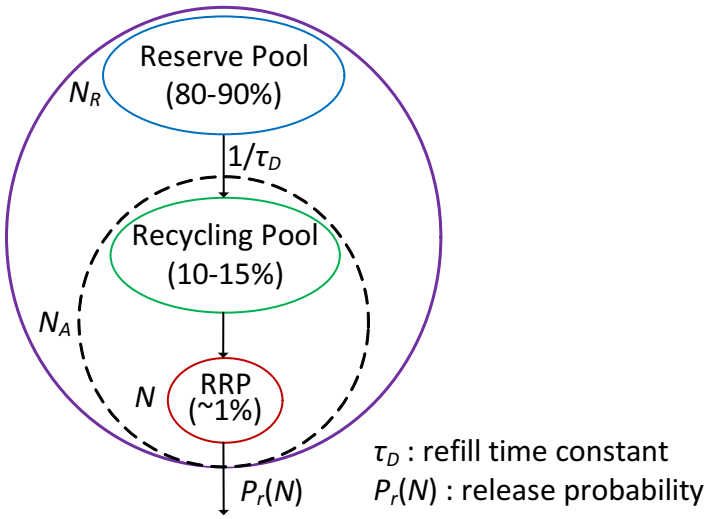

Figure 3.2: The pool-based synapse model.

membrane. Vesicles in the neural terminal can be grouped into three sub-pools according to their relative mobilities: the readily releasable pool (RRP), the recycling pool and the reserve pool, which differ on the basis of the relative mobility of vesicles in each pool [142]. It takes the longest to mobilize the vesicles in the reserve pool while in RRP, vesicles are ready to mobilize upon arrival of a spike.

Let the pool sizes, i.e., the number of vesicles in pools, be denoted as N, $N_A - N$, and N_R, for RRP, the recycling pool and the reserve pool, respectively. N_A is the total vesicle size in the recycling pool and RRP. The recycling pool is close to the cell membrane, and tends to be cycled at moderate stimulation, so that the rate of vesicle release is the same as, or lower than, the rate of vesicle formation. Once the RRP and the recycling pool are exhausted, the reserve pool is mobilized [142]. A pool-based synapse model is illustrated in Fig. 3.2.

In the pool model shown in Fig. 3.2, $p_r(N)$ is the release probability per stimulus, and the available pool is considered to be exhausted with a rate $1/\tau_D$. Therefore, the reserve pool should recover the available, i.e., docked, pool with a time constant τ_D [110].

The release of a single vesicle upon arrival of a spike is governed by a Poisson process with non-constant presynaptic firing rate $\lambda(t)$. Then, the fusion rate, i.e., the rate at which the vesicles are expelled from the cell through exocytosis [110], for a single vesicle is determined

as

$$\alpha_{v_k} = \int_0^{\Delta t_k} \lambda(t)\, \mathrm{d}t, \tag{3.19}$$

where the integration is evaluated over the duration of the presynaptic pulse [110]. In the calculation of α_{v_k}, we divide $\lambda(t)$ into windows of equal durations. If we choose sufficiently large number of windows of equal duration, there exists at most one spike at each window. Discretizing the fusion rate, as soon as the spike is within a specified window and the window size is small enough, the fusion rate is the same independent of at which time point the spike is. This makes sense because the fusion rate stays constant for a sufficiently small interval. This is also a realistic assumption since we need to discretize the time axis in our simulations. In (3.19), subscript k denotes the window index, and the integration on the right hand side is from the start of the presynaptic stimulus taken as the time origin until the end of k^{th} time window of the stimulus denoted as Δt_k.

Additional to presynaptic firing rate, the level of activation of inhibitory auto-receptors, i.e., the receptors located in the presynaptic membrane that serve as a part of a feedback loop in signal transduction by inhibiting further release or synthesis of the neurotransmitters, also affect the fusion rate [110]. Furthermore, the vesicle release probability is dependent on a power of the spike-triggered Ca^{2+} influx. Therefore, the vesicle fusion rate can be replaced with $\alpha_{v_k} \rightarrow \frac{\alpha_{v_k}}{(1+C_x x(t))^q}$, where the constant C_x controls the strength of the inhibitory effect, and parameter q specifies Ca^{2+} cooperativity of vesicle release [110]. However, to simplify our analysis, we ignore the effect of inhibitory auto-receptors.

Using the vesicle fusion rate defined in (3.19), the single-vesicle release probability is $p_{v_k} = 1 - \exp(-\alpha_{v_k})$. The release probability per stimulus is the complement of the failure probability, which is the probability that no vesicle is released during the window of interest, given by

$$p_r(N_k) = 1 - \exp(-\alpha_{v_k} N_k), \tag{3.20}$$

where N_k is the number of vesicles available for release at the window of interest and the failure probability is $1 - p_r(N_k) = \exp(-\alpha_{v_k} N_k)$ [42].

For the more realistic case where each release site is permitted to have its own release probability, the probability that no vesicles fuses on the k^{th} interval can be calculated as $\prod_{j=1}^{N_k}(1 - p_{v_{jk}})$,

where $p_{v_{jk}} = 1 - \exp\left(-\alpha_{v_{jk}}\right)$, as explicitly pointed out in [43]. Here $p_{v_{jk}}$ and $\alpha_{v_{jk}}$ are the probability that the j^{th} vesicle fuses on during k^{th} interval, and its fusion rate, respectively, and N_k is the number of vesicles in the RRP at the k^{th} window.

To find the mutual release probability, i.e., $p^*_{v_k}$, that gives the same result as the calculation with different release probabilities per vesicle, we set $\prod_{j=1}^{N_k}(1-p_{v_{jk}}) = (1-p^*_{v_k})^{N_k}$.

$$p^*_{v_k} = \frac{1}{N_k}\sum_{j=1}^{N_k} p_{v_{jk}}. \tag{3.21}$$

$p^*_{v_k}$ is the average release probability per vesicle for the pool of vesicles. Using the $p_{v_{jk}}$ expression and (3.21), the mutual fusion rate, i.e., $\alpha^*_{v_k}$, can be obtained as

$$\alpha^*_{v_k} = \ln(N_k) - \ln\left(\sum_{j=1}^{N_k}\exp\left(-\alpha_{v_{jk}}\right)\right). \tag{3.22}$$

Equation (3.22) gives a compact expression when each vesicle has a distinct fusion rate depending on the distinct release sites on presynaptic neuron, regional differences in the strength of inhibitory effects, Ca^{2+} concentration levels, and presynaptic auto-receptors.

There is some previous work concentrating on univesicular release mechanism [159, 47]. The all-or-none synaptic transmission that arises from the saturation of postsynaptic receptors by neurotransmitter content of a single vesicle is suggested in [163], implying the same postsynaptic response regardless of the number of vesicles released. In [106], it is assumed that each action potential yields at most one vesicle release and the vesicle release process is modeled by a Z-channel because without stimuli the probability of spontaneously generated vesicles is very low, and hence, ignored. Additional to single vesicle release case, multivesicular release is studied in [110]. Moreover, it is found that the temporal correlation between stochastic responses to a repetitive train of stimuli behaves differently depending on whether multiple releases are allowed.

In univesicular release case, the probability of release is given by p_{v_k}. This is equivalent to saying that vesicle release at k^{th} spike arrival is bernoulli distributed with probability p_{v_k}. Hence, expected number of vesicles released at k^{th} spike is equivalent to p_{v_k}. In multivesicular release, on the other hand, each vesicle has an independent (not necessarily identical) release probability, i.e, $p_{v_{jk}}$. Therefore, in multivesicular case, each vesicle also has Z-channel model with an average release probability p_{v_k} as calculated in (3.21). The model for multivesicular release can be represented by a non-binary Z-channel. Binary symbols of the SISO Z-channel

are scaled by N_k, which is the total number of available vesicles in the RRP to be released upon spike generation at the presynaptic terminal. This assumption is valid since the vesicle release rate is scaled by N_k in multivesicular release case. Thus, expected number of released vesicles in multivesicular case is $p_{v_k}N_k$.

In this section, we study the multivesicular release case. We model the number of vesicles released in response to an action potential exerted at k^{th} window with a random variable denoted as W_k. W_k is determined by a binomial distribution with parameters p_{v_k} and N_k. The average number of vesicles released is then given by $\langle W_k \rangle = p_{v_k}N_k$ for fixed N_k.

$$P(W_k = i) = \binom{N_k}{i} (p_{v_k})^i (1 - p_{v_k})^{N_k - i}. \tag{3.23}$$

Assuming that each vesicle has the same probability of release, i.e., p_{v_k}, upon a stimulus, the expected number of vesicles released on window k can be calculated as

$$\langle W_k \rangle = \sum_{i=0}^{N_k} iP(W_k = i) = p_{v_k}N_k. \tag{3.24}$$

The release probability, i.e., the probability that at least one vesicle is released, on window k is

$$P_k \quad = \quad 1 - (1 - p_{v_k})^{N_k}. \tag{3.25}$$

The release probability on the next window, i.e., P_{k+1}, can be iteratively calculated using $p_{v_{k+1}}$ and N_{k+1} by applying the relation

$$N_{k+1} = N_k - \langle W_k \rangle + N_{k+1}^{rf} = N_k(1 - P_k)^{\frac{1}{N_k}} + N_{k+1}^{rf} \tag{3.26}$$

into (3.25), where P_k is the measured release probability for the previous, i.e., k^{th} time window, $\langle W_k \rangle$ is the average number of vesicles released on k^{th} window and N_{k+1}^{rf} is the number of vacancies in the releasable pool refilled by the reserve pool during the time difference between consecutive windows, i.e., one inter-spike interval (ISI), which can be calculated as $N_{k+1}^{rf} = N_R P_{k+1}^{rf}$. N_R and P_{k+1}^{rf} are the reserve pool size and the vesicle refill probability during one ISI, respectively. According to the derivation in [110], the reserve pool fills the vacancies with a time constant τ_D, which is the refill time constant. Therefore, it takes τ_D time for the system to reach $1 - 1/e$ of its final value, which is $P_k^{rf*} = 1$. Hence, provided the reserve pool size remains unchanged, the refill probability is

$$P_k^{rf} = 1 - \exp(-\Delta t_k / \tau_D), \tag{3.27}$$

where Δt_k is the time interval between the start of the stimulus until the end of k^{th} window and τ_D is the refill time constant which is inverse of vacancy refill rate [110].

3.2.3 Postsynaptic Response with Variability in Vesicle Release

The postsynaptic response function to the release of a single vesicle is denoted by $h(t)$. Output of this response filter is subject to additive white gaussian noise denoted as $n(t)$ and the channel output is the postsynaptic voltage, i.e., $Z(t)$.

We model the postsynaptic response by a function $h(t)$, which corresponds to the EPSP waveform of a fast, voltage-independent AMPA-like synapse modeled as an alpha function [138],

$$h(t) = h_p \frac{t}{t_p} \exp\left(1 - \frac{t}{t_p}\right), \tag{3.28}$$

where h_p is the peak EPSP magnitude and t_p is the corresponding time-to-peak. The Fourier transform of $h(t)$, denoted as $H(f)$ can be calculated as $H(f) = h_p \exp(1)/t_p \left(\frac{1}{t_p} + j2\pi f\right)^2$, which is utilized in the rate region analysis for synaptic communication channel in Section 3.3.2.

We assume that the postsynaptic responses to a sequence of vesicle releases add linearly. We incorporate synaptic variability by multiplying the response $h(t)$ by a random variable q drawn from a probability distribution $P(q)$, which can be measured empirically. q models the trial-to-trial variability in the amplitude of the postsynaptic responses observed for central neurons. In some cases, the variance in the size of EPSP is as large as the mean. Despite being possibly biased due the inability of measuring very small synaptic events, the experimentally observed amplitude distributions are usually skewed to high amplitudes and can be modeled by a Gamma distribution [25]. Here, we model $P(q)$ by a gamma distribution. A gamma-distributed random variable Q with shape α and rate β is denoted by $Q \sim \Gamma(\alpha, \beta)$. The probability density function (pdf) of Q is

$$\mathrm{f}(q; \alpha, \beta) = \beta^{\alpha} \frac{1}{\Gamma(\alpha)} q^{\alpha-1} \exp(-\beta q) \text{ for } q \geq 0 \text{ and } \alpha, \beta > 0, \tag{3.29}$$

where α is the order of the distribution. If α is a positive integer, then $\Gamma(\alpha) = (\alpha - 1)!$.

The mean $\bar{q}$, standard deviation σ_q and the coefficient of variation of the gamma distribution are defined as $\bar{q} = \alpha/\beta$, $\sigma_q = \alpha/\beta^2$ and $c_q = 1/\beta$, respectively. In this section, we choose $\alpha = \beta = 0.6^{-1}$, consistent with the postsynaptic quantal variation, i.e., the variation in the transmitter content among vesicles as determined by vesicle volume, model proposed in [106].

Four parameters are thought to be particularly important in determining trial-to-trial EPSC variability: the time course and probability of quantal release, i.e., the amount of neurotrans-

mitter released following neural stimulation,, the number of release sites, where the secretion of a quantum of neurotransmitter occurs, and the quantal size, which is the postsynaptic response to the release of neurotransmitter from a single vesicle [147]. Although in [147], authors claim that multivesicular release can cause postsynaptic saturation, i.e., full receptor occupancy, in this section, we assume that receptors at the postsynaptic terminal are not saturated by multivesicular release assuming the available number of postsynaptic receptors is high enough.

The postsynaptic membrane voltage is

$$Z(t) = \sum_{l=1}^{M} \sum_{i} q_i^l W_i^l h^l(t - t_i) + n(t), \tag{3.30}$$

where q is the random EPSP amplitude and W is a binomial variable representing the spike-conditioned vesicle release process. Superscript l refers to the l^{th} synaptic connection. If the synapses are distributed at different electrotonic locations, i.e., positions along the excitable cell with unequal electrical state in the absence of repeated action potentials, on the postsynaptic neuron, the corresponding EPSP waveforms $h^l(t)$ are different [106]. In this chapter, to simplify the analysis, we assume that synaptic connections are at the same electrotonic location, and hence, they are identical and have the same EPSP characteristics.

Assuming a point-to-point synaptic connection between a pre- and postsynaptic neuron terminal pair, the postsynaptic membrane voltage can be calculated as

$$Z(t) = \sum_{i} q_i W_i h(t - t_i) + n(t) = \left[h(t) * \sum_{i} q_i W_i \delta(t - t_i) \right] + n(t), \tag{3.31}$$

where W_i is a binomial random variable representing the spike-conditioned vesicle release process to a spike generated at t_i^{th} time instant. If the spike generated at time t_i does not lead to vesicle release at input neurons, $W_i = 0$. The model for the SISO neuro-spike channel model is given in Fig. 3.3. In Section 3.3, we extend the single-input synaptic model to multi terminal input case, and investigate its rate region.

3.3 Multiple-Access Neuron Channel

We extend the SISO channel model to MISO, i.e., multiple-access, channel model. In this model, we assume that presynaptic terminals are identical, i.e., the axons share the LNP model features and spike generation mechanisms, and the EPSP characteristics are the same.

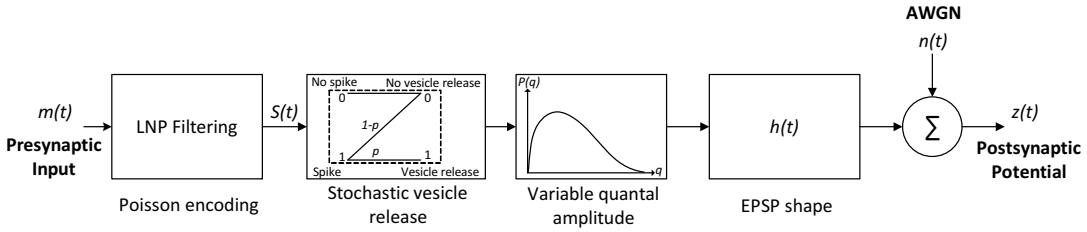

Figure 3.3: Single-input single-output neuro-spike channel model between presynaptic and postsynaptic neuron terminals.

A conceptual model for the multiple-access synaptic communication channel and the main blocks of the multiuser neuronal channel are illustrated in Fig. 3.4 and 3.5, respectively.

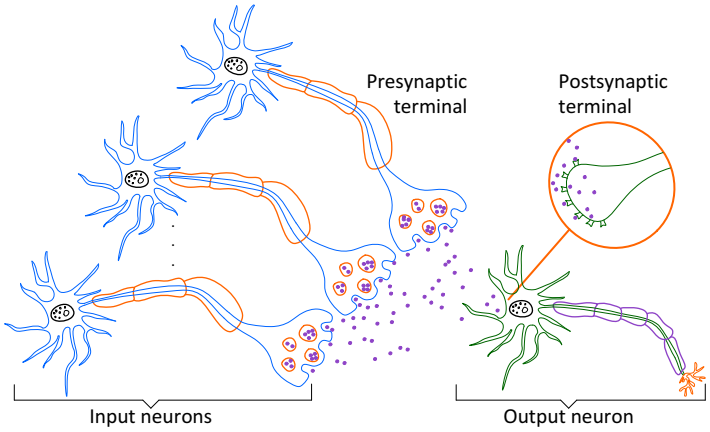

Figure 3.4: Multiple-access synaptic communication channel model.

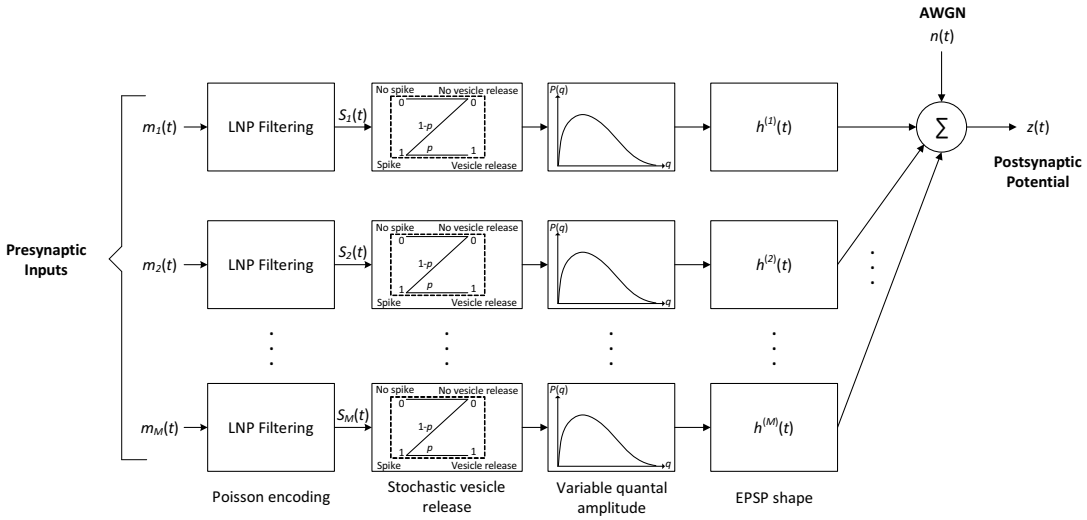

Figure 3.5: Multiple-access channel model between presynaptic and postsynaptic neuron terminals.

In Fig. 3.5, the hypothetical model for multiple-access channels among neuron terminals is illustrated. Each presynaptic terminal generates its own stochastic impulse train. Upon arrival of the spike train, the presynaptic terminals release vesicles with an average probability of p independent of each other. Therefore, the vesicle release instances are determined by each presynaptic terminal's own spike characteristics. The released vesicles are directed to a common postsynaptic terminal through distinct synapses with separate input terminals. In this chapter, we assume that the synaptic impulse responses, i.e., the EPSP characteristics, are identical in shape. However, each synaptic channel is characterized by a random amplitude determined by a Gamma distributed variable q. Hence, the synaptic channels can be independently characterized. At the end of the transmission process, each presynaptic terminal delivers vesicles to the same postsynaptic terminal through a succession of stochastic processes. Hence, the voltage seen at the postsynaptic terminal is stochastically determined by the random spike generation and vesicle release processes at each input terminal, and the channel variabilities at each synaptic channel. In this section, we analyze the rate region for multiple-access synaptic communication channel.

3.3.1 Modulated Input Power Spectral Density

Using the approximation for the PSD of the spike train in (3.17), we have

$$S_s(f) \approx \bar{\lambda} + \left(\bar{\lambda} b\right)^2 |K(f)|^2 S_m(f) + \bar{\lambda}^2 \delta(f) \tag{3.32}$$

$$\sigma_\lambda^2 = \int \left[\left(\bar{\lambda} b\right)^2 |K(f)|^2 S_m(f) + \bar{\lambda}^2 \delta(f) \right] \mathrm{d}f. \tag{3.33}$$

Similar to spike generation process, the vesicle release process is also Poisson with rate $p_{v_k} N_k \lambda(t)$. Therefore, the PSD for vesicle release process at k^{th} window, i.e., $S_w^{(k)}$ can be obtained as

$$S_w^{(k)}(f) \quad = \quad (p_{v_k} N_k)^2 \left[\left(\bar{\lambda} b\right)^2 |K(f)|^2 S_m(f) + \bar{\lambda}^2 \delta(f) \right] + (p_{v_k} N_k)\, \bar{\lambda}. \tag{3.34}$$

Next, by considering the effect of channel variability, represented by the random variable q, we define $S_l^{(k)}(f)$ as the PSD of the modulated input l at k^{th} window of interest. Here, modulated input is the presynaptic neuron stimulus passing through LNP filter to be Poisson encoded, and converted into binomial vesicle release form and then scaled with random quantal amplitude to be filtered with postsynaptic response function. Modulated input is a function of frequency and random due to the stochastic variables denoting vesicle release and synaptic

filter amplitude.

$$S_l^{(k)}(f) = \bar{q}^2(p_{v_k}N_k)^2\left[(\bar{\lambda_l}b)^2|K(f)|^2S_{m_l}(f)+(\bar{\lambda_l})^2\delta(f)\right]+(\bar{q}^2+\sigma_q^2)(p_{v_k}N_k)\bar{\lambda_l} \quad (3.35)$$

following from (3.34), the linear encoding restriction and the approximation of $Var(qp\lambda_l(t))$ as

$$\begin{aligned} Var(qp\lambda_l(t)) &= \mathrm{E}\left[q^2(p_{v_k}N_k)^2\lambda_l^2(t)\right]-\bar{q}^2(p_{v_k}N_k)^2\bar{\lambda}_l^2 \\ &= \left(\bar{q}^2+\sigma_q^2\right)(p_{v_k}N_k)^2\sigma_{\lambda_l}^2+\left(\bar{q}^2+\sigma_q^2\right)(p_{v_k}N_k)^2\bar{\lambda}_l^2-\bar{q}^2(p_{v_k}N_k)^2\bar{\lambda}_l^2 \\ &\approx \sigma_q^2(p_{v_k}N_k)^2\bar{\lambda}_l^2+\bar{q}^2(p_{v_k}N_k)^2\sigma_{\lambda_l}^2. \end{aligned} \quad (3.36)$$

Approximation in (3.36) follows from the fact that the mean firing rate is at least three times larger than the standard deviation of firing rate to ensure linear encoding [106]. Hence, $c_\lambda = \sigma_\lambda/\bar{\lambda} \leq 1/3$ should be satisfied, and the $\sigma_q^2(p_{v_k}N_k)^2\sigma_{\lambda_l}^2$ term in (3.36) is negligible.

From (3.36), variability of q only affects the frequency independent part of the modulated input, i.e., the term $(p_{v_k}N_k)\bar{\lambda}_l$ in (3.34), due to linear encoding condition. As a result of linear encoding assumption, the variation at the frequency dependent part is ignored.

For single synapse channel, the power spectrum of $z(t)$ can be calculated as in [106], i.e.,

$$S_Z(f) = |H^{(l)}(f)|^2S_l^{(k)}(f)+S_n(f). \quad (3.37)$$

Extending this model to multiple input case for M number of presynaptic neurons, we obtain

$$S_Z(f) = \sum_{l=1}^{M}|H^{(l)}(f)|^2S_l^{(k)}(f)+S_n(f). \quad (3.38)$$

3.3.2 Multiuser Channel Rate Regions

The multiaccess coding theorem asserts that if source l, $1 \leq l \leq M(l \geq 2)$ has rate R_l and is constrained to a PSD S_l over the given bandwidth B, then, arbitrarily small error probability can be achieved for all sources if for each subset $A \subseteq \{1,2,\ldots,M\}$ [58],

$$\sum_{l\in A}R_l < \int_{-B/2}^{B/2}\log\left(1+\frac{\sum_{l\in A}S_l|H^{(l)}(f)|^2}{N_0}\right)\mathrm{d}f, \quad (3.39)$$

where $H^{(l)}(f)$ is the Fourier transform of $h^{(l)}(t)$. The quantity on the right hand side of (3.39) is the conditional average mutual information per unit time, $I(A)$, between the inputs in A and

Table 3.1: Analysis parameters.

Parameter	**Symbol**	**Value / Range**
Soma time constant	$\tau = RC$	20 ms
AWGN bandwidth	B_n	100 Hz
AWGN standard deviation	σ_n	0.1 mV
Peak magnitude of the EPSP waveform	h_p	1 mV
Time at which EPSP reaches its peak	t_p	0.5 ms
Firing rate control parameter	a	$1/0.029^\circ$
Voltage at half the maximum firing rate	$v_{1/2}$	0.036°
The vesicle release probability	p_{v_k}	0.4
Average firing rate	α_{v_k}	$10\,spikes/\mathrm{s}$
Available pool size	N_A	$3-10$
Reserve pool size	N_R	60
Vesicle refill time constant	τ_D	2 s
Quantal amplitude CV	c_q	0.6
Mean of quantal amplitude	$\bar{q}$	1

the output, conditional on the inputs not in A; this assumes that the inputs are independent stationary white Gaussian noise processes over the bandwidth B. From multiaccess coding theorem,

$$\begin{aligned}\sum_{l\in A} R_l \quad &< \quad \max_{S_l^{(k)}(f)} \int_{-B/2}^{B/2} \log\left(1+\frac{\sum\limits_{l\in A}\left|H^{(l)}(f)\right|^2 S_l^{(k)}(f)}{N_0}\right)\mathrm{d}f \\ &\text{s.t.} \sum_{l\in A}\int S_l^{(k)}(f)\,\mathrm{d}f \le \sum_{l\in A} P_l^{(k)}, \end{aligned} \tag{3.40}$$

for multiple input synaptic communication channel, where $P_l^{(k)}$ is the power constraint of the l^{th} presynaptic neuron over the bandwidth B, and the input subset is denoted by $A \subseteq \{1,\ldots,M\}$.

3.4 Performance Evaluation

In this section, we evaluate the analytical expressions obtained in Sections 3.2-3.3. The parameters for numerical evaluations, as tabulated in Table 3.1, are obtained from [42], [106], [41].

Initially, we generate spike trains using the LNP model discussed in Section 3.2.1. The linearized LNP model with $\lambda_{\max} = 36.03$ Hz is illustrated in Fig. 3.6(a). We apply a normal distributed stimulus to each presynaptic neuron terminal. The outputs of the LNP filters, i.e., the generated spike trains based on the firing rates are illustrated in Fig. 3.6(b).

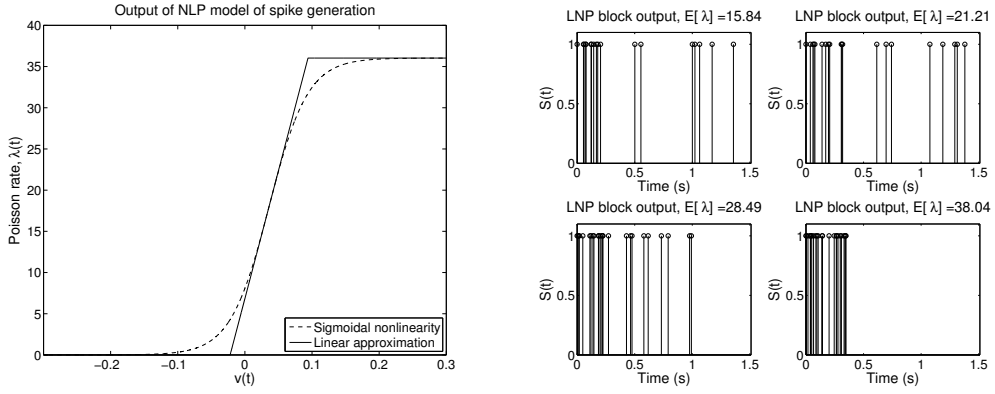

(a) (b)

Figure 3.6: (a) Linear approximation for the rate of the Poisson arrival process, and (b) the spike train at the output of the LNP filter under varying firing rates.

Spike trains, i.e, action potentials, are converted into the form of vesicle release. Rate of the spike trains determines the triggering level for vesicle release mechanism. During each repetition of the train, the RRP decreases by 1 each time a vesicle is released. The release probability at a synapse is directly correlated with the size of its readily releasable vesicle pool, which is N. In [42], authors choose $N_A = 3-10$ in their simulations. For the vesicle refill time constant they use a value of $\tau_D = 2$ s, which agrees with the time of recovery of the RRP measurements in hippocampal slice experiments. Therefore, we choose the refill rate and reserve pool size based on these experiments. The simulation result for the dynamic vesicle release process, which is initiated with the spike train given in Fig. 3.6(b) with $\mathrm{E}[\lambda] = 15.84$, is depicted in Fig. 3.7.

Passing through the synaptic channel, the released molecules are modulated. Modulation is due to the variability in the number of available receptors on the surface of the postsynaptic neuron. Furthermore, the synaptic channel behaves like an alpha-shaped filter, the input and the output of which are the modulated input and the postsynaptic potential observed at the destination neuron, respectively. A segment of a typical EPSP waveform is shown in Fig. 3.8.

We observe the vesicle release probability during a spike train to characterize how the average rate per spike varies. We analyze the fusion rate by dividing the spike train into 100 windows of equal duration. As fusion rate, i.e, α_v, is solely dependent on the integration duration of $\lambda(t)$, it increases during train as seen in Fig. 3.9(a). Furthermore, the average vesicle release probability, i.e., p_v, also increases with α_v, which agrees with the results obtained in [43]. Therefore, average number of vesicles released increases during train, which is illustrated in

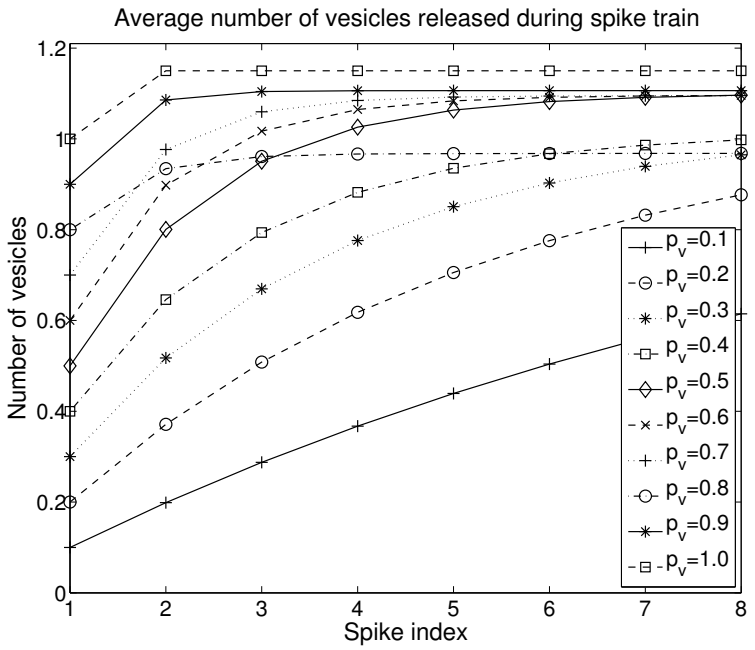

Figure 3.7: Random vesicle release process in the course of Poisson distributed spike train.

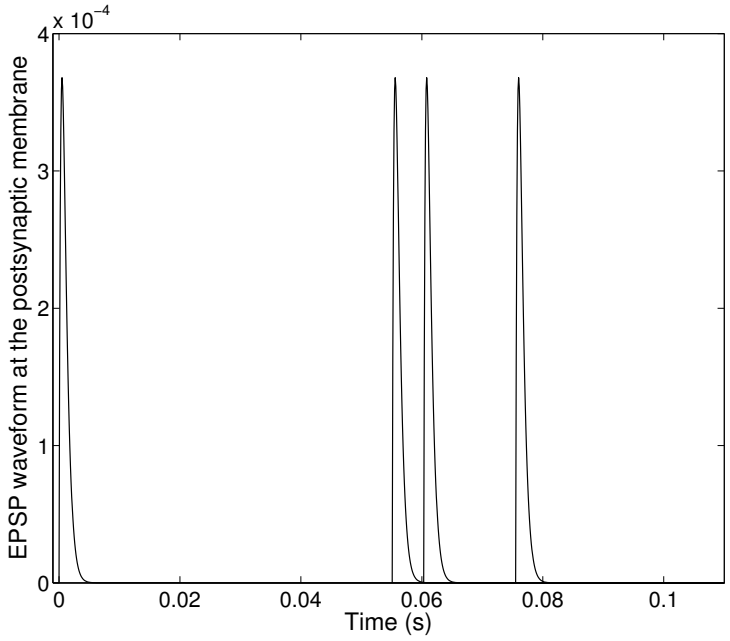

Figure 3.8: A segment of the EPSP waveform at the postsynaptic membrane, $E[\lambda] = 15.84$.

Fig. 3.9(b). Hence, the information rate is also augmented with impulse train duration as shown in Fig. 3.9(c).

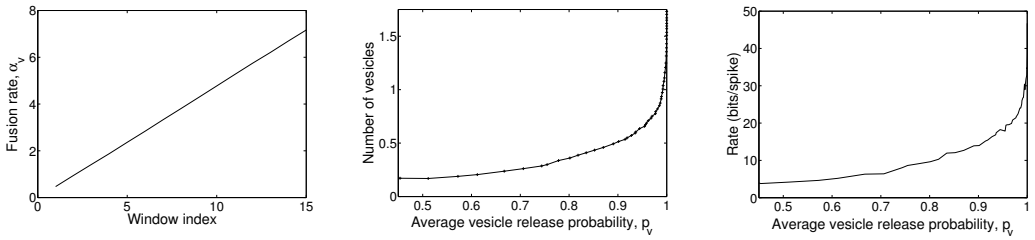

(a) (b) (c)

Figure 3.9: Time dependent neuronal (a) vesicle fusion rate, (b) vesicle release process, and (c) average rate during spike train.

As the presynaptic firing rate enhances, the information bits delivered per spike increases. Making realistic assumptions on the rate of spike trains, authors in [42] come across the typical spike rate of neurons, which is 1 spike per 100 ms. Therefore, we limit $\lambda(t)$ to be around this typical value in our simulations. Using (3.40), we can obtain the rate region for SISO neuro-spike communication channel. The rate region for varying RRP size, i.e., N_A, and reserve pool size, i.e, N_R, and vesicle refill time constant, i.e., τ_D, is pointed out in Fig. 3.10. As N_A increases the available number of vesicles ready for release gets higher. For large N_R values since the refill rate gets larger, size of the available pool gets larger during the stimulus, causing improved rate values at the postsynaptic terminal. As τ_D increases, as more time is required to fill the docked pool, the docked pool depletes faster, and the rate drops.

Although in [56], authors calculate that the maximum amount of information that can be transmitted by an ideal synapse is approximately equal to 1.13 bits per spike, their analysis is based on unitary vesicle release. In this chapter, as we allow multivesicular release, higher information rates become possible. We hypothetically show that rate is affected by firing of presynaptic terminal, vesicle pool sizes and refill process, vesicle fusion rate and postsynaptic receptors. Furthermore, in this study, the saturation of postsynaptic receptors, which, in fact, adversely influences the vesicle release process, is ignored. The model could be extended to observe the feedback relationship between the postsynaptic receptors and vesicle release process.

Extension of the model to multiple-access neuro-spike channel is the next step. Using (3.40), we can obtain the rate upper bounds for any user subset $A \subseteq \{1,\ldots,M\}$. Depending on whether the set of users has correlation among them or not, in this section, we investigate the rate regions.

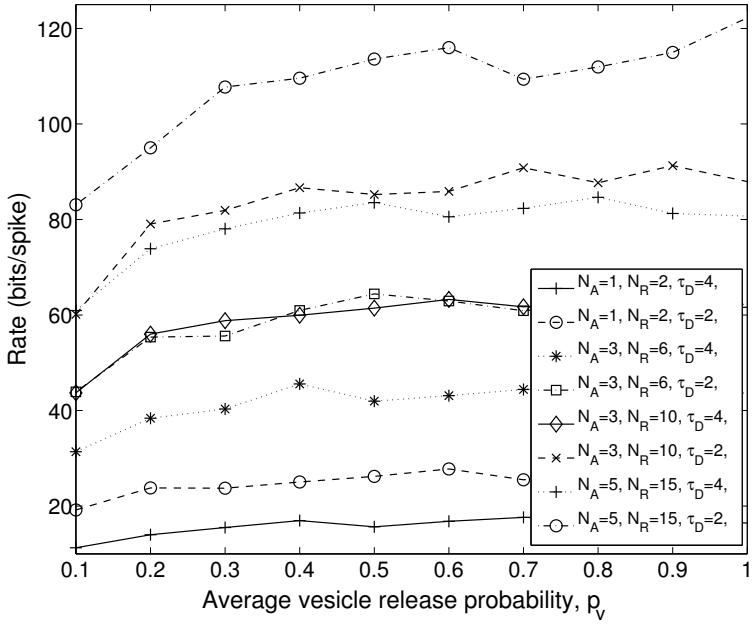

Figure 3.10: The achievable rate region for SISO synaptic communication channel under variable vesicle pool conditions.

Assume that M neurons are fired with an input vector $\underline{m}(t) = \{m_1(t), m_2(t), ..., m_M(t)\}$, and neurons release their vesicles through the channel, i.e., the synapse. We investigate two different cases regarding the dependence of the individual presynaptic neurons.

3.4.1 Independent Firing of Neurons

Let $S_l \sim Pois(\lambda_l)$, for $l \in \{1,\ldots,M\}$ be an inhomogeneous and independent Poisson process with rate $\lambda_l(t)$ corresponding to the model of spike generation at l^{th} input neuron. The probability mass function (pmf) of S_l is given by

$$\mathrm{f}(k;\lambda_l(t)) = P(S_l = k) = \frac{\lambda_l^k(t)}{k!}\exp\left(-\lambda_l(t)\right),\ l \in \{1,\ldots,M\},\ k \in \mathbb{Z}_{\geq 0}. \tag{3.41}$$

We define a new random process S, denoting the sum of individual independently but not necessarily identically distributed random processes S_l, i.e., S$=\sum_{l=1}^{M} S_l$. The pmf of S is

$$P(S) = P(S_1 = k_1, S_2 = k_2, \ldots, S_M = k_M) = \prod_{l=1}^{M}\frac{\lambda_l^{k_l}}{k_l!}\exp\left(-\lambda_l\right) = \exp\left(-\sum_{l=1}^{M}\lambda_l\right)\prod_{l=1}^{M}\frac{\lambda_l^{k_l}}{k_l!} \tag{3.42}$$

In independent firing of neurons, l^{th} neuron releases vesicles with rate $\lambda_l(t)$ independent of other neurons. Therefore, at the l^{th} input neuron, the vesicle release probability is determined

by a Poisson distribution with a rate parameter $\lambda_l(t)p$, where $p = p_{v_k}N_k$ at k^{th} window of interest. Let X_l be the random process modeling the vesicle release at l^{th} input neuron. Hence, $X_l \sim Pois(\lambda_l(t)p)$, for $l \in \{1,\ldots,M\}$ independently vesicle releasing input neurons.

The vesicles released by all input neurons are accumulated at the synaptic channel. Therefore, the total vesicle release to the synaptic channel can be determined by the process $X = \sum_{l=1}^{M} X_l$, the rate of which is $\sum_{l=1}^{M}\lambda_l(t)p = p\sum_{l=1}^{M}\lambda_l(t) = p\lambda(t)$, where $\lambda(t) = \sum_{l=1}^{M}\lambda_l(t)$. Therefore, the vesicle release process can be modeled by a Poisson distribution, $X \sim Pois\left(p\sum_{i=1}^{M}\lambda_l(t)\right)$.

Under independently firing of presynaptic neurons, Fig. 3.4.2 illustrates the rate region for a subset $A \subseteq \{1,\ldots,M\}$ of $M = 35$ user synaptic multiple-access channel determined by (3.40). As shown in Fig. 3.4.2, the total rate does not scale with the same order as the raise in the number of users as the multiple-access synaptic communication channel experiences interference.

3.4.2 Correlated Firing of Neurons

Let $T_l \sim Pois(\theta_l)$, for $l \in \{1,\ldots,M\}$ are independent random variables. Consider the random variables $S_l = T_l + T_0$, $\forall l \in \{1,\ldots,M\}$. Then, $\{S_1, S_2, \ldots, S_M\}$ jointly follow a multivariate Poisson distribution [29]. The joint pmf $P(S) = P(S_1 = k_1, S_2 = k_2, \ldots, S_M = k_M)$ is given by

$$P(S) \;=\; \exp\left(-\sum_{l=1}^{M}\theta_l\right)\prod_{l=1}^{M}\frac{\theta_l^{k_l}}{k_l!}\sum_{l=0}^{k_{\min}}\prod_{j=1}^{M}\binom{k_j}{l}l!\left(\theta_0/\prod_{l=1}^{M}\theta_l\right)^{l}, \tag{3.43}$$

where $k_{\min} = \min(k_1, k_2, \ldots, k_M)$. Marginally, each presynaptic input S_l follows a Poisson distribution with rate parameter $\theta_l + \theta_0$. Therefore, $\mathrm{E}[S_l] = \theta_l + \theta_0$, and $Var[S_l] = \theta_l + \theta_0$. The correlation coefficient between S_i and S_j, i.e., ρ_{ij}, can be calculated as

$$\rho_{ij} = corr(S_i, S_j) = \frac{\mathrm{E}\left[(S_i - \mathrm{E}[S_i])(S_j - \mathrm{E}[S_j])\right]}{\sigma_i\sigma_j} = \begin{cases} \frac{\theta_0}{\sqrt{(\theta_i+\theta_0)}\sqrt{(\theta_j+\theta_0)}} & \text{if } i \neq j \\ 1 & \text{if } i = j \end{cases}. \tag{3.44}$$

Hence, given the rate parameters (θ_i) of uncorrelated distributions (T_i), and assuming the correlation coefficients (ρ_{ij}) are experimentally known, θ_0 can be determined as

$$\theta_0 = \frac{(\theta_i+\theta_j)\rho_{ij} + \sqrt{(\theta_i+\theta_j)^2\rho_{ij}^2 + 4(1-\rho_{ij})\theta_i\theta_j\rho_{ij}}}{2(1-\rho_{ij})}. \tag{3.45}$$

θ_0 is the covariance between all the pairs of random variables. In this section, we assume common covariance for all pairs, which is a simple yet powerful conjecture enough to demonstrate

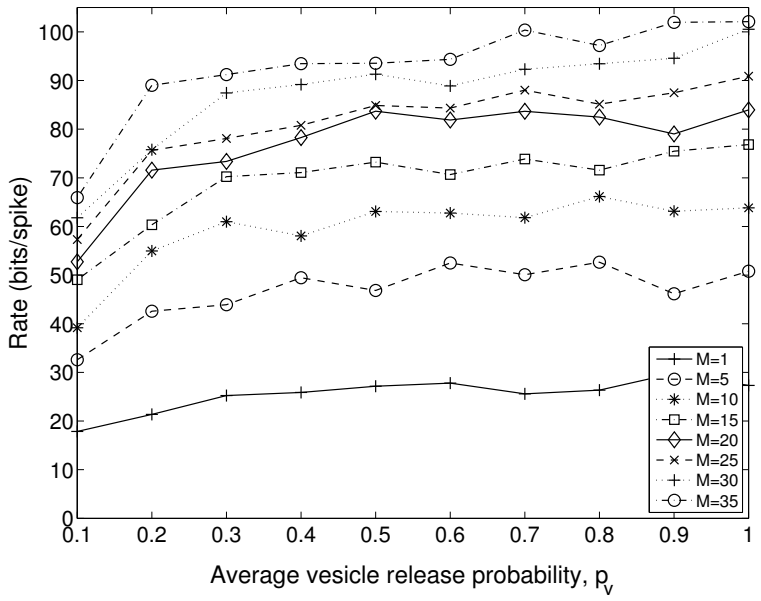

Figure 3.11: The rate region for multiple-access synaptic communication channel under independent firing of presynaptic neurons for a subset $A \subseteq \{1,\ldots,M\}$ of $M = 35$ presynaptic terminals

the improvement in additive rate compared to the case where presynaptic inputs are uncorrelated.

In correlated firing of neurons, l^{th} neuron releases vesicles with rate $\lambda_l(t) = \theta_l + \theta_0$, where θ_0 denotes the common correlation parameter between any two neurons. At the l^{th} input neuron, the vesicle release probability is determined by a Poisson distribution with a rate parameter $(\theta_l + \theta_0)\, p$, where $p = p_{v_k} N_k$. Let X_l be the random process modeling the vesicle release at l^{th} input neuron. Hence, in correlated firing of presynaptic neurons, the vesicle release process at each presynaptic terminal can be modeled by $X_l \sim Pois\,((\theta_l + \theta_0)\, p)$, for $l \in \{1,\ldots,M\}$.

The vesicles released by all input neurons are accumulated at the synaptic channel. Therefore, the total vesicle release to the synaptic channel can be determined by the process $X = \sum_{l=1}^{M} X_l = p\sum_{l=1}^{M} T_l + pMT_0$, the rate of which is $\sum_{l=1}^{M} (\theta_l + \theta_0)\, p = p\sum_{l=1}^{M} (\theta_l + \theta_0) = p\theta + pM\theta_0$, where $\theta = \sum_{l=1}^{M} \theta_l$. Since T_l s are independent of each other, $\sum_{l=1}^{M} T_l$ has a Poisson distribution with rate parameter $\sum_{l=1}^{M} \theta_i$, which is independent from the rate coming from distribution of MT_0. However, it is nontrivial to characterize the pdf of X because MT_0 is not Poisson distributed.

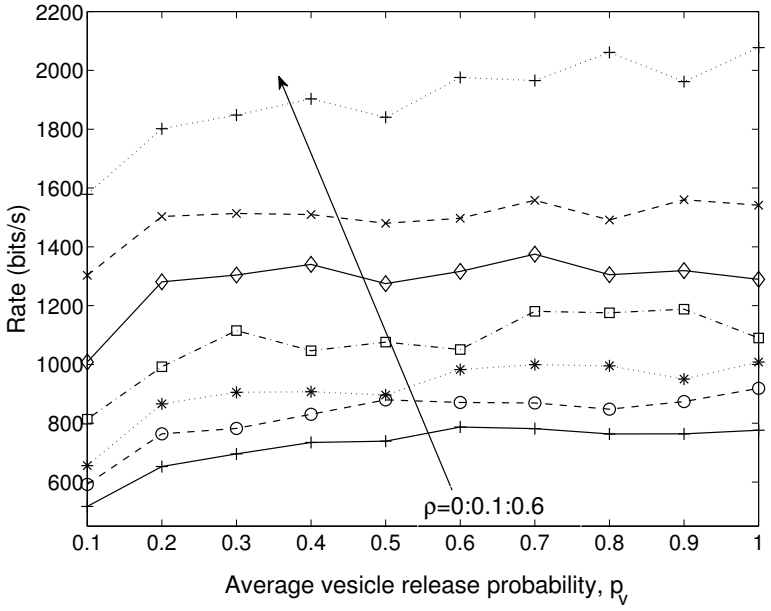

Figure 3.12: The rate region for multiple-access synaptic communication channel under correlated firing of presynaptic neurons for $M = 5$ presynaptic terminals with $\rho = 0 : 0.1 : 0.6$.

Note that when $\theta_0 = 0$, $X \sim Pois\left(p\sum_{l=1}^{M}\theta_l\right)$, which simplifies to the case of independently firing of input neurons. A constant correlation, i.e., θ_0, among each pair of input neurons increases the overall vesicle release rate to the synaptic cleft by $pM\theta_0$.

Fig. 3.4.2 illustrates the rate region for $M = 5$ user synaptic multiple-access channel determined by (3.40) given that users' firing rates have first-order correlation. Since the transmitted information bits per spike remains the same independent of the correlation amount, we scale the delivered information per spike by spike count in a second, and obtain the rate as information bits per second. Compared to uncorrelated firing of neurons, the curve corresponding to $\rho = 0$, as the firing rates become more correlated, total rate in bits per second enhances. Hence, incorporating correlation, more information is conveyed through synapses to the postsynaptic end.

3.5 Implications of Synaptic Communication on Neurological Disorders

Neurons are susceptible to electrochemical and structural disruption. Disorders of neuromuscular transmission are due to a wide variety of agents, such as genetic disorders, systemic

diseases, drugs, environmental health problems, infections, lifestyle, hormones, some are genetically determined, many are of unknown etiology [161]. All such disorders interfere with one or more events in the sequence whereby a nerve impulse excites an action potential. Here, we establish relations between synaptic communication problems and the neuronal disorders, focusing on the presynaptic, synaptic and postsynaptic abnormalities.

3.5.1 Disorders Characterized by Presynaptic Abnormality

Impairments in action potential generation, vesicle fusion process and neurotransmitter release are the main causes for presynaptic abnormalities.

3.5.1.1 Action Potential and Neural Transmission Performance

Action potentials get amplified and degraded depending on outside factors. For example, nicotine enhances neurotransmission rate by causing more action potentials in the presynaptic neuron [127]. This dependence between the action potentials and transmission rate is also shown in Fig. 3.9, utilizing the relation between action potential and fusion rates as in (3.19). Alcohol, on the other hand, blocks neurotransmission by inhibiting the excitatory channels on the postsynaptic neuron, and then lowering the rate of action potentials from the presynaptic neuron [61]. As a result, fusion rate decays, and hence, the synaptic performance drops as shown in Fig. 3.9(c).

3.5.1.2 Vesicle Fusion Rate, Neurotransmitters and Neural Transmission Performance

Diminishing neurotransmitter release is directly linked to neurological syndromes. Depression is associated with fewer neurotransmitters released per vesicle [177]. Cocaine provides a sense of euphoria by blocking the reuptake of dopamine by the presynaptic neuron. As the reuptake rate drops, higher amount of vesicles, i.e., N_A, would be available for release as illustrated in Fig. 3.10. This leads to a higher dopamine concentration in the synapse, which increases neurotransmission in brain reward system, i.e., the brain circuit that reinforces behavior by inducing pleasurable effects, hence more postsynaptic firing [60]. Heroin is thought to increase the rate of vesicle fusion in the presynaptic neurons that use dopamine as a neurotransmitter [118]. Fig. 3.13 depicts the deteriorating effect of drug use and depression on

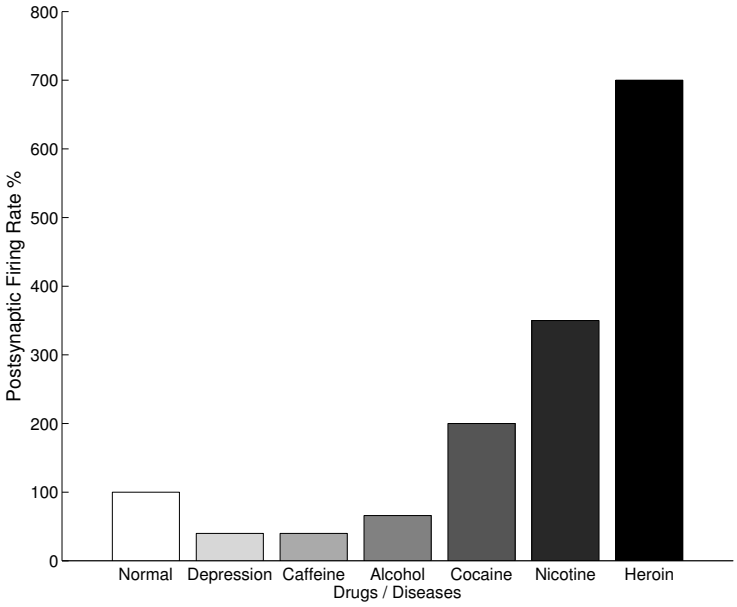

Figure 3.13: The effects of drugs and diseases on synaptic transmission [118].

postsynaptic firing of neurons.

3.5.2 Disorders Characterized by Synaptic Abnormality

Synaptic transmission is the most vulnerable step in neuronal signaling because synaptic plasticity has a crucial role in learning and memory.

3.5.2.1 Synaptic Depression

Depletion of the readily releasable vesicles leads to synaptic fatigue and depression. Decrease in RRP, i.e., N_A, leads to significant drop in postsynaptic firing rates. The neural transmission rate pattern under variable pool conditions is also drawn in Fig. 3.10.

3.5.2.2 Abnormal Synaptic Plasticity

Synaptic plasticity is the ability of the synapse to change in strength in response to either use or disuse of transmission over synaptic pathways. Quantal variations of neurotransmitters re-

leased into a synapse and the postsynaptic response variability cooperate to achieve plasticity [57]. As in (3.30), the postsynaptic voltage directly depends on the quantal variations in EPSP. Furthermore, variations in quantal amplitude change the PSD of the modulated presynaptic inputs as in (3.35), affecting the neural communication performance.

3.5.3 Disorders Characterized by Postsynaptic Abnormality

Excessive postsynaptic firing rates and disorders arising from postsynaptic receptor saturation are the main health problems attributed to postsynaptic abnormalities.

3.5.3.1 Postsynaptic Firing Rate and Neural Disorders

High postsynaptic firing rates could lead to sleepiness at synapses where adenosine is the primary transmitter. Caffeine inhibits sleepiness by inhibiting adenosine receptors [140]. Hence, available neurotransmitter amount at synapses decreases, yielding to decrement in postsynaptic firing rates, as previously indicated in Fig. 3.10.

3.5.3.2 Postsynaptic Receptor Saturation and Neural Transmission Performance

Various neurodegenerative disorders including schizophrenia, epilepsy, Alzheimer's and Huntington's diseases are associated with increased and decreased stimulation of a special type of postsynaptic receptor, i.e., NMDA receptor [75]. Variable stimulation of postsynaptic receptors causes alterations in EPSP amplitudes and neuronal communication performance as indicated in (3.30) and (3.40), respectively.

Multivesicular release could cause postsynaptic receptors to be saturated. When receptors are saturated, the quantal variability, i.e., q, drops, yielding to decreased level of postsynaptic firing rates as derived in (3.35) and (3.40). When specific receptor types take up too much of glutamate, a neurotransmitter known for exciting neurons and is very important in neural signal propagation in the brain, it can result in mass cell death and, over time, neurodegeneration [139].

CHAPTER 4

ADAPTIVE WEIGHT UPDATE IN CORTICAL NEURONS AND ESTIMATION OF CHANNEL WEIGHTS IN SYNAPTIC INTERFERENCE CHANNEL

Synaptic channels automatically adapt their weights in order to compensate the variations depending on the synapse input and output characteristics, i.e., spike frequency, correlation if there are multiple inputs, time difference between presynaptic and postsynaptic action potentials. Modification of the synaptic conductances, i.e., channel weights, is the main mechanism that enables learning in neurons. In this chapter, we approach this learning mechanism from a different perspective. First, we use an optimal linear estimation method to estimate the channel weights for both single-input single-output (SISO) and multi-input single-output (MISO) synaptic interference channels. Next, using this estimation method, we derive an optimal learning algorithm, which minimizes the interference in the synaptic channel in the presence of multiple presynaptic neuron terminals, and analyze the mean square error performance for SISO and MISO synaptic interference channels. Moreover, we provide the natural adaptive weight update algorithm for neurons based on experimental findings. Then, we compare the performance of the natural learning algorithm conducted by neurons to the optimal learning algorithm we developed. Our results demonstrate that neurons are capable of mitigating the interference, and achieve rates close to the capacity.

4.1 Introduction

The biological spiking neuron model is a mathematical description of the properties of neurons, which is designed to accurately characterize the biological processes. A simple model

of the response of an excitable cell to a periodic stimulus is provided by the integrate-and-fire model [86], [80]. In this model, the membrane potential $v(t)$ is assumed to behave linearly unless the threshold is reached. If the threshold is reached, then, the membrane fires and is immediately reset to zero. In another model, Hodgkin-Huxley model, the cell membrane can be modeled as a capacitor in parallel with an ionic current. FitzHugh-Nagumo model is a simplified form of the Hodgkin-Huxley model. The Hodgkin-Huxley model is the most important model in all of the physiological literature [81].

Neuro-spike communication, i.e., the communication of spiking neurons through the release of neurotransmitter molecules to the synaptic clefts, is an interdisciplinary research area, which combines the fields of neuroscience, communications and nanotechnology [21]. The point-to-point synaptic communication channel is studied in the literature widely as in [21], [66] and [74], and the multiple-access neuro-spike communication channel is studied in [105]. Development of these channel models is promising for future nanoscale and molecular communication techniques and applications. However, considering the essential roles of neurons and synaptic connections in memory and learning processes, more analysis is needed to correctly characterize neuro-spike communication.

Synapses are able to adjust their channel conductances depending on the action potential (AP) characteristics, called as neural plasticity (NP) in the neuroscience literature [37]. NP aims at building stronger connections among neurons so that actively transmitting neurons are sustained to carry information, but on the other hand, other connections, which are usually not correlated with the most of the transmitted information, are fade away. In this chapter, we investigate the sustainability of the synaptic connections from a communication theory perspective. We treat the synapses that do not provide useful information transmission as interfering connections. Information transfer via interfering connections should be cancelled out at the output neuron. To achieve this task, neurons, through feedback mechanisms, manage to adjust the synaptic conductances, i.e., synaptic weights. These mechanism among neuronal connections enables the reduction of interference caused by uncorrelated synapses. In this study, we investigate the optimality of this adaptive interference canceling method. To the best of our knowledge, the effect of interference among a cluster of neurons has not been investigated yet.

In this chapter, we consider the most basic model of a neuron, which consists of an input with

some synaptic weight vector and an activation function or transfer function inside the neuron determining output. This is the basic structure used in artificial neurons. We model neurons as linear systems, to estimate their channel weights. Depending on the which have optimal solutions when certain conditions are satisfied. Estimation of input signal waveforms are conducted through Minimum Mean Square Error (MMSE) estimators, which minimize the estimation error. Furthermore, MMSE estimation is also shown to be an optimal approach for solving interference problems [144]. Here, we compare the Signal-to-Noise plus Interference Ratio (SNIR) obtained for actual interference cancellation mechanism seen in neurons and to the optimal interference prevention technique. The results show that neurons are actually good interference canceling elements that are already available in the nature. This finding could be exploited to build strong connections enabling the transfer of most common data seen in the input side.

The remainder of this chapter is organized as follows. In Section 4.2, we give a background on neural signaling and neural communication. In Section 4.3, we provide the discrete linear system models for the SISO and MISO synaptic interference channels by projecting the stochastic processes, i.e., inputs and the channel noise, onto interference eigenfunctions. Then, we investigate and analyze the SISO and MISO synaptic interference channel after introducing the interference eigenfunction concept. In Section 4.4, we provide the maximum information rate for single input and multiple-access neuron interference channels. In Section 4.5, we provide a technique for linear estimation of the synaptic channel weights for the point and multiple-access neurons, and the optimal solutions to obtain maximum Signal-to-Interference Ratio (SIR). In Section 4.6, we analyze the average power dissipation in the neural communication channel incorporating the channel noise and the neural input correlation. In Section 4.7, by explaining the neural learning algorithm through synaptic weight modification, i.e., STDP, we interpret the output neuron SIR, analytically. In Section 4.8, we provide the performance results of optimal detection and STDP algorithms on the output SIR, and interpret the results.

4.2 Background and System Model

4.2.1 Background on Neural Signaling

In this section, we provide the essential components of neural signaling. These include *AP generation*, *neural firing*, *vesicle release* processes and the *postsynaptic potential*.

AP is a short-lasting event in which the electrical membrane potential of a cell rapidly rises and falls, following a consistent trajectory [21]. During the action potential, part of the neural membrane opens to allow positively charged ions inside the cell and negatively charged ions out. This process causes a rapid increase in the positive charge of the nerve fiber. When the charge reaches +40mV, the impulse is propagated down the nerve fiber. This electrical impulse is carried down the nerve through a series of action potentials. *Neural firing* is the response of a neuron when it is stimulated. A neuron that emits an action potential is often said to fire.

Synaptic vesicles store neurotransmitters to be released at synapses and constantly reproduced by the cells. These vesicles are essential for conduction of nerve impulses among neurons. Action potentials trigger the complete fusion of the synaptic vesicle with the cellular membrane, and then, the excretion from the cell through exocytosis, which is called *vesicle release* [110].

Postsynaptic potential is the membrane potential at the postsynaptic terminal of a chemical synapse. In neuroscience, an EPSP is the temporary increase in the postsynaptic membrane potential caused by the flow of positively charged ions into the postsynaptic cell due to the vesicle release [22]. An Inhibitory PostSynaptic Potential (IPSP), which is the opposite of an EPSP, is a kind of synaptic potential that makes a postsynaptic neuron less likely to generate an action potential.

Postsynaptic potentials are subject to spatial and temporal summation. *Spatial summation* occurs when a neuron is receiving input at two synapses that are near each other. In this case, their postsynaptic potentials add together. If the neuron is receiving two Excitatory PostSynaptic Potentials (EPSPs), they combine so that the membrane potential is depolarized by the sum of the two changes. If there are two inhibitory potentials, they also sum, and the membrane is hyperpolarised by that amount. If the cell is receiving both inhibitory and

excitatory postsynaptic potentials, they can cancel out, or one can be stronger than the other, and the membrane potential will change by the difference between them. The threshold of firing is typically -50mV [145]. Therefore, to fire a neuron, the addition of the potentials of Excitatory Synapses (EXS) and Inhibitory Synapses (INS) should be equal to or greater than -50mV. *Temporal summation* occurs when a neuron receives inputs that are close together in time. In this case, these inputs are added together, even if they are from the same synapse. Thus, if a neuron receives an EPSP, and then the presynaptic neuron fires again, creating another EPSP, then the membrane of the postsynaptic cell is depolarized by the total of the EPSPs.

4.2.2 Background on Neural Communication

4.2.2.1 Transmitting Node: The Presynaptic Neuron

When a random stimulus is applied, the presynaptic neuron terminal generates a Poisson distributed AP train, $S(t)$, at its axon, which has a firing rate λ. Neuronal response characteristics are usually characterized by Linear-Nonlinear-Poisson (LNP) model. The details of the firing and AP train generation can be found in [105]. AP train, i.e., $S(t)$, triggers the *vesicle release process* from the presynaptic terminal. The release process is shaped according to the rate of AP generation, i.e., λ.

4.2.2.2 Transmission Process: The Synaptic Channel

AP generated by the presynaptic terminal enables vesicle release to the synaptic channel. Release amount depends on the strength of the AP train, the size of available vesicle pool located in the neural terminal, and the quantal release parameters. *Quantal release* is the secretion process denoting the neurotransmitter amount excreted from *release sites* following neural stimulation, i.e., AP generation. *Quantal size* is the synaptic response to the release of neurotransmitter from a single vesicle, and *quantal content* is the number of effective vesicles released in response to a nerve impulse [73]. *Quantal variation* is the alteration in the transmitter content among vesicles as determined by vesicle volume [73]. These concepts are explained in [110].

Input the synaptic channel, $S(t)$, is scaled by the synaptic conductance. Synaptic channels have variable conductances. These conductances, i.e., weights, are adjusted through spike-timing-dependent plasticity (STDP), which will be discussed in Section 4.7. In this section, we simply call the synaptic weight, w, to use in our linear system model.

4.2.2.3 Receiving Node: The Postsynaptic Neuron

At the postsynaptic terminal, each input propagated through the soma is summed linearly in the point neuron, i.e., perceptron, model. Perceptron can be described by

$$r_i(t) = \sqrt{P_i}\beta_i w_i S_i(t) + Z_i(t) = h_i S_i(t) + Z_i(t), \tag{4.1}$$

where $Z_i(t)$ is assumed to be an independent interference stochastic waveform that may be composed of both thermal noise and interfering signals of other transmitting neurons, i.e., presynaptic terminals. For a single bit, the fundamental problem is to build a receiver which guesses β with minimum probability of error. Alternatively, when β is one bit in a stream of coded bits, we would like to produce a soft estimate of b with high SNIR. When $Z_i(t)$ is composed of known waveforms in addition to independent Gaussian noise, that is

$$Z_i(t) = \sum_{j \neq i}^{M} \sqrt{P_j}\beta_j \alpha_{ij} S_j(t) + N(t), \tag{4.2}$$

multiuser receivers have been designed for a variety of objectives, e.g., minimum probability of error, maximum SNIR, or zero interference from other users. These multiuser systems share the property that the receiver does as best it can given the set of transmitter signals $S_i(t)$.

In (4.2), $Z_i(t)$ is the interference signal seen at the soma [135], α_{ij}'s and $S_j(t)$'s are the synaptic interference weights and unit power synaptic inputs, respectively. β_j denotes whether the inputs coming from either EXS or INS. It is bipolar, 1 if the synapse is an EXS, -1 if an INS. P_j is the input power at the j^{th} synaptic connection, and finally $N(t)$ stands for the axonal noise, and $M = M_{EX} + M_{IN}$, where M_{EX} and M_{IN} are for the total number of EXSs and INSs, is for the total number of EXSs and INSs to the soma.

From the perspective of the receiver neuron i for $S_i(t)$, the interference $Z_i(t)$ is simply a stochastic process, which we assume zero mean with no loss of generality. Ideally, we would like to obtain a set of uncorrelated (and preferably independent) sufficient statistics and then optimally combine these either to detect the bit β_j or to derive an estimate of β_j. When $Z_i(t)$

is Gaussian, these projections would indeed be independent Gaussian random variables and the optimal estimation (detection) problem would be easily solved. A complete and rigorous development of the ideas can be found in [12].

4.2.2.4 Processing of Axonal Information

the perceptron equation is defined as

$$y_i(t) = \Theta\left(r_i(t) - \theta\right) = \Theta(v_i(t)) = \Theta\left(\sqrt{P_i}\beta_i w_i S_i(t) + \sum_{j=1, j\neq i}^{M} \sqrt{P_j}\beta_j \alpha_{ij} S_j(t) + N(t) - \theta\right) \quad (4.3)$$

In current applications, the sigmoidal AF is used, which is as

$$y_i(t) = \Theta(v_i(t)) = \left(1 + \exp\left(-v_i(t)\right)\right)^{-1}, \quad (4.4)$$

where Θ is the neural activation function (AF), and θ is the threshold at which a postsynaptic response is exerted. $y_i(t)$ is the output of the node, and $v_i(t)$ is the weighted sum of the input synapses [87], [156], [40]. The heaviside step function can also be used as an AF.

4.3 Synaptic Interference Channel

In this section, we first describe the *interference eigenfunctions* concept, and then, based on this concept, we present a discrete-time linear neuron model. Then, using this linear model, we investigate two different types of neuron interference channel. First, we investigate SISO neuron interference channel, and then, we analyze the MISO neuron interference channel.

4.3.1 Interference Eigenfunctions

In general, for the given stochastic process, $Z(t)$, we seek an orthonormal representation

$$Z(t) = \lim_{N\to\infty} \sum_{k=1}^{N} Z_k \Phi_k(t), \qquad Z_k = \langle Z(t), \Phi_k(t) \rangle = \int_0^T Z(t)\Phi_k(t)\,\mathrm{d}t, \quad (4.5)$$

where $\Phi_k(t)$'s are the *interference eigenfunctions* and $\langle \cdot, \cdot \rangle$ denotes inner product operation [144]. Assuming that the orthonormal representation for $Z(t)$ exists and converges, we seek a special set of orthonormal Φ_k which produce uncorrelated projections, i.e., Z_k's. Hence, we

require that

$$\left\langle \Phi_i(t), \Phi_j(t) \right\rangle = \int_0^T \Phi_i(t)\Phi_j(t)\,\mathrm{d}t = \delta_{ij}, \tag{4.6}$$

where δ_{ij} is the Kronecker delta. Hence, we the following is required for the projections a_k being uncorrelated:

$$\mathrm{E}\left[Z_i Z_j\right] = \mathrm{E}\left[\left\langle \Phi_i(t), Z(t) \right\rangle \left\langle \Phi_j(t), Z(t) \right\rangle\right] = \mathrm{E}\left[\int_0^T \int_0^T \Phi_i(\tau) Z(\tau) \Phi_j(t) Z(t)\,\mathrm{d}t\mathrm{d}\tau\right] = \lambda_j \delta_{ij}. \tag{4.7}$$

Defining the autocorrelation function (ACF) of $Z(t)$ $R_Z(t,\tau) = \mathrm{E}\left[Z(t)Z(\tau)\right]$, and using (4.7), we obtain the following integral equation

$$\int_0^T \Phi_j(t) \underbrace{\left(\int_0^T R_Z(t,\tau)\Phi_i(\tau)\,\mathrm{d}\tau \right)}_{*} \mathrm{d}t = \lambda_j \delta_{ij}, \tag{4.8}$$

where the requirement on $*$ is

$$* = \int_0^T R_Z(t,\tau)\Phi_i(\tau)\,\mathrm{d}\tau = \lambda_i \Phi_i(t). \tag{4.9}$$

Using an equivalent discrete representation of (4.9), and assuming that the set of the interference eigenfunctions, i.e., $\Phi_i(t)$'s, is a convenient basis function set over the time interval, we define r_{ij} in terms of the projections Z_n as follows

$$r_{ij} = \mathrm{E}\left[\int_0^T \int_0^T Z(t)Z(\tau)\Phi_i(t)\Phi_j(\tau)\,\mathrm{d}t\mathrm{d}\tau\right] = \mathrm{E}\left[Z_i Z_j\right]. \tag{4.10}$$

If $\Phi_i(t)$ is not a convenient basis function set, then, we can represent it by a finite sum $\Phi_i(t) = \sum_{n=1}^{N} \phi_{in}\Psi_n(t)$, where $\Psi_n(t)$ is a convenient basis function set over the interval. Then, using (4.9), we need to follow a few steps to find the relation between λ_j and r_{nk}.

The receiver i, i.e., the soma of the postsynaptic terminal i, observes the signal $r_i(t)$ as input on the interval $[0,T]$. Projecting the received signal onto the interference eigenfunctions, $\Phi_1(t), \Phi_2(t), \ldots, \Phi_n(t)$, we obtain the following vector output, which is a standard matrix eigenvalue eigenvector equation of the form

$$\mathrm{E}[\underset{\sim}{\underset{\sim}{\mathbf{z}\mathbf{z}^{\mathsf{T}}}}]\phi_k = \mathbf{R}\phi_k = \lambda_k \phi_k. \tag{4.11}$$

Here, $\phi_k = [\phi_{k1} \dots \phi_{kN}]^\mathsf{T}$ and $\underset{\sim}{\mathbf{z}} = [Z_1 \dots Z_N]^\mathsf{T}$. Each eigenvector corresponds to an eigenfunction of (4.9) and it is easily verified that each eigenvalue is the amount of interference signal energy carried by that eigenfunction. It is also easy to verify that since $R_{\underset{\sim}{\mathbf{z}}}(t,\tau) = \mathrm{E}[\underset{\sim}{\mathbf{z}}\underset{\sim}{\mathbf{z}}^\mathsf{T}]$ is an ACF, $\mathbf{R}$ is symmetric and positive semi-definite. This implies that $\mathbf{R}$ has nonnegative eigenvalues and an associated full set of orthonormal eigenvectors which span $\mathbb{R}^\mathrm{N}$.

4.3.2 Single-Input Single-Output Neuron Synaptic Interference Channel

In the case of single input neuron channel, the receiver neuron i, i.e, the i^{th} postsynaptic terminal axon, observes the signal

$$r_i(t) = h_i S_i(t) + Z_i(t), \tag{4.12}$$

as input on the interval $[0,T]$. Projecting the received signal onto the interference eigenfunctions $\Phi_1(t), \dots, \Phi_N(t)$ as described in Section 4.3.1, we obtain the vector output

$$\underset{\sim}{\mathbf{r_i}} = h_i \underset{\sim}{\mathbf{s_i}} + \underset{\sim}{\mathbf{z_i}} \tag{4.13}$$

where $\underset{\sim}{\mathbf{s_i}}$ and $\underset{\sim}{\mathbf{z_i}}$ have n^{th} components $s_{in} = \langle S_i(t), \Phi_n(t) \rangle$, $z_{in} = \langle Z_i(t), \Phi_n(t) \rangle$ and the z_{in}'s are mutually uncorrelated. In (4.13), $\underset{\sim}{\mathbf{s_i}}$ is an $N \times 1$ vector with user' signature, and h_i is the channel gain parameter equal to $h_i = \sqrt{P_i}\beta_i w_{ii}$, and $\underset{\sim}{\mathbf{z_i}} = \begin{bmatrix} z_1 & z_2 & \dots & z_N \end{bmatrix}^\mathsf{T}$ is the channel interference vector combined with the AWGN noise vector with zero mean and covariance matrix $\sigma^2 \mathbb{I}_\mathbf{N}$ with size $N \times N$, and $\sigma^2 = \mathrm{E}\left[n_k^2\right] = N_0/2$.

Here, to simplify the analysis, we first work with unit vectors, and then, generalize our analysis to non-unit vectors. With no loss of generality we assume that the basis functions $\Phi_n(t)$ also span the signal space for $S_i(t)$, and $h_i \underset{\sim}{\mathbf{s_i}}$ contains all available information about $h_i S_i(t)$.

The correlation matrix of the received signal in vector form is

$$\mathbf{R}_{\underset{\sim}{\mathbf{r_i}}} = \mathrm{E}\left[\underset{\sim}{\mathbf{r_i}}\underset{\sim}{\mathbf{r_i}}^\mathsf{T}\right] = \mathrm{E}\left[\left(h_i \underset{\sim}{\mathbf{s_i}} + \underset{\sim}{\mathbf{z_i}}\right)\left(h_i \underset{\sim}{\mathbf{s_i}}^\mathsf{T} + \underset{\sim}{\mathbf{z_i}}^\mathsf{T}\right)\right] = h_i^2 \mathrm{E}\left[\underset{\sim}{\mathbf{s_i}}\underset{\sim}{\mathbf{s_i}}^\mathsf{T}\right] + \mathrm{E}\left[\underset{\sim}{\mathbf{z_i}}\underset{\sim}{\mathbf{z_i}}^\mathsf{T}\right], \tag{4.14}$$

which will be utilized in Section 4.4 in the rate analysis for SISO synaptic channel.

Using the perceptron equation given in (4.3), the vector output at the neural node is obtained as

$$\underset{\sim}{\mathbf{y}} = \Theta\left(h\underset{\sim}{\mathbf{s}} + \underset{\sim}{\mathbf{z}} - \underset{\sim}{\theta}\right) = \Theta(\underset{\sim}{\mathbf{v}}), \tag{4.15}$$

where Θ is the neural activation function (AF), and $\underset{\sim}{\theta}$ is the projection of θ onto the interference basis vectors.

4.3.3 Multi-Input Single-Output Neuron Synaptic Interference Channel

When there are multiple presynaptic neuron terminals sending APs simultaneously, the receiver neuron i, i.e, the postsynaptic terminal i^{th} axon, observes a summation of signals

$$r_i(t) = \sum_{j=1}^{M} h_j S_j(t) + N(t) \tag{4.16}$$

as input on the interval $[0,T]$, where $h_j = \sqrt{P_j}\beta_j w_{ij}$. For multiple presynaptic terminal case, projecting the received signal onto the interference eigenfunctions $\Phi_1(t),\ldots,\Phi_N(t)$, we obtain the the following linear system relation for the vector output

$$\underset{\sim}{\mathbf{r_i}} = \mathbf{S}\underset{\sim}{\mathbf{h_i}} + \underset{\sim}{\mathbf{n_i}}, \tag{4.17}$$

where $\mathbf{S} = \left[\underset{\sim}{\mathbf{s_1}} \quad \underset{\sim}{\mathbf{s_2}} \quad \ldots \quad \underset{\sim}{\mathbf{s_M}}\right]$ is an $N \times M$ matrix with users' signatures, and $\underset{\sim}{\mathbf{s_j}}$ is the projection component of $S_j(t)$ onto interference eigenfunctions. and $\underset{\sim}{\mathbf{h_i}} = \left[h_{i1} \quad h_{i2} \quad \ldots \quad h_{iM}\right]^{\mathsf{T}}$, is the channel gain vector where $h_{ij} = \sqrt{P_j}\beta_j w_{ij}$, and $\underset{\sim}{\mathbf{z_i}} = \left[z_1 \quad z_2 \quad \ldots \quad z_N\right]^{\mathsf{T}}$ is the channel interference vector combined with the AWGN noise vector with zero mean and covariance matrix $\sigma^2\mathbb{I}_{\mathbf{N}}$ with size $N \times N$, and $\sigma^2 = \mathrm{E}\left[n_k^2\right] = N_0/2$.

The correlation matrix of the received signal in vector form is

$$\mathbf{R}_{\underset{\sim}{\mathbf{r_i}}} = \mathrm{E}\left[\underset{\sim}{\mathbf{r_i}}\underset{\sim}{\mathbf{r_i}}^{\mathsf{T}}\right] = \mathrm{E}\left[\left(\mathbf{S}\underset{\sim}{\mathbf{h_i}} + \underset{\sim}{\mathbf{n_i}}\right)\left(\underset{\sim}{\mathbf{h_i}}^{\mathsf{T}}\mathbf{S}^{\mathsf{T}} + \underset{\sim}{\mathbf{n_i}}^{\mathsf{T}}\right)\right] = \mathbf{S}\mathbf{P}\mathbf{S}^{\mathsf{T}} + \mathrm{E}\left[\underset{\sim}{\mathbf{n_i}}\underset{\sim}{\mathbf{n_i}}^{\mathsf{T}}\right], \tag{4.18}$$

where $\mathbf{P}$ is the power matrix obtained as

$$\mathbf{P} = \mathrm{E}\left[\underset{\sim}{\mathbf{h_i}}\underset{\sim}{\mathbf{h_i}}^{\mathsf{T}}\right] = \mathrm{diag}\left(w_{i1}^2P_1,\ldots,w_{iM}^2P_M\right), \tag{4.19}$$

because we assume $\beta_j = 1$ or $\beta_j = -1$ with equal probability, and each synapse could be either excitatory or inhibitory independent of each other. Hence, $\mathrm{E}[\beta_i] = 0$, and $\mathrm{E}[\beta_i\beta_j] = \delta_{ij}$. (4.18) will be utilized in Section 4.4 in the rate analysis for MISO synaptic channel.

4.4 Achievable Communication Rates in Synaptic Interference Channel

As neurons have very large-scale connections, and multiple neurons simultaneously transfer data through synaptic connections among them, they suffer from interference. In this section,

we investigate the capacity of single and multiple-access synaptic interference channels using the linear system model developed in Section 4.3 and provide the output SNIR for both cases.

In the classical communication schemes, interference is treated as noise. Therefore, the channel capacity (or the rate of the communication) can be obtained using

$$R = \log\left(1 + \frac{SNR}{1 + INR}\right) = \log\left(1 + SNIR\right). \tag{4.20}$$

Assuming that there are M transmitting nodes directed to a receiving neuron node, i.e., the axon hillock of the receiver neuron, the fictitious SNIR at the output neuron is

$$\zeta_i(t) = \frac{w_{ii} S_i(t)}{n_i + \sum\limits_{j=1, j\neq i}^{M} \alpha_{ij} S_j(t)}, \tag{4.21}$$

where $\zeta_i(t)$ is the fictitious SNIR at time step t, $S_i(t)$ is the state of the neuron, w_{ii} is the feedback coefficient from its state to its input layer, and α_{ij} is the weight from the output of the j^{th} neuron to the input of the i^{th} neuron. n_i represents the noise at the receiver neuron.

4.4.1 Single-Input Single-Output Neuron Synaptic Interference Channel

4.4.1.1 Total Signal Power at the Output

Total signal power at the output node can be found using

$$\begin{aligned} \underset{\sim}{\mathbf{r_i}} &= h_i \underset{\sim}{\mathbf{s_i}} + \underset{\sim}{\mathbf{z_i}}, \\ \|\underset{\sim}{\mathbf{r_i}}\|_2^2 &= \underset{\sim}{\mathbf{r_i}}^{\intercal} \underset{\sim}{\mathbf{r_i}} = h_i^2 \sum_{k=1}^{N} s_{ik}^2 + 2h \sum_{k=1}^{N} s_{ik} z_{ik} + \sum_{k=1}^{N} z_{ik}^2. \end{aligned} \tag{4.22}$$

Hence, the SNIR at the output axon hillock i can be computed as

$$\text{SNIR}_{out,i} = \frac{\mathrm{E}\left[h_i^2 \sum\limits_{k=1}^{N} s_{ik}^2\right]}{\mathrm{E}\left[2h_i \sum\limits_{k=1}^{N} s_{ik} z_{ik} + \sum\limits_{k=1}^{N} z_{ik}^2\right]} = \frac{w_{ii}^2 P_i}{\mathrm{E}\left[\mathrm{Tr}(\underset{\sim\sim}{\mathbf{z}\mathbf{z}}^{\intercal})\right]} \sum_{k=1}^{N} s_{ik}^2, \tag{4.23}$$

where we assume that interference signal is independent from the input signal, and zero mean, and (4.23) depends on the channel weight, i.e., w_{ii}, which changes adaptively depending on the AP patterns. Hence, the time dependent output SIR can be calculated using the algorithm described in Section 4.7.1.

4.4.1.2 Channel Capacity

Using (4.20), for the node at the output side, and assuming unit power constraint on the presynaptic terminal, we obtain the following rate expression

$$R_i = \frac{1}{2}\log\left(1+\mathrm{SNIR}_{out,i}\right) = \frac{1}{2}\log\left(1+\frac{w_{ii}^2 P_i}{\mathrm{E}\left[\mathrm{Tr}(\underset{\sim}{\mathbf{z}}\underset{\sim}{\mathbf{z}}^{\intercal})\right]}\right) = \frac{1}{2}\log\left(1+\frac{w_{ii}^2 P_i}{\sum\limits_{j\neq i}^{M} P_j\alpha_{ij}^2+\sigma^2 N}\right) \quad (4.24)$$

Using (4.13), and assuming no synaptic interference, the capacity expression for the single input neural communication channel can be simplified to AWGN channel with the capacity as

$$C(\underset{\sim}{\mathbf{s}};\underset{\sim}{\mathbf{r}}) = \max_{p(\underset{\sim}{\mathbf{s}})} I(\underset{\sim}{\mathbf{s}};\underset{\sim}{\mathbf{r}}) = H(\underset{\sim}{\mathbf{r}}) - H(\underset{\sim}{\mathbf{n}}) = \frac{1}{2}\log\left(1+\frac{w_{ii}^2 P_i}{\sigma^2 N}\right). \quad (4.25)$$

4.4.2 Multi-Input Single-Output Neuron Synaptic Interference Channel

4.4.2.1 Total Signal Power at the Output: Multiaccess Channel

Total signal power at the output node can be found using

$$\begin{aligned} \underset{\sim}{\mathbf{r_i}} &= \mathbf{S}\underset{\sim}{\mathbf{h_i}} + \underset{\sim}{\mathbf{n_i}}, \\ \|\underset{\sim}{\mathbf{r_i}}\|_2^2 &= \underset{\sim}{\mathbf{h_i}}^{\intercal}\mathbf{S}^{\intercal}\mathbf{S}\underset{\sim}{\mathbf{h_i}} + 2\underset{\sim}{\mathbf{h_i}}^{\intercal}\underset{\sim}{\mathbf{n_i}} + \underset{\sim}{\mathbf{n_i}}^{\intercal}\underset{\sim}{\mathbf{n_i}}. \end{aligned} \quad (4.26)$$

Hence, the SNIR at the output axon hillock can be computed as

$$\begin{aligned} \mathrm{SNIR}_{out,i} &= \frac{\mathrm{E}\left[\underset{\sim}{\mathbf{h_i}}^{\intercal}\mathbf{S}^{\intercal}\mathbf{S}\underset{\sim}{\mathbf{h_i}}\right]}{\mathrm{E}\left[2\underset{\sim}{\mathbf{h_i}}^{\intercal}\underset{\sim}{\mathbf{n_i}} + \underset{\sim}{\mathbf{n_i}}^{\intercal}\underset{\sim}{\mathbf{n_i}}\right]} = \frac{\mathrm{E}\left[\mathrm{Tr}(\underset{\sim}{\mathbf{h_i}}^{\intercal}\mathbf{S}^{\intercal}\mathbf{S}\underset{\sim}{\mathbf{h_i}})\right]}{\mathrm{E}\left[2\underset{\sim}{\mathbf{h_i}}^{\intercal}\underset{\sim}{\mathbf{n_i}}\right] + \mathrm{E}\left[\mathrm{Tr}(\underset{\sim}{\mathbf{n_i}}^{\intercal}\underset{\sim}{\mathbf{n_i}})\right]} \\ &= \frac{\mathrm{E}\left[\mathrm{Tr}(\mathbf{S}\underset{\sim}{\mathbf{h_i}}\underset{\sim}{\mathbf{h_i}}^{\intercal}\mathbf{S}^{\intercal})\right]}{\mathrm{E}\left[\mathrm{Tr}(\underset{\sim}{\mathbf{n_i}}\underset{\sim}{\mathbf{n_i}}^{\intercal})\right]} = \frac{\mathrm{Tr}(\mathbf{S}\mathrm{E}[\underset{\sim}{\mathbf{h_i}}\underset{\sim}{\mathbf{h_i}}^{\intercal}]\mathbf{S}^{\intercal})}{\mathrm{Tr}(\mathrm{E}[\underset{\sim}{\mathbf{n_i}}\underset{\sim}{\mathbf{n_i}}^{\intercal}])} \\ &= \frac{1}{\mathrm{Tr}(\mathrm{E}[\underset{\sim}{\mathbf{n_i}}\underset{\sim}{\mathbf{n_i}}^{\intercal}])}\sum_{k=1}^{N} w_{ik}^2 P_k \,\mathrm{Tr}(\underset{\sim}{\mathbf{s_k}}\underset{\sim}{\mathbf{s_k}}^{\intercal}) \end{aligned} \quad (4.27)$$

(4.27) depends on the channel weights, i.e., $w_k's$, which change adaptively depending on the AP patterns. Using the algorithm for modification of the synaptic weight as described in Section 4.7.1, the time dependent SIR at the output neuron could be iteratively calculated.

4.4.2.2 Channel Capacity

Using (4.20), for the node at the output side, and assuming unit power constraint on the presynaptic terminals, we obtain the following rate expression

$$R_i = \frac{1}{2}\log\left(1+\mathrm{SNIR}_{out,i}\right) = \frac{1}{2}\log\left(1+\frac{\sum_{k=1}^{M} w_{ik}^2 P_k}{\mathrm{E}\left[\mathrm{Tr}(\underset{\sim}{\mathbf{n_i}}\underset{\sim}{\mathbf{n_i}}^{\intercal})\right]}\right) = \frac{1}{2}\log\left(1+\frac{\sum_{k=1}^{M} w_{ik}^2 P_k}{\sigma^2 N}\right). \quad (4.28)$$

Using the expression in (4.17), and assuming no synaptic interference, the capacity expression for the multiaccess neural communication channel can be simplified to AWGN channel with the capacity as

$$C(\mathbf{S};\underset{\sim}{\mathbf{r}}) = \max_{p(\mathbf{S})} I(\mathbf{S};\underset{\sim}{\mathbf{r}}) = H(\underset{\sim}{\mathbf{r}}) - H(\underset{\sim}{\mathbf{n}}) = \frac{1}{2}\log\det\left(\frac{\mathbf{SPS}^{\intercal}+\mathbb{I}_{\mathbf{N}}\sigma^2}{\sigma^2}\right). \quad (4.29)$$

4.5 Classical Communication Techniques for Avoiding Interference in Neurons

Multiuser receivers have been designed for a variety of objectives, e.g., minimum probability of error, maximum SIR, or zero interference from other users [168]. These multiuser systems share the property that the receiver does as best it can given the set of transmitter signals $S_j(t)$.

Using linear MMSE estimation techniques, we can measure the synaptic channel weights for both point-to-point and multiple-access neuron interference channels.

4.5.1 Linear Estimation of the Channel Weight in Single Input Neural Channel

The signal at the receiver neuron is

$$r(t) = hS(t) + Z(t), \quad (4.30)$$

where $h = \sqrt{P}bw$. A matched filter on the rescaled signal vector components s_k/λ_k is then performed to complete the detection process.

It is worthwhile to note that in a CDMA system where $Z(t)$ consists of the other usersï¿½ known signature waveforms and additive white Gaussian noise, the vector $\underset{\sim}{\mathbf{c}}$ with components

$c_k = s_k/\lambda_k$ is a scaled version of the well known minimum mean squared error (MMSE) linear filter and the decision rule [164] is the MMSE multiuser detector. We see that the filter output (and decision statistic) is

$$\hat{h} = \underset{\sim}{\mathbf{c}}^{\mathsf{T}}\underset{\sim}{\mathbf{r}} = \sum_{k=1}^{N} c_k r_k = \left(\sum_{k=1}^{N} \frac{s_k^2}{\lambda_k}\right) h + \sum_{k=1}^{N} \frac{s_k z_k}{\lambda_k}. \tag{4.31}$$

Hence, the output SNIR can be calculated as

$$\mathrm{SNIR}_h = \frac{\mathrm{E}\left[\left(h\sum_{k=1}^{N}\frac{s_k^2}{\lambda_k}\right)^2\right]}{\mathrm{E}\left[\left(\sum_{k=1}^{N}\frac{s_k z_k}{\lambda_k}\right)^2\right]} = \frac{Pw^2\left(\sum_{k=1}^{N}\frac{s_k^2}{\lambda_k}\right)^2}{\sum_{k=1}^{N}\sum_{l=1}^{N}\frac{s_k s_l \mathrm{E}[z_k z_l]}{\lambda_k\lambda_l}} = Pw^2\sum_{k=1}^{N}\frac{s_k^2}{\lambda_k}. \tag{4.32}$$

It is well known that among all linear filters $\underset{\sim}{\mathbf{c}}$, the MMSE filter maximizes the output SNIR [104]. However, (4.32) demonstrates that it remains possible to obtain a higher output SIR by altering the components s_k of the desired signal $S(t)$. That is, when $S(t)$ is subject to the unit energy constraint $\sum_k s_k^2 = 1$, we can maximize SNIR_h by choosing $s_k = 1$ for any $\lambda_k = \lambda^* = \min_j \lambda_j$. In this case, we have $S(t) = \Phi_k(t)$. Equivalently, we could distribute the signal energy in some arbitrary way over all such $\Phi_k(t)$. Hence, to obtain maximum SNIR, we need to place all the signal energy where there is least interference.

4.5.2 Linear Estimation of the Channel Weights in Multiple-Access Neural Interference Channel

When there is no interference, but AWGN only, the signal at the receiver neuron is $\underset{\sim}{\mathbf{r}} = \mathbf{S}\underset{\sim}{\mathbf{h}} + \underset{\sim}{\mathbf{n}}$. Hence, using the best linear minimum variance estimator for linear AWGN, the channel weight estimation is

$$\underset{\sim}{\hat{\mathbf{h}}} = \mathbf{W}\underset{\sim}{\mathbf{r}}, \qquad \mathbf{W} = \left(\mathbf{S}^{\mathsf{T}}\mathbf{C}_{\mathbf{n}}^{-\mathbf{1}}\mathbf{S}\right)^{-1}\mathbf{S}^{\mathsf{T}}\mathbf{C}_{\mathbf{n}}^{-\mathbf{1}},$$

where C_n is the covariance matrix for the AWGN.

In this section, we investigate the effect of interference between multiple-access neurons. For a single input neuron k, we observe that $\mathbf{S}\mathbf{S}^{\mathsf{T}} = \mathbf{R}_k + \underset{\sim}{\mathbf{s_k}}\underset{\sim}{\mathbf{s_k}}^{\mathsf{T}}$, where $\mathbf{R}_k = \sum_{i\neq k}\underset{\sim}{\mathbf{s_i}}\underset{\sim}{\mathbf{s_i}}^{\mathsf{T}}$, the correlation matrix of the interference faced by user k, is analogous to the matrix $\mathbf{R}$ introduced in Section 4.3.1.

Using $\mathbf{Z_k} = \mathbf{R_k} + \sigma^2\mathbb{I}$,

$$\underset{\sim}{\mathbf{c_k}} = (\underset{\sim}{\mathbf{s_k}}^{\intercal}\mathbf{Z_k^{-1}}\underset{\sim}{\mathbf{s_k}})^{-1}\mathbf{Z_k^{-1}}\underset{\sim}{\mathbf{s_k}}.$$

Replacing this with unit energy MMSE receiver filter, we obtain

$$\underset{\sim}{\mathbf{c_k}} = (\underset{\sim}{\mathbf{s_k}}^{\intercal}\mathbf{Z_k^{-2}}\underset{\sim}{\mathbf{s_k}})^{\frac{1}{2}}\mathbf{Z_k^{-1}}\underset{\sim}{\mathbf{s_k}}, \quad k = 1,\ldots,M. \tag{4.33}$$

Hence, $\hat{h} = \underset{\sim}{\mathbf{c_k}}^{\intercal}\underset{\sim}{\mathbf{r}} = \sum_{l=1}^{N} c_{lk}\left(\sum_{i=1}^{M} s_{li}h_i + n_l\right)$, where $s_{li} = [\mathbf{S}]_{li}$.

$$\begin{aligned}
\hat{h} &= \underset{\sim}{\mathbf{c_k}}^{\intercal}\underset{\sim}{\mathbf{r}} = (\underset{\sim}{\mathbf{s_k}}^{\intercal}\mathbf{Z_k^{-2}}\underset{\sim}{\mathbf{s_k}})^{\frac{1}{2}}\underset{\sim}{\mathbf{s_k}}^{\intercal}\mathbf{Z_k^{-1}}(\mathbf{S}\underset{\sim}{\mathbf{h}} + \underset{\sim}{\mathbf{n}}) \\
&= (\underset{\sim}{\mathbf{s_k}}^{\intercal}\mathbf{Z_k^{-2}}\underset{\sim}{\mathbf{s_k}})^{-\frac{1}{2}}\underset{\sim}{\mathbf{s_k}}^{\intercal}\mathbf{Z_k^{-1}}\left(\sum_{i=1}^{M}\underset{\sim}{\mathbf{s_i}}h_i + \underset{\sim}{\mathbf{n}}\right) \\
&= (\underset{\sim}{\mathbf{s_k}}^{\intercal}\mathbf{Z_k^{-2}}\underset{\sim}{\mathbf{s_k}})^{-\frac{1}{2}}\left(\sum_{i=1}^{M}\underset{\sim}{\mathbf{s_k}}^{\intercal}\mathbf{Z_k^{-1}}\underset{\sim}{\mathbf{s_i}}h_i + \underset{\sim}{\mathbf{s_k}}^{\intercal}\mathbf{Z_k^{-1}}\underset{\sim}{\mathbf{n}}\right) \\
&= (\underset{\sim}{\mathbf{s_k}}^{\intercal}\mathbf{Z_k^{-2}}\underset{\sim}{\mathbf{s_k}})^{-\frac{1}{2}}\left(h_k(\underset{\sim}{\mathbf{s_k}}^{\intercal}\mathbf{Z_k^{-1}}\underset{\sim}{\mathbf{s_k}}) + \sum_{i\neq k}\underset{\sim}{\mathbf{s_k}}^{\intercal}\mathbf{Z_k^{-1}}\underset{\sim}{\mathbf{s_i}}h_i + \underset{\sim}{\mathbf{s_k}}^{\intercal}\mathbf{Z_k^{-1}}\underset{\sim}{\mathbf{n}}\right).
\end{aligned} \tag{4.34}$$

Hence, the output SNIR, SNIR_h can be calculated as

$$\begin{aligned}
\mathrm{SNIR}_h &= \frac{\mathrm{E}\left[h_k^2(\underset{\sim}{\mathbf{s_k}}^{\intercal}\mathbf{Z_k^{-1}}\underset{\sim}{\mathbf{s_k}})^2\right]}{\mathrm{E}\left[\sum_{i\neq k}\sum_{j\neq k}(h_ih_j\underset{\sim}{\mathbf{s_k}}^{\intercal}\mathbf{Z_k^{-1}}\underset{\sim}{\mathbf{s_i}}\underset{\sim}{\mathbf{s_j}}^{\intercal}\mathbf{Z_k^{-1}}\underset{\sim}{\mathbf{s_k}}) + \underset{\sim}{\mathbf{s_k}}^{\intercal}\mathbf{Z_k^{-1}}\underset{\sim}{\mathbf{n}}\underset{\sim}{\mathbf{n}}^{\intercal}\mathbf{Z_k^{-1}}\underset{\sim}{\mathbf{s_k}}\right]} \\
&= \frac{h_k^2(\underset{\sim}{\mathbf{s_k}}^{\intercal}\mathbf{Z_k^{-1}}\underset{\sim}{\mathbf{s_k}})^2}{\sum_{i\neq k}(h_i^2\underset{\sim}{\mathbf{s_k}}^{\intercal}\mathbf{Z_k^{-1}}\underset{\sim}{\mathbf{s_i}}\underset{\sim}{\mathbf{s_i}}^{\intercal}\mathbf{Z_k^{-1}}\underset{\sim}{\mathbf{s_k}}) + \sigma^2(\underset{\sim}{\mathbf{s_k}}^{\intercal}\mathbf{Z_k^{-2}}\underset{\sim}{\mathbf{s_k}})} \\
&= \frac{P_kw_k^2\left(\sum_{l=1}^{N}\frac{a_{lk}^2}{\lambda_l}\right)^2}{\sum_{i\neq k}P_iw_i^2\left(\sum_{l=1}^{N}\frac{a_{lk}a_{li}}{\lambda_l}\right)^2 + \sigma^2\sum_{l=1}^{N}\frac{a_{lk}^2}{\lambda_l^2}}.
\end{aligned} \tag{4.35}$$

In (4.35), we make the assumption that z_n's are uncorrelated. This yields $\mathbf{Z_k} = Q\Lambda Q^{\intercal}$ and $\underset{\sim}{\mathbf{s_k}}^{\intercal}\mathbf{Z_k}^{-1}\underset{\sim}{\mathbf{s_k}} = \underset{\sim}{\mathbf{s_k}}^{\intercal}Q\Lambda^{-1}Q^{\intercal}\underset{\sim}{\mathbf{s_k}}$. We replace $Q^{\intercal}\underset{\sim}{\mathbf{s_k}}$ by $\underset{\sim}{\mathbf{a_k}}$, where $\underset{\sim}{\mathbf{a_k}} = \begin{bmatrix} a_{1k} & \ldots & a_{Nk}\end{bmatrix}^{\intercal}$, and obtain (4.35). Using $Q^{\intercal}\underset{\sim}{\mathbf{s_k}} = \underset{\sim}{\mathbf{a_k}}$, the total power constraint on at each signal component is $\|\underset{\sim}{\mathbf{a_k}}\|_2^2 = \|\underset{\sim}{\mathbf{s_k}}\|_2^2 = 1$.

It is possible to obtain a higher output SNIR by altering the components s_k of the desired signal $S(t)$. That is, when $S(t)$ is subject to the unit energy constraint $\sum_l s_l^2 = 1$, we can maximize

SNIR_h by choosing $s_l = 1$ for any $\lambda_l = \lambda^* = \min_j \lambda_j$. In this case, we have $S(t) = \Phi_l(t)$. Equivalently, we could distribute the signal energy in some arbitrary way over all such $\Phi_l(t)$.

We need to maximize the SNIR_h expression in (4.35).

$$\max_{\substack{\text{s.t.} \sum_{l=1}^{N} a_{lk}^2 = 1 \\ k \in \{1,\ldots,M\}}} \frac{P_k w_k^2 \left(\sum_{l=1}^{N} \frac{a_{lk}^2}{\lambda_l} \right)^2}{\sum_{i \neq k} P_i w_i^2 \left(\sum_{l=1}^{N} \frac{a_{lk} a_{li}}{\lambda_l} \right)^2 + \sigma^2 \sum_{l=1}^{N} \frac{a_{lk}^2}{\lambda_l^2}}, \tag{4.36}$$

so that power distribution is managed among the input nodes in the best possible way in order to minimize the interference.

4.6 Power Consumption of the Synaptic Interference Communication Channel

The probability of a given code is the product of the probabilities for each individual binary value in that code. This is mathematically defined as

$$Pr(C_k) = \prod_{j=1}^{M} Pr(x_j = C_k(j)) \tag{4.37}$$

The average power dissipation of the codebook, i.e., the set of all possible codes, at output node can be calculated as

$$\text{E}[\text{Codebook Power}] = \sum_k Pr(C_k) \, \text{Power}(C_k), \tag{4.38}$$

where $\text{Power}(C_k)$ is the power dissipation of code C_k, which can be calculated as

$$\text{Power}(C_k) = \sum_{j=1}^{M} \text{Power}(C_k(j)) = \left(\sum_{S_j = C_k(j)} \sqrt{P_j} \beta_j w_{ij} S_j \right)^2 = \left(\sum_{S_j = C_k(j), S_j = 1} \sqrt{P_j} \beta_j w_{ij} \right)^2 \tag{4.39}$$

The average power dissipation of the code k at the output node is hence,

$$\begin{aligned} \text{E}[\text{Power}(C_k)] &= \text{E}\left[\left(\sum_{S_j = C_k(j)} \sqrt{P_j} \beta_j w_{ij} S_j \right)^2 \right] = \sum_{S_j = C_k(j)} \sum_{S_l = C_k(l)} h_j \text{E}[S_j S_l] h_l \\ &= \underset{\sim}{\mathbf{h}}^{\mathsf{T}} \text{corr}(\bar{\mathbf{S}}) \underset{\sim}{\mathbf{h}} = \underset{\sim}{\mathbf{h}}^{\mathsf{T}} \Sigma_{\bar{\mathbf{S}}} \underset{\sim}{\mathbf{h}} + \underset{\sim}{\mathbf{h}}^{\mathsf{T}} \mu_{\bar{\mathbf{S}}} \mu_{\bar{\mathbf{S}}}^{\mathsf{T}} \underset{\sim}{\mathbf{h}}, \end{aligned} \tag{4.40}$$

where $\bar{\mathbf{S}} = \begin{bmatrix} S_1 & \ldots & S_M \end{bmatrix}^{\mathsf{T}}$ is the input vector containing binary codeword bits, and $\mu_{\bar{\mathbf{S}}}$ and $\Sigma_{\bar{\mathbf{S}}}$ are its mean and covariance vectors, respectively.

We assume that the inputs are binary and bernoulli distributed with parameter p, and not necessarily i.i.d. Hence, the correlation coefficient ρ_{ij} among S_i and S_j can be determined as

$$\rho_{ij} = \frac{\text{E}[S_i S_j] - p^2}{p - p^2}, \tag{4.41}$$

where $\mathrm{E}[S_i] = \mathrm{E}[S_i^2] = p$. Hence, the entries of the correlation matrix are obtained as $[\mathrm{corr}(\bar{\mathbf{S}})]_{ij} = \mathrm{E}[S_i S_j] = \rho_{ij}(p - p^2) + p^2$, which follows from (4.41). Hence,

$$\begin{aligned}
\mathrm{E}[\mathrm{Power}(C_k)] &= \sum_{i=1}^{M} h_i^2 + \sum_{i \neq j} 2[\mathrm{corr}(\bar{\mathbf{S}})]_{ij} h_i h_j \\
&= \sum_{i=1}^{M} h_i^2 + \sum_{i \neq j} 2[\rho_{ij}(p - p^2) + p^2] h_i h_j \\
&= \sum_{i=1}^{M} P_i w_i^2 + 2 \sum_{i \neq j} [\rho_{ij} p + \overline{\rho_{ij}} p^2] \sqrt{P_i P_j} \beta_i \beta_j w_i w_j, \qquad (4.42)
\end{aligned}$$

where $\overline{\rho_{ij}}$ is the complement of ρ_{ij}, i.e., $\overline{\rho_{ij}} = 1 - \rho_{ij}$.

4.7 Neural Plasticity (Learning) with Synaptic Conductance Modification

In this section, we focus on the actual characteristics of synaptic weights. First, we introduce the mechanism behind the synaptic weight modification. Then, we incorporate the factors, such as synaptic strength decrease and increase functions, synaptic conductance modification characteristics, that enable us to understand these changes, and build an algorithm to describe the synaptic weight update mechanism. Later, in the performance evaluation, in Section 4.8, we compare the ideal synaptic communication rate to actual adaptive communication between neuron terminals. Hence, this section provides a mean to understand the tradeoffs between optimum and actual achievable transmission performance among multiple-access synaptic connections.

Spike-timing-dependent plasticity (STDP) is a biological process that adjusts the strength of connections between neurons in the brain. The process adjusts the connection strengths based on the relative timing of a particular neuron's output and input APs (or spikes). The STDP process is a tentative candidate for a hypothesis that partially explains the development of an individual's brain, especially with regards to long-term potentiation and long-term depression [37].

If an input spike to a neuron tends to occur immediately before that neuron's output spike, then that particular input is made somewhat stronger. If an input spike tends to occur immediately after an output spike, then that particular input is made somewhat weaker, which is called the STDP process. Thus, inputs that might be the cause of the post-synaptic neuron's excitation are made even more likely to contribute in the future, whereas inputs that are not the cause of

the post-synaptic spike are made less likely to contribute in the future. The process continues until a subset of the initial set of connections remain, while the influence of all others is reduced to 0. Since a neuron produces an output spike when many of its inputs occur within a brief period the subset of inputs that remain are those that tended to be correlated in time. In addition, since the inputs that occur before the output are strengthened, the inputs that provide the earliest indication of correlation will eventually become the final input to the neuron.

4.7.1 Spike Timing Dependent Plasticity (STDP) Algorithm

Δt is a random variable standing for the time difference between presynaptic potential and postsynaptic potential at a neuron. We know the relation between δt and synaptic modification. $\bar{g}_{\max} g(\delta t)$ is the modification amount in the peak synaptic conductance. $g(\delta t)$ determines the amount of synaptic modification arising from a single pair of pre- and postsynaptic spikes separated by a time δt.

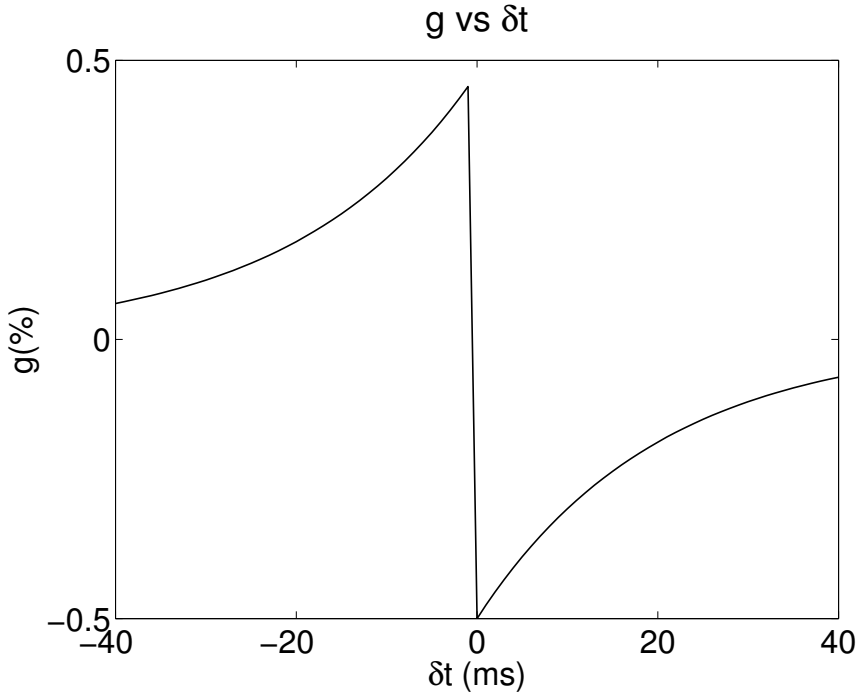

Figure 4.1: Spike Timing Dependent Plasticity (STDP).

Hence, at each time step δt, the peak synaptic conductance is modified as

$$\bar{g}_{\max}(t+\delta t)) = \bar{g}_{\max}(t) + \bar{g}_{\max} g(\delta t), \tag{4.43}$$

where $g(\delta t)$ is the percentage of modification and described as follows

$$g(\delta t) = \begin{cases} A_+ \exp(\delta t/\tau_+) & \text{if } \delta t < 0 \\ -A_- \exp(-\delta t/\tau_-) & \text{if } \delta t \geq 0 \end{cases}, \tag{4.44}$$

where A_+ and A_-, which are both positive, determine the maximum amounts of synaptic modification when δt is close to zero [157]. The parameters τ_+ and τ_- determine the ranges of pre-to-postsynaptic interspike intervals over which synaptic strengthening and weakening occur. In this chapter, to be consistent with [157], we choose $\tau = \tau_+ = \tau_- = 20$ms, and $A_+ = 0.005$ and $A_- = 1.05A_+$, respectively. The STDP algorithm is presented in Fig. 4.1.

In order to determine the modification in conductance, or in exact words, the probability density function (pdf) of conductance modification, we need to extract the pdf of δt.

Under the condition that neurons are *regularly fired*, δt is uniformly distributed, as stated in [2].

$$f_{\Delta t}(\delta t) = \begin{cases} \frac{1}{2\tau} & \text{if } -\tau < \delta t < \tau \\ 0 & \text{if } otherwise \end{cases}, \tag{4.45}$$

Hence, using the following relation for functions of random variables

$$f_Y(y) = f_{\Delta t}(g^{-1}(y)) \left| \frac{dg^{-1}(y)}{dy} \right|, \tag{4.46}$$

the pdf of $Y = g(\Delta t)$ can be obtained as

$$f_Y(y) = \begin{cases} \frac{1}{|2y|} & \text{if } e^{-1}A_+ \leq y < A_+, -A_- \leq y < -e^{-1}A_- \\ 0 & \text{otherwise} \end{cases}. \tag{4.47}$$

Synaptic weight w and the percentage synaptic weight modification δw can be obtained through scaling the synaptic conductance and the percentage of synaptic conductance modification as

$$w = \bar{g}_{\max}/R, \quad \delta w = \bar{g}_{\max} g(\delta t)/R, \tag{4.48}$$

respectively [157].

In this chapter, we assume that the APs are Poisson distributed. Hence, at each synapse, the inter-arrival times are exponential distributed. Furthermore, $\delta t = t_{pre} - t_{post}$ is uniform

Table 4.1: Function and variable definitions.

Definition	**Symbol**	**Value / Range**
EXS conductance	$g_{ex}(t)$	—
INS conductance	$g_{in}(t)$	—
AWGN at axon, mean and standard deviation	μ_N, σ_N	$0, \mathrm{O}\left(10^{-4}\right)$
Peak magnitude of the EPSP waveform	h_p	50 mV
Time at which EPSP reaches its peak	t_p	0.5 ms
Synaptic strength decrease function	$M(t)$	—
Synaptic strength increase function	$P_a(t)$	—
Range of pre-to-postsynaptic interspike intervals over which strenghtening occurs	τ_+	20 ms
Range of pre-to-postsynaptic interspike intervals over which weakening occurs	τ_-	20 ms
Max amount of synaptic modification	A_-	$1.05A_+$
Max amount of synaptic modification	A_+	0.005
Percentage of synaptic conductance modification	$g(\delta t)$	$[-0.5, 0.5]$
Peak synaptic conductance	$\bar{g}_{\max}$	0.035
Peak EXS conductance	$\bar{g}_a$	$0 \leq \bar{g}_a \leq \bar{g}_{\max}$
Peak INS conductance	$\bar{g}_{in}$	$0 \leq \bar{g}_{in} \leq \bar{g}_{\max}$

distributed. Hence, $f_{T_{Post}}(t_{post}) = f_{T_{Pre}}(t_{pre}) * f_{\Delta t}(\delta t)$, where $t_{pre} \sim Pois(\lambda)$ for each EXSs or INSs. Hence, we use the pdfs for t_{pre} and t_{post} to generate the random AP patterns and postsynaptic potentials, respectively.

On arrival of a presynaptic AP, EXS and INS conductances are modified as

$$g_{ex} \Rightarrow g_{ex} + \bar{g}_a, \qquad g_{in} \Rightarrow g_{in} + \bar{g}_{in}, \tag{4.49}$$

where $\bar{g}_a$ and $\bar{g}_{in}$ are the peak synaptic conductances. When there is no presynaptic AP, both g_{ex} and g_{in} decay exponentially as $g_{ex} = \exp(-t/\tau_{EX}), \quad g_{in} = \exp(-t/\tau_{IN})$, where τ_{EX} and τ_{IN} are the EXS and INS time constants, respectively [157]. Synaptic modification is generated through $M(t)$ and $P_a(t)$ functions. These decay exponentially as

$$M(t) = \exp(-t/\tau_-) \qquad P_a(t) = \exp(-t/\tau_+), \tag{4.50}$$

where $M(t)$ and $P_a(t)$ are used to decrease and increase the strength of synapses, respectively. Synaptic conductance is modified according to the arrival of presynaptic AP at EXSs or INSs. If synapse a receives a presynaptic AP at time t, $P_a(t)$ is incremented by an amount of A_+, and $\bar{g}_a -> \bar{g}_a + M(t)\bar{g}_{\max}$. Every time the postsynaptic neuron fires an AP, $M(t)$ is decremented by an amount A_-, and $\bar{g}_a -> \bar{g}_a + P_a(t)\bar{g}_{\max}$. Thus, we need to know the time dependent arrival probability to estimate the synaptic conductance changes. The details of the synaptic modification are described in [157]. In Algorithm 1, we summarize the synaptic weight modification characteristics. The definitions of the functions and variables in the algorithm are

given in Table 4.1.

4.8 Performance Evaluation

In this section, we analyze the SISO and MISO synaptic channels under interference, respectively. First, we evaluate the estimation performance of the SISO and MISO synaptic interference channels and evaluate the MSE for the channel weight estimations. Furthermore, we investigate the SNIR performance of both channels and their achievable rates.

4.8.1 SISO Synaptic Interference Channel Performance Analysis

We first analyze the SISO channel performance, where there exists no interference, but axonal noise only. The rate of the communication channel can be calculated using (4.24). In Fig. 4.2, we show how the Signal-to-Noise Ratio (SNR) varies with the axonal noise variance, i.e., σ^2. The SNR at the soma is sufficiently large provided that the axonal noise variance $\sigma^2 < 0.5 \times 10^{-7}$. In the same figure, we also illustrate the dependence of the capacity of the SISO channel on the axonal noise.

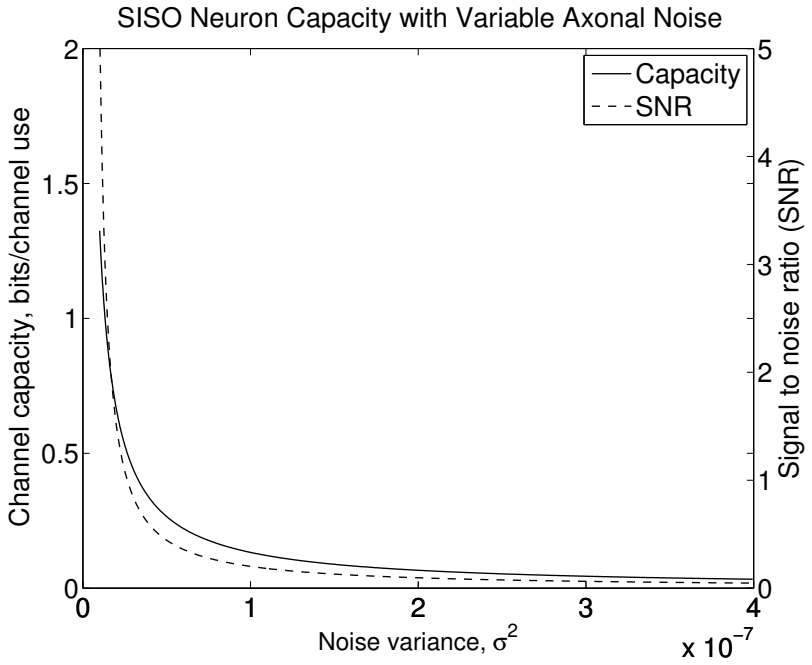

Figure 4.2: Capacity of the SISO neuron channel with respect to noise variance σ^2.

Algorithm 1 Modification of the Synaptic Weight

Require: $t_{pre}(1) = 0, t_{post}(1) = 0$

Ensure: $T = 1000\text{ms}, \Delta t = 0.01\text{ms}$

for $i = 1, i{+}{+}$, while $i < \frac{T}{\Delta}$ **do**
  $t_{pre}(i+1) - t_{pre}(i) \sim \text{Exp}(1/\lambda)$
  $t_{post}(i+1) - t_{post}(i) \sim \text{Exp}(1/\lambda) * f_{\Delta t}(\delta t) * f_{\Delta t}(\delta t)$
end for
for $k = 1, k{+}{+}$, while $k < \frac{T}{\Delta}$ **do**
  $t = t + \Delta t$
  $M(t) = \exp(-t/\tau_{-})$
  $P_a(t) = \exp(-t/\tau_{+})$
  if $t_{pre}(k) = t$ **then** {Synapse **a** receives an AP}
    $t_{pre} \Leftarrow t$
    if AP=1 **then** {Presynaptic AP is excitatory}
      $g_{ex} \Leftarrow g_{ex} + \bar{g}_a$
    else[AP=-1] {Presynaptic AP is inhibitory}
      $g_{in} \Leftarrow g_{in} + \bar{g}_{in}$
    end if
    $P_a(t) \Leftarrow P_a(t) + A_{+}$
    $\bar{g}_a \Leftarrow \bar{g}_a + M(t)\bar{g}_{\max}$
    if $\bar{g}_a < 0$ **then**
      $\bar{g}_a \Leftarrow 0$
    end if
    if $t_{post}(k) = t$ **then** {Postsynaptic neuron fires an AP}
      $t_{post} \Leftarrow t$
      $\delta t \Leftarrow t_{pre} - t_{post}$
      if $\delta t < 0$ **then**
        $g(\delta t) = A_{+}\exp(\delta t/\tau_{+})$
      else[$\delta t \geq 0$]
        $g(\delta t) = -A_{-}\exp(-\delta t/\tau_{-})$
      end if
      $\bar{g}_{\max} \Leftarrow \bar{g}_{\max} + \bar{g}_{\max} g(\delta t)$
      $M(t) \Leftarrow M(t) - A_{-}$
      $\bar{g}_a \Leftarrow \bar{g}_a + P_a(t)\bar{g}_{\max}$
      if $\bar{g}_a > \bar{g}_{\max}$ **then**
        $\bar{g}_a \Leftarrow \bar{g}_{\max}$
      end if
    end if
  else[$t_{pre}(k) \neq t$] {Synapse **a** does not receive an AP}
    $g_{ex} = \exp(-t/\tau_{EX})$
    $g_{in} = \exp(-t/\tau_{IN})$
  end if
end for

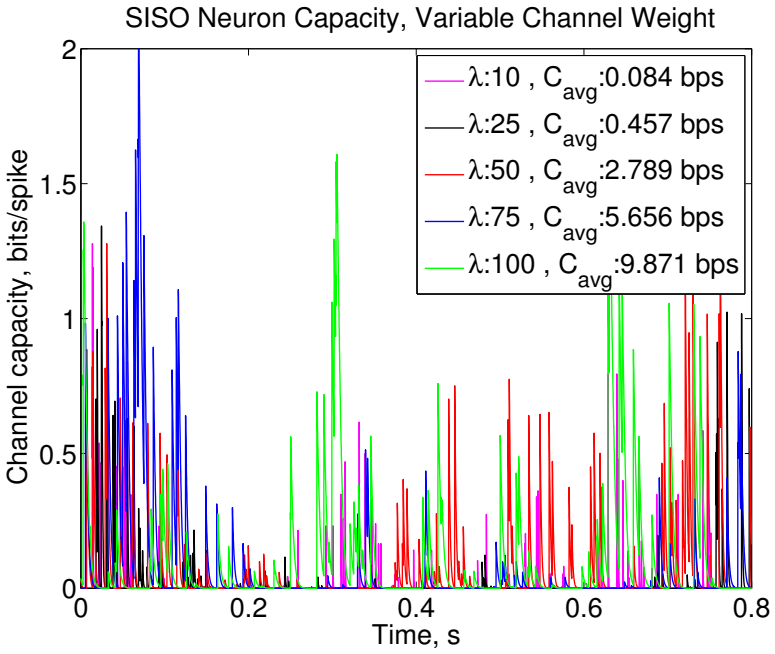

Figure 4.3: Capacity of the SISO neuron channel with respect to time, which is dependent on the actual dynamics of the synaptic channel weight w for $\sigma^2 = 2.5 \times 10^{-8}$.

The neuron synaptic weights are automatically updated by the synaptic channel itself according to spike timing characteristics. This is also summarized in Algorithm 1 in Section 4.7. Using the algorithm, we analyze how the capacity for the SISO interference channel changes adaptively for a low axonal noise variance of $\sigma^2 = 2.5 \times 10^{-8}$. In Fig. 4.3, we illustrate the time course of the capacity in bits/spike for the SISO channel for different AP generation rates. As seen from the figure, the average capacity of the channel is proportional to the AP generation rate. Higher rates are achievable as long as the presynaptic neuron terminal is not saturated.

In Fig. 4.4, we illustrate how the MSE in the channel weight w estimation with respect to the number of excitatory and inhibitory presynaptic inputs changes. In Fig. 4.4, we choose the ratio for the excitatory to inhibitory synapses as 2.5, i.e., $M_{EX}/M_{IN} = 2.5$. As seen from the figure, the estimation error is less than 1×10^{-5} for $M_{EX} \leq 100$. In the same plot, the linear estimation filter output SNIR, i.e., $SNIR_h$, with respect to M_{EX} is also drawn.

Besides the SNR analysis, we also analyze the SNIR and the channel capacity for the SISO synaptic interference channel. The performance result for the communication rate is shown in Fig. 4.5 for varying ratios of M_{EX} to M_{IN}. As the M_{EX}/M_{IN} ratio increases, the interference

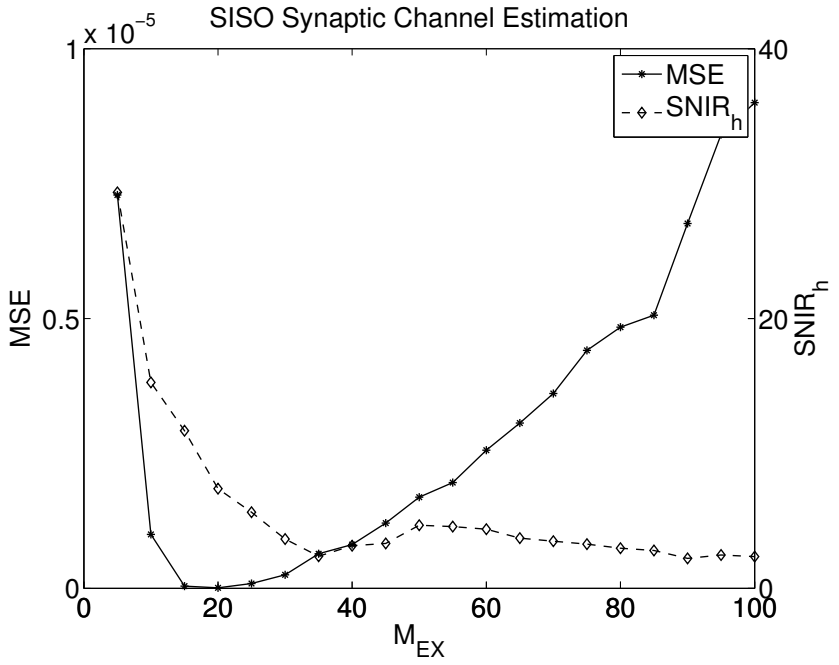

Figure 4.4: MSE performance of weight estimation of the SISO neuron interference channel for $M_{EX}/M_{IN} = 2.5$.

on the SISO synaptic interference channel increases. Hence, the communication rate drops. For $\sigma^2 = 2.5 \times 10^{-8}$, for small number of interfering presynaptic inputs, communication rates around 3 bits/channel use are achievable.

4.8.2 MISO Synaptic Interference Channel Performance Analysis

In this section, we extend the interference analysis for SISO synaptic interference channel to MISO synaptic interference channel. We analyze the interference depending on the synaptic weights, i.e., strengths. We assume that at least one presynaptic input is strong, i.e., at least one input has $w = \bar{g}_{\max}$. In the performance analysis, other inputs are given weights $w = \alpha\bar{g}_{\max}$, where $\alpha < 1$. We denote the number of strong and weak presynaptic inputs by N_S and N_W, respectively.

In Fig. 4.6, we illustrate how the total MSE in the channel weights w's estimation with respect to M_{EX}. In Fig. 4.6, we use different number of strong inputs N_S and weak inputs N_W with variable synaptic strengths. In Fig. 4.6(a), the MSE for $N_S = 2$ is investigated for varying number of presynaptic inputs. The weak presynaptic inputs are assigned an average weight of $w = \alpha\bar{g}_{\max}$, where $\alpha = [0.1, 0.7]$ is incremented with a step size 0.2. As α increases, the total

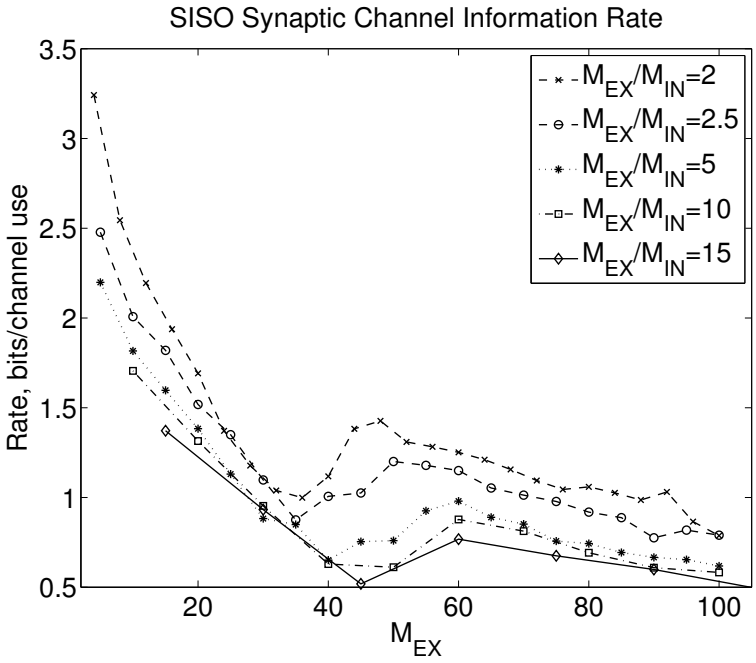

Figure 4.5: Communication rate of the SISO neuron interference channel for various values of M_{EX} and M_{IN}, where $\sigma^2 = 2.5 \times 10^{-8}$.

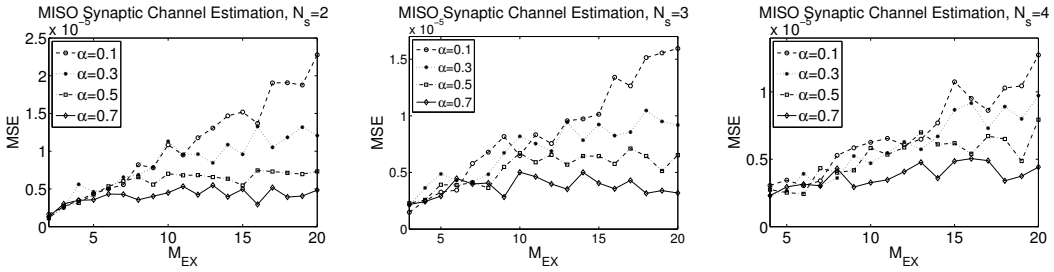

(a) (b) (c)

Figure 4.6: MISO synaptic interference channel estimation, (a) MSE for $N_S = 2$, (b) MSE for $N_S = 3$, and (c) MSE for $N_S = 4$, $\sigma^2 = 2.5 \times 10^{-4}$.

weight of the presynaptic inputs, and the output SNR increases. Therefore, the estimation performance increases, and thus, the MSE drops. The analysis is repeated for $N_S = 3$ and $N_S = 4$ in Fig. 4.6(b) and 4.6(c), respectively. Performance analyses show that as the number of strong inputs, i.e., N_S, increases, lower MSE values could be achievable.

We also investigate the communication rate of the multiple-access synaptic interference channel. We analyze the communication rate of the multiuser channel under varying number of M_{EX}'s with varying axonal noise levels. The dependence of the rate on the axonal noise and channel weight are shown in Fig. 4.7. In Fig. 4.7(a), the channel capacity in bits/channel

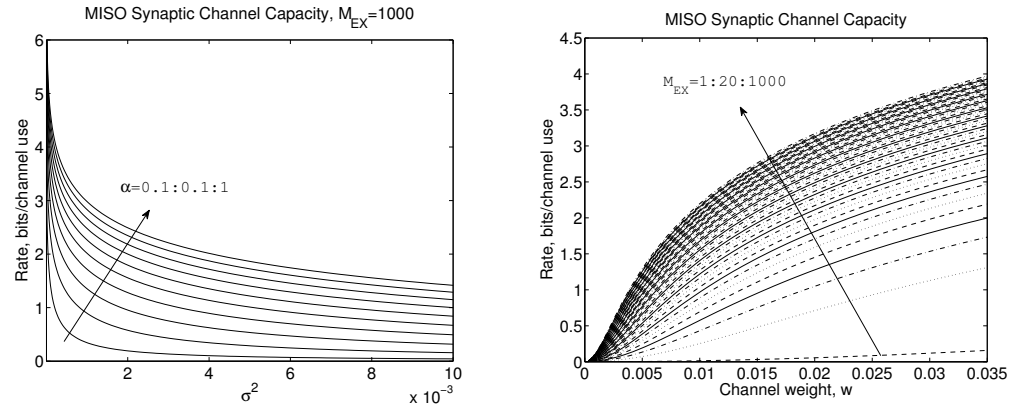

(a) (b)

Figure 4.7: MISO synaptic interference channel communication rate with respect to (a) noise variance σ^2, and (b) channel weight w, where $\sigma^2 = 2.5 \times 10^{-4}$.

use for varying synaptic strengths and for $M_{EX} = 1000$ and a high level of axonal noise with $\sigma^2 = 2.5 \times 10^{-4}$ is investigated. As α increases, the bits/channel use capacity increases. In Fig. 4.7(b), the capacity in bits/channel use with respect to channel weight, i.e., w, is shown. As M_{EX} increases, the total rate of communication is enhanced. Furthermore, as w increases towards the maximum, the maximum achievable rate per channel use can be incremented. As seen from Fig. 4.7(b), as the number of strong inputs increases, the total communication rate is enhanced. Furthermore, as the number of weak inputs increases, the rise in the output rate is rather incremental. Here, the axonal noise variance is taken as $\sigma^2 = 2.5 \times 10^{-4}$.

In Fig. 4.8, we illustrate how the communication rate for the MISO channel changes depending on the variable synaptic strengths of multiple users and the number of M_{EX} and axonal noise variance. In Fig. 4.8(a), the communication rate in bits/channel use for $\sigma = 10^{-4}$ is investigated for varying number of presynaptic inputs. The presynaptic inputs are assigned an average weight of $w = \alpha \bar{g}_{\max}$, where $\alpha = [0.1, 0.7]$ is incremented with a step size 0.2. As α increases, the total weight of the presynaptic inputs, and the output rate increases. The analysis is repeated for $\sigma = 10^{-3}$, $\sigma = 10^{-2}$ and $\sigma = 10^{-1}$ in Fig. 4.8(b), 4.8(c) and 4.8(d), respectively. Performance analyses points out the downward trend of the total rate of synaptic communication as the axonal variance increases.

In Fig. 4.9, using the Algorithm 1 presented in Section 4.7, the time course of MISO synaptic channel capacity is investigated. Using the algorithm, we analyze how the capacity for the MISO interference channel changes adaptively for a low axonal noise variance of $\sigma^2 = 2.5 \times 10^{-8}$. In Fig. 4.9, we illustrate the time course of the capacity in bits/spike for the MISO

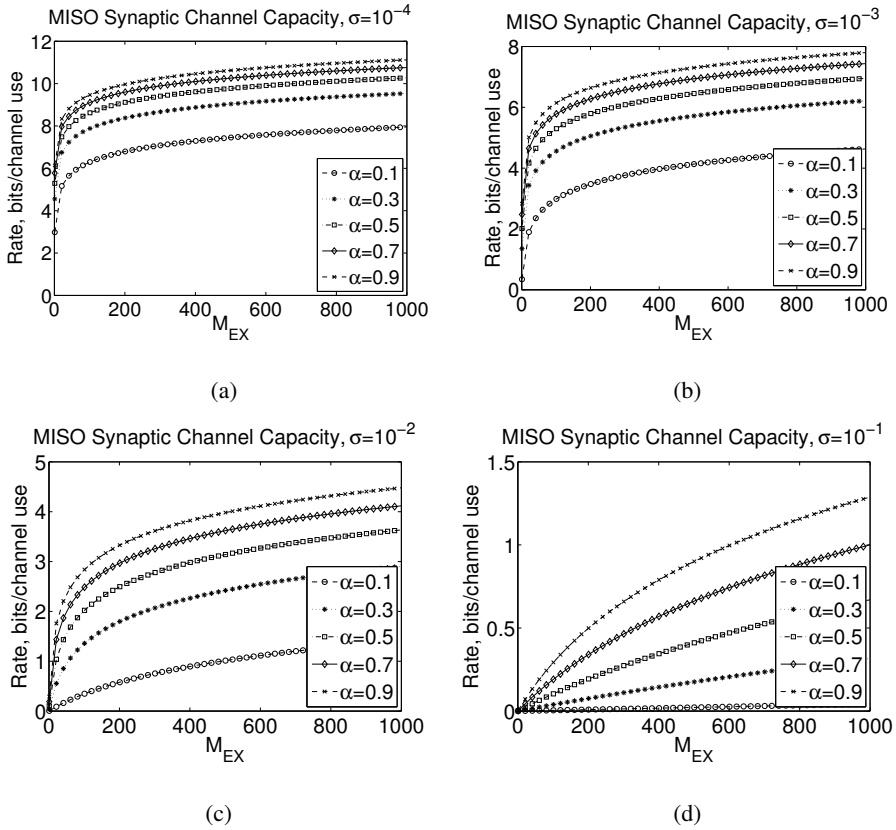

Figure 4.8: MISO synaptic interference channel capacity for (a) $\sigma = 10^{-4}$, (b) $\sigma = 10^{-3}$, (c) $\sigma = 10^{-2}$, and (d) $\sigma = 10^{-1}$.

channel for AP generation rate $\lambda = 10$ $spike/s$ for different M_{EX} values. As seen from the figure, the average capacity of the communication channel is incremented as M_{EX} increases, and higher rates are achievable at the postsynaptic neuron terminal. Comparing Fig. 4.9 to Fig. 4.8, we infer that as the number of excitatory synapses increases, MISO synaptic channel performs close to the maximum channel capacity curves drawn in Fig. 4.8(a).

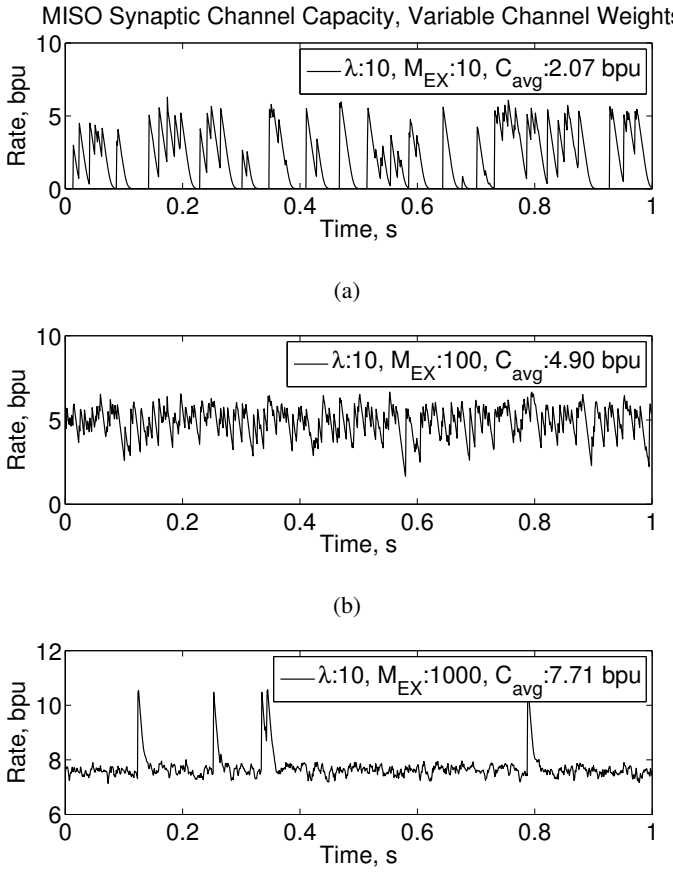

Figure 4.9: MISO synaptic interference channel capacity for $\sigma^2 = 2.5 \times 10^{-8}$, (a) for $M_{EX} = 10$, (b) for $M_{EX} = 100$, and (c) for $M_{EX} = 1000$.

CHAPTER 5

RATE-DELAY TRADEOFF WITH NETWORK CODING IN MOLECULAR NANONETWORKS

Molecular communication is a novel nanoscale communication paradigm, in which information is encoded in messenger molecules for transmission and reception. However, molecular

communication is unreliable and has highly varying long propagation delays mainly due to the stochastic behavior of the freely diffusing molecules. Thus, it is essential to analyze its delay characteristics, as well as the tradeoff between the rate and delay, in order to reveal the capabilities and limitations of molecular information transmission in nanonetworks. In this chapter, first, a new messenger-based molecular communication model, which includes a nano-transmitter sending information to a nano-receiver, is introduced. The information is encoded on a polyethylene molecule, $CH_3(CHX)_nCH_2F$, where X stands for H and F atoms representing 0 and 1 bits, respectively. The emission of the molecules is modeled by puffing process which is inspired by the alarm pheromone release by animals in dangerous situations. In this work, the rate-delay characteristics of this messenger-based molecular communication model are explored. Then, a Nano-Relay is inserted in the model, which XOR's the incoming messages from two different nanomachines. Performance evaluation shows that indeed, a simple network coding mechanism significantly improves the rate given delay of the system, and vice versa.

5.1 Introduction

Advances in nano and biotechnology require the development of biocompatible nanomachines, which have fundamental roles in complex bio-hybrid structures. These machines have a wide range of duties such as assisting the biological cells in performing the sustainment of vital activities and taking charge of disorders in biological entities, i.e., molecules, cells, organs. In order to attain macro scale objectives, nanomachines need to communicate with each other to realize cooperative tasks, which leads to the development of nanoscale communication techniques. Molecular communication, as one of these techniques, is inspired by the natural behaviors of the existing biological structures, which paves the way for upcoming communication applications in nanoscale environments.

Since molecular communication inherently exists in nature, it is biocompatible, biostable and it has also the capability of operating at nanoscale. Hence, it may be applied to a wide variety of areas such as environmental applications, which include water and air pollution control, industrial applications, which include development of nanorobots, nano-processors and nano-memory, and medical applications, which are drug delivery, disease treatment and health monitoring [3].

Molecular communication differentiates from standard wireless communication applications with its dramatically higher and varying propagation delays [121], operational uncertainties and proneness to noise and interference. To design nanomachines that compensate these drawbacks, the operation limits of molecular communication systems should be thoroughly investigated.

Although molecular communication is a very new alternative for nanoscale communication, the concept is physically implemented. In [115], Cu^{2+} ions are propagated where gemini peptid lipid is used as a molecular switch which acts as an artificial receptor. With the help of fluorescence microscopic observations, in [174], the hybridization of DNA is used to employ a molecular communication path between vesicles. A physical reception mechanism is discussed in [149] where a biomimetic nanosensory device is implemented for detection and amplification of biologically important entities.

In the literature, the studies are concentrated on theoretical models for molecular communication [129], analysis of upper and lower bounds on information rates [46], capacity of molecular channels [11], [9], noise analysis of molecular channels [131], and gain and delay with respect to input frequency and transmission range [129]. None of these studies investigates the rate-delay tradeoff in molecular domain, which is very crucial to determine the possible application areas. One of these areas is delay tolerant networks used for applications such as health monitoring, drug delivery, and molecular computers [3], [150].

Molecular communication is unreliable and suffering from long propagation delays, even up to hours [54], due to diffusion of large molecules. Moreover, the nanomachine spends time generating multiple redundant molecules for a single message to guarantee the delivery of the message and preparing them for transmission. This unfortunately yields low rates. Therefore, a joint rate and delay analysis for molecular communication is needed to investigate its capabilities and shortcomings.

In classical communications domain, the rate-delay tradeoffs are examined to accommodate different types of traffic in electro-magnetic networks with composite links [96], to optimize rate for two-layered, namely, physical and network packet transmission system [167], and mitigate delay in multipath routed and network coded networks [170]. Albeit these studies point out the rate-delay tradeoffs for classical communication domains, no study has concentrated on the trade-off between rate and delay in molecular communications, which led us to

this very study.

In this chapter, a new diffusion-based model for molecular communication, whose main distinction with respect to previously proposed models, such as [11] and [129], arises from the utilization of a messenger molecule as information carrier, is introduced. A hydrofluorocarbon molecule, fluorinated polyethylene, is chosen as the messenger molecule on the grounds of biocompatibility of hydrofluorocarbons, which are the basic molecules used as reversible oxygen carriers in artificial blood formulations [176].

We analyze the stochastic nature of a basic point-to-point messenger-based molecular communication model with one nano-transmitter and one nano-receiver, named Nano-Alice and Nano-Bob, respectively, from information encoding and transmission up to reception and decoding processes. A set of message molecules, i.e., puff, is generated and transmitted from the surface of the spherical shaped nano-transmitter. Furthermore, a nanonetwork consisting of two transmitting and receiving nanomachines and a nano-relay is established. Then, a simple network coding is applied on this nanonetwork, and the rate and delay for both uncoded and network coded cases are derived to reveal the tradeoff between propagation delay and reception rate. With network coding, we attain higher rates with the same delay compared to the uncoded case, and lower delays for the same rate of operation, as discussed in Section 5.4.

The remainder of this chapter is organized as follows. Using the messenger-based molecular communication model introduced in Section 5.2, we investigate the delay characteristics of this model. In Section 5.3, to examine an analysis of rate-delay tradeoff over a networking case with a single Nano-Relay, a simple network coding is applied. The expressions derived in Section 5.2 and 5.3 are evaluated numerically and the results on the rate-delay tradeoff are discussed thoroughly in Section 5.4. The improvement achieved by network coding is highlighted by comparing the delays in both coded and uncoded cases.

5.2 A Messenger-Based Molecular Communication Model

Messenger-based molecular communication inherently exists in different types of cells from the simplest prokaryotic cells such as bacteria using quorum sensing to more complex mammalian cells using intracellular communication [17]. For example, nitric oxide, an intracellular messenger molecule, provides cell-to-cell communication system in mammalians,

which is exploited in artificial intracellular communication for the purpose of gene regulation [17]. Since messenger-based molecular communication is ubiquitous, it is crucial to build an analytical model of it by benefiting from inherent communication mechanisms, which also promotes nanomedicine applications.

In this section, a messenger-based molecular communication model is proposed. This messenger-based model includes partially fluorinated polyethylene messenger molecules, $CH_3(CHX)_nCH_2F$, carrying n bits of information on predefined X atoms by diffusion. X is replaced by an Hydrogen (H) or Fluorine (F) atom representing the bit 0 or 1. n can reach up to 10^9 bits, which is a practically high amount of information for a single messenger molecule despite its longer propagation delay [54]. Therefore, the messenger-based approach is an intriguing case for realizing the rate-delay tradeoff.

In this approach, the transmitter only supplies the kinetic energy for the messenger molecules to reach to the emission boundary, which is defined in Section 5.2.2. When the molecules arrive to the emission boundary, the transmitter releases these molecules into the fluid medium where these molecules are propagated by Brownian motion with drift, where the drift arises from the mean drift velocity of the fluid medium. Then, they reach the receiver boundary where the information embedded on them is decoded.

The transmitter and the receiver mentioned in this model are nanomachines which are capable of performing some simple predefined tasks. In our model, the transmitter nanomachine is capable of producing molecules on which the information is encoded, combining them into puffs, and releasing the puffs to the medium. After, the receiver nanomachine, which has the receptors that bind the propagating molecules, picks the molecules, it decodes them. The radii of these nanomachines are assumed to be a few nanometers. Hence, they are capable of handling fluorinated polyethylene molecules, the size of which is in the order of $10^{-2} \times n\ nm^3$. Moreover, the nanomachines are assumed to be separated by a few micrometers so that the size of the nanomachines are negligible compared to the distance travelled by the messenger molecule [54].

Our model embodies five main processes; information encoding process, transmission process, propagation process, reception process and information decoding process. In the following subsections, we investigate these five main processes.

5.2.1 Information Encoding Process

In this model, it is assumed that nanomachines use information-storing molecular packets, i.e., messenger molecules for the transfer of information. These molecular packets are similar to data link-layer packets in classical wireless communication systems. These two differ in that the molecular packets store information physically on themselves so that they cannot interfere with each other. Besides, the messenger molecules are assumed to be bioinactive, i.e., not easily corrupted or destroyed by natural processes. They are easily recognized by nano-receptors such as molecular pumps or sorting rotors due to the special structure of these molecules containing a distinctive head. Thus, the entire message need not be read in order to identify the intended recipient [54].

The partially fluorinated polyethylene molecules [54] are candidates for such messenger molecules. Suggested in [44] for nanocomputer memory systems, a partially fluorinated polyethylene messenger molecule is in the form $CH_3(CHX)_nCH_2F$, where X stands for H and F atoms representing 0 and 1 bits, respectively. These coded atoms are in one side of the chain while the other side of the chain is full of H atoms so that the receiver can recognize the coded side easily, which facilitates reading. Otherwise, since the head and tail of the molecule have the same symmetry axis as seen in Fig. 5.1, the receiver cannot decide which side is coded. To overcome the ambiguity, only one side of the molecule is coded and the other side is filled with H atoms. Hence, the receiver can decide which side is coded.

This molecule carries 50% H and 50% F atoms on the coded side of the molecule to equalize the molecular weight, hence the diffusion coefficient of all the intended symbols, which simplifies the analytical complexity of this work. Still, for any source distribution, the ratio of the H and F atoms can be kept fixed doing an appropriate encoding at the nano-transmitter. However, for the operation of the proposed model, any ratio of H and F atoms is feasible in the expense of unequal diffusion coefficients.

The messenger molecule has a message molecule density of $r_{message} \sim 1000\ kg/m^3$ and message molecule volume $V_{message} \sim (3.82 \times 10^{-29})n\ m^3$ [54]. Since one molecule carries n bits of information in volume $V_{message}$, the information density of this molecule is calculated as $d_{message} \sim 26\ bits/nm^3$ which gives a distinguishably higher density when compared to DNA whose information density is $\sim 1\ bit/nm^3$ [54]. This is the reason why partially fluorinated

polyethylene molecule is preferred to DNA in this study. During preparation for transmission, these hydrofluorocarbon molecules with $n > 20$ can be wound onto a bobin or can be folded into a compact spherical shape ensuring easy reading and high packing density [44].

A partially fluorinated polyethylene molecule can carry l_m bits of information which is approximately given by

$$l_m \approx \frac{4}{3}\pi r^3 d_{message}, \tag{5.1}$$

where r is the spherical radius of the messenger molecule and $d_{message}$ is the information density [54]. $n \neq l_m$ because of the non-information carrying H atoms on one side of the molecule for easy reading and the allocation of some part of n bits for extra information about the message such as message ID. In this study, to ease the decoding process at the receiver nanomachine, we allocate $n - l_m$ bits (a few) at predefined locations for message ID declaration. Therefore, actual information density is slightly less compared to $d_{message}$. The distinctive head and tail structure of the molecule, CH_3 and CH_2F forming the two ends of the molecule, provides a decoding order for the message in such a way that the bits carrying the extra information such as message ID are read before the entire message.

To increase the information carrying capacity of messengers, one needs to create larger molecules. However, larger molecules diffuse more slowly in liquid environment. According to the Einstein-Stokes relation [98], the diffusion coefficient D is inversely related with the size of the particles, i.e.,

$$D = \frac{k_B T}{6\pi\eta r}, \tag{5.2}$$

where k_B is Boltzmann's constant, T is the absolute temperature and η is viscosity.

The information encoding process described here can exploit a molecular modulation technique such as Molecule Shift Keying modulation (MoSK) introduced in [89]. This modulation scheme requires 2^n different molecules to represent n bit logical information. For the transmission of an intended symbol, one of these molecules are released by the transmitter and the receiver decodes the intended symbol according to the type of the received molecule. Inspired by [89], a $n = 2$ bit constellation diagram for Quadruple MoSK realized by fluorinated polyethylene is shown in Fig. 5.1.

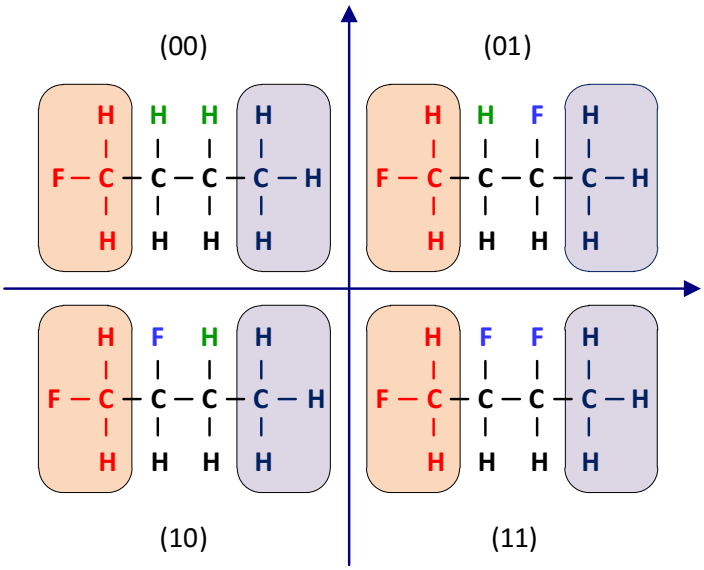

Figure 5.1: Constellation diagram for QMoSK modulation, $n = 2$.

5.2.2 Transmission Process

The transmitter nanomachine is assumed to have a spherical shape and the messenger molecules are released to the medium from the boundary of the nanomachine. This emission process is uniformly distributed over this spherical boundary called emission boundary. If a living cell is chosen as the nanomachine, the emission boundary corresponds to the cell membrane.

The transmission strategy is chosen as *puffing of messengers*, i.e., instantaneous emission of puffs which are sets of released message molecules. Since the information is encoded in the type of molecule and not in its concentration, the transmitter does not need to continuously fill the medium with molecules. Instantaneous emission is a more suitable scheme than continuous emission for the messenger-based communication model proposed in this study. As the model relies on the diversity of message molecules, it requires rapid fade out to increase the number of messages that can be transmitted by a single transmitter nanomachine [125]. In nature, puffing is usually used for modeling pheromone release in alarm situations such as presence of predators and enemies, fight, injured conspecifics, exposure to toxic compounds [173]. Those alarm situations require a sudden release of a limited amount of pheromones. Examples include insect pheromones dispersed within forest canopies [160] and pheromones of ant *Acanthomyops claviger* [93].

When a nanomachine needs to transmit a single message, it generates puffs of N_M molecules. The probability of successful transmission of the message with just one puff is very low, therefore, for a single message N_P puffs are sent. Thus, a single message consists of N_P puffs of N_M molecules.

Accordingly, the transmission rate can be defined as

$$R^{(TX)} = \frac{l_m}{N_P T_M}, \tag{5.3}$$

where T_M is the process time required to prepare a puff. The transmitter nanomachine does not prepare the molecules in advance, and does not store the molecules generated for future use. This is mainly due to the sudden need for communication with pheromones in alarm situations [173]. It requires $N_P T_M$ time to produce a message of N_P puffs, with each puff containing N_M molecules to be released immediately after message generation.

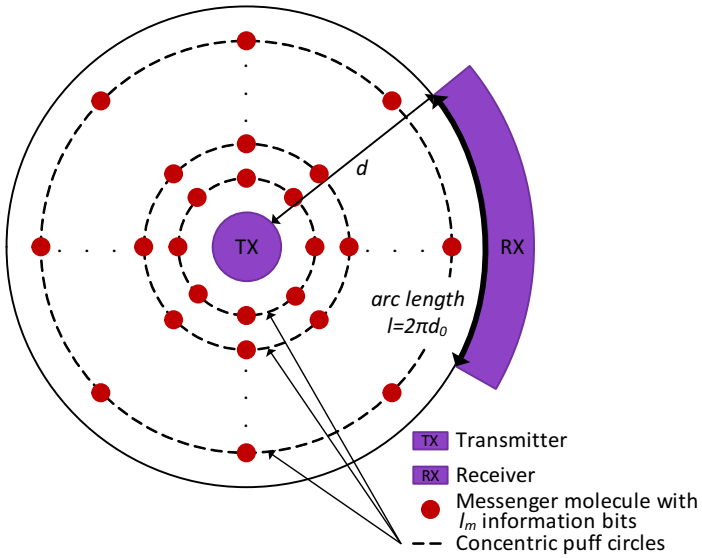

Figure 5.2: Particle propagation and detection processes.

5.2.3 Propagation Process

The position of a messenger molecule due to random thermal noise as a function of time is modeled as a Brownian motion. The radial position of a molecule with respect to the transmitter is a stochastic process given by

$$R_t = \nu t + \sqrt{2D} W_t, \tag{5.4}$$

where W_t is a standard Wiener process, v is the mean drift velocity of the medium, D is the diffusion coefficient.

Therefore, the first hitting time, τ, to a spherical surface at a distance d away from the emission boundary is distributed according to an inverse Gaussian probability density function [158], i.e.,

$$\tau = min\{\tau | R_t = d\} \sim f_\tau(\tau), \tag{5.5}$$

$$f_\tau(\tau) = \frac{d}{\sqrt{4\pi D\tau^3}} \exp\left(-\frac{(v\tau - d)^2}{4D\tau}\right), \quad \tau \geq 0. \tag{5.6}$$

The random variable τ can also be defined as the propagation delay of a single puff for a distance d.

5.2.4 Reception Process

A messenger molecule is assumed to be received at the time instant when it hits the boundary of the receiver and it is removed after the decoding takes place.

To calculate the reception rate, an interval of time beginning with the reception of the first message, t_1, and ending with the reception of the $(k+1)^{th}$ message, t_{k+1}, is considered. The length of this time interval is

$$\Delta t = t_{k+1} - t_1. \tag{5.7}$$

Assume that $t_{k+1} - t_1 = \tau_{k+1} - \tau_1 + kN_P T_M$, where τ_{k+1} is the propagation delay for the $(k+1)^{th}$ message and τ_1 is the propagation delay for the first message. We assume that $E\{\tau_{k+1}\} = E\{\tau_1\}$ for all k regarding that the channel imposes the same expected delay to all messages. Hence, expected length of Δt can be calculated by

$$E\{\Delta t\} = kN_P T_M. \tag{5.8}$$

During this time interval, kl_m information carrying bits are received. Thus, reception rate is expressed as

$$R^{(RX)} = \frac{l_m}{N_P T_M}. \tag{5.9}$$

Having a closed-form expression for rate, we try to obtain an analytical expression for delay. To obtain the *Cumulative Distribution Function* (CDF) of delay, the probability of receiving the message is considered first.

If the reception boundary is the entire spherical surface that encapsulates the transmitter source, then, the probability of receiving the message before time t can be denoted by $P_M(t)$. It is the probability of the complementary event that none of $N_M N_P$ molecules that are released for one message is received before time t.

For each molecule of the i^{th} puff, $F_\tau(t-iT_M)$ is the probability that it is received before time t, hence, $1-F_\tau(t-iT_M)$ is the probability that it is not received. Thus, for that entire puff, $(1-F_\tau(t-iT_M))^{N_M}$ is the probability that all N_M molecules of i^{th} puff is not received before time t. Multiplying these probabilities for all puffs of a message, we obtain $\overline{P_M(t)} = \prod_{i=1}^{N_P}(1-F_\tau(t-iT_M))^{N_M}$, representing the probability that none of $N_M N_P$ molecules is received before t. Finally, the probability that at least one molecule carrying the intended message is arrived, P_M, can be found by $1-\overline{P_M(t)}$. $P_M(t)$ can be expressed by

$$P_M(t) = 1 - \prod_{i=1}^{N_P}[1-F_\tau(t-iT_M)]^{N_M}, \tag{5.10}$$

where $F_\tau(\tau)$ is the CDF of the propagation delay τ. For simplicity, the initiation time of the message, i.e., release time of the first puff is taken as 0.

However, the reception boundary cannot encapsulate the transmitter source practically. Thus, there should be a probability P_d for detecting a messenger molecule when it is d away from the emission boundary. We assume that P_d is inversely proportional to the distance because it can be expressed as the ratio of the length of receiving boundary, l ($= 2\pi d_0$, for the shell shaped receiver), to the perimeter of the circle at distance d. P_d is expressed by

$$P_d = \begin{cases} 1, & \text{if } d \le d_0 \\ \frac{d_0}{d}, & \text{if } d > d_0 \end{cases}, \tag{5.11}$$

where the constant d_0 is proportional to l and depends on the geometry of the receiver. Up to a critical distance, d_0, i.e., in the vicinity of the transmitter, the probability of reception is close to 1. However, when the receiver moves away beyond d_0, the receiving boundary do no longer cover the nano-transmitter. Hence, the probability of receiving falls below 1. As the receiver has a spherical shape, the receiving boundary cannot fit the arc with radius d completely as the shell shaped receiver shown in Fig. 5.2. Thus, d_0 is not directly equal to $l/2\pi$ but it is proportional with $l/2\pi$ in this case.

At a distance d, the probability that a molecule is not received is $1-P_d$. Hence, the probability that none of the N_M released molecules for a puff is received becomes $(1-P_d)^{N_M}$. When N_P

puffs are released, the probability for receiving the message as time goes to infinity becomes

$$P_r = 1 - (1 - P_d)^{N_P N_M}. \tag{5.12}$$

Then, to calculate the delay, we are conditioned that the message has to be received. Otherwise, we cannot define a finite delay for a non-received message. The probability $P_M(t)$ in (5.10) can be modified as a conditional probability, where M is the event that the message is received, i.e.,

$$P_M(t|\mathrm{M}) = \frac{1 - \prod_{i=1}^{N_P} \left[1 - P_d F_\tau(t - iT_M)\right]^{N_M}}{P_r}. \tag{5.13}$$

The probability that the message is received before t corresponds to the CDF of the message propagation delay, i.e., $F_{\tau_M}(\tau_M) = P_M(t|\mathrm{M})$. Note that $P_M(t|\mathrm{M})$ goes to 1 as t goes to infinity, hence, it can be the CDF of the message propagation delay τ_M given that the message M is received as proposed.

Since τ_M is a nonnegative random variable, the expected message propagation delay can be calculated by integrating the complementary CDF of τ_M,

$$E\left\{\tau_M|\mathrm{M}\right\} = \int_0^\infty \left(1 - F_{\tau_M}(t)\right) dt. \tag{5.14}$$

For a single puff containing a single molecule, i.e., $N_M = 1$ and $N_P = 1$ in (5.12) and (5.13), the CDF of the delay denoted by $F_{\tau_M}(t)$ becomes equal to $F_\tau(t)$ whose pdf is given in (5.6). Hence, the expected message propagation delay is equal to d/ν, the expected value of $F_\tau(t)$, which is an inverse gaussian distribution. This expected delay is utilized in Section 5.3 to approximate puff propagation delays.

5.2.5 Information Decoding Process

Decoding of the messages is realized as the demodulation of the incoming molecule stream according to MoSK described in Section 5.2.1. This demodulation is based on differentiating between different molecule types containing different numbers of H and F atoms. In nature, such a differentiating mechanism is found in pheromone receptors. For example, a very sensitive reception of pheromones exists in a male moth who can recognize potential mates, prey, and specific features of the environment such as food sources through the antennas placed on its olfactory system [94]. The olfactory system of moths produces electrical signals in

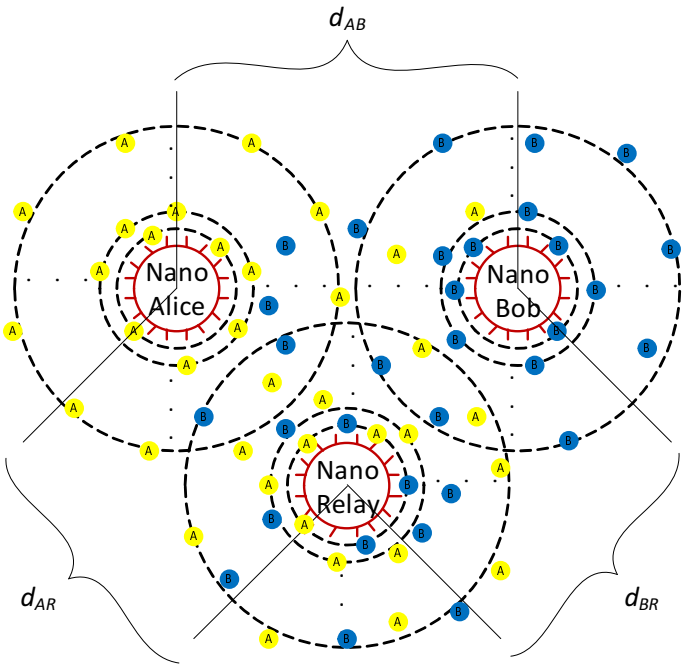

Figure 5.3: A simple uncoded network mechanism.

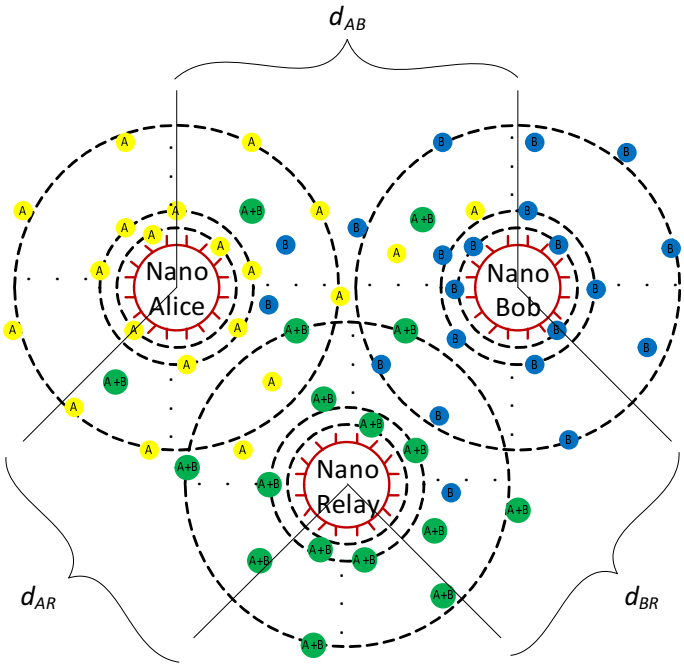

Figure 5.4: A simple network coding mechanism.

their neurons according to the type of the received pheromone. A similar system of antennas may be used by the receiver nanomachine which will process the information brought by the messenger molecule.

Another decoding mechanism may be constructed to read the encoded information on the molecule, bit by bit using a convenient probe as suggested in [23]. In such a system, the receiver nanomachine may be equipped with the specific C_5H_5B or $C_3H_3N_2B$ probe to identify the H or F atom using the difference in interaction energies between B atom of the probe and H/F atoms of the polyethylene molecule.

In this study, we assume that the receiver nanomachines use the second mechanism described above. After decoding the message with the probing mechanism, the receiver needs to reveal the meaning of the decoded bits. As suggested in Section 5.2.1, some portions of the bits, i.e., $n-l_m$ bits, may be used to encode a message ID which will be the same for all N_M molecules of all N_P puffs carrying the same message.

A nanomachine may receive a message multiple times since there are redundant messenger molecules in the communication medium. Upon detecting the first molecule for a message, it ignores the remaining molecules carrying the same message. Once a message is received and its ID is decoded, the subsequent molecules, which have the same ID, are not taken into consideration. Assuming that the puff preparation time T_M is the same for each type of molecule, the whole message preparation time is $N_P T_M$. To reduce the energy for decoding the redundant molecules, the receiver nanomachine may wait a time proportional to $N_P T_M$, defined as $T_{wait} = \alpha N_P T_M$, where $\alpha > 1$, after the reception of the first message since a second message cannot be generated by the transmitter in a time duration of $N_P T_M$.

5.3 Rate-Delay Tradeoff with Network Coding

In this section, a mathematical model is derived for a relay network to characterize the rate-delay tradeoff of a molecular nanonetwork. This section also describes a simple network coding mechanism that improves the rate-delay performance of the molecular nanonetwork.

Consider a relay network containing a Nano-Relay as shown in Fig. 5.3, where Nano-Alice and Nano-Bob need to send each other a message in a sufficiently long time interval.

Nano-Alice and Nano-Bob function as both nano-transmitter and nano-receiver. These nanomachines realize all the five main processes mentioned in Section 5.2. Thus, rate and delay derivations carried out in Section 5.2 are valid for both Nano-Alice and Nano-Bob. Assume

also that Nano-Alice and Nano-Bob are not in the communication range of each other but in the communication range of Nano-Relay, i.e., $d_{AR} < d_0, d_{RB} < d_0, 2d_0 > d_{AB} > d_0$. This means that the messages of Nano-Alice and Nano-Bob are guaranteed to be received by Nano-Relay. Nano-Relay can operate both as a nano-transmitter and a nano-receiver. Additionally, Nano-Relay combines the incoming molecules from Nano-Alice and Nano-Bob and determines whether to generate new molecules or relay the incoming molecules. Depending on the arrival times of molecules sent from Nano-Alice and Nano-Bob, relay queues the molecules to be forwarded.

In order to improve the rate-delay characteristics of this system, in the second part of this section, we introduce a basic network coding mechanism where Nano-Relay XORs the messages coming from Nano-Alice and Nano-Bob. In molecular level, such an XOR operation is feasible. Although there is no study on XOR operation for fluorinated polyethylene, an XOR gate can be implemented at the molecular level by pseudorotaxane as described in [38].

In this scheme, the ultimate goal is that Nano-Alice and Nano-Bob exchange a pair of messages. Without network coding, Nano-Alice sends its message to Nano-Relay which forwards it to Nano-Bob and Nano-Bob sends its message to Nano-Relay which forwards it to Nano-Alice. Thus, we have four transmissions in total.

When the network coding mechanism is considered, Nano-Alice and Nano-Bob send their messages to Nano-Relay which XORs and sends the combined message back to both Nano-Alice and Nano-Bob which requires a total of three transmissions instead of four. By doing so, we decrease the total number of transmissions by one. As Nano-Alice and Nano-Bob know their sent message, they can decode Nano-Relay's message and extract the messages of their respective partners. Thus, the molecular network coding can be an efficient way of increasing the rate since the same information is sent now with less number of transmission, i.e., in a shorter time interval.

As described in Section 5.2, a partially fluorinated polyethylene molecule carries l_m bits of information by H and F atoms, denoting binary 0 and 1, respectively. Since a molecule can convey l_m bits of information through distinct sequences of H and F atoms, a molecular XOR scheme can be generated such that Nano-Relay combines the information coming from Nano-Alice and Nano-Bob by XORing l_m number of H and F atoms sequentially, i.e., starting from head of the molecule until its tail, which is in fact similar to binary XOR operation on a string

of zeros and ones. More specifically, if the message strings coming from both Nano-Alice and Nano-Bob contain the same atom to be XORed, Nano-Relay outputs H. Otherwise, it transmits F. Hence, knowing the bit they sent, Nano-Alice and Nano-Bob decide what was sent by the other.

5.3.1 Rate-Delay Tradeoff for Uncoded Case

Assume that Nano-Alice and Nano-Bob start transmitting their messages at the same time instant. Both of them do not know about the position of the other and release N_P puffs of messenger molecules into the communication medium. Since the propagation delay for a Brownian message is a random variable, Nano-Relay receives messages from Nano-Alice and Nano-Bob at random time instants. The forwarding procedure for a message starts when it is received by Nano-Relay. However if a second message arrives during the transmission of the first, Nano-Relay puts it in the queue and this second message waits until the transmission of the first is finished. The waiting time of a message in the queue is denoted as T_q.

Let A and B be the messages of Nano-Alice and Nano-Bob, respectively. Both messages A and B can reach their destinations directly or from the transmission path over Nano-Relay. Then, the expected delay time $E\{T_D\}$ for a message to reach its destination can be calculated as

$$E\{T_D\} = E\{T_D|AB\}P(AB) + E\left\{T_D|\overline{AB}\right\}P(\overline{AB}), \tag{5.15}$$

where AB is the event when the same message is transferred on both Nano-Relay and the direct path between Nano-Alice and Nano-Bob, simultaneously. $\overline{AB}$ represents the complement event when the message is transferred on only Nano-Relay.

The probability $P(AB)$ can be calculated as

$$P(AB) = 1 - \left(1 - \frac{d_0}{d_{AB}}\right)^{N_P}. \tag{5.16}$$

If the message fails to reach its destination on the direct path ($\overline{AB}$ case), then, the delay is completely determined by the transmission path over Nano-Relay, which is given by

$$E\left\{T_D|\overline{AB}\right\} = E\{T_{ARB}\}, \tag{5.17}$$

where T_{ARB} is the delay for the path ARB.

Otherwise, i.e., when AB event takes place, the delay is the minimum of time delays to which the message molecules are exposed for paths ARB and AB, namely,

$$E\{T_D|AB\} = E\{\min(T_{AB}, T_{ARB})\}, \tag{5.18}$$

where T_{AB} is the delay time for the path AB.

$E\{T_D|AB\}$ is upper bounded by $E\{T_{AB}\}$ since $E\{T_{AB}\} < E\{T_{ARB}\}$ due to the triangle inequality

$$E\{T_D|AB\} < E\{T_{AB}\} = E\{\tau_M\}. \tag{5.19}$$

Then, the expected message delay between A and B is

$$E\{\tau_M\} = \int_0^\infty \left[\frac{\prod_{i=1}^{N_P} (1 - P_d F_\tau(t - iT_M))^{N_M} - (1-P_d)^{N_P N_M}}{1 - (1-P_d)^{N_P N_M}} \right] dt. \tag{5.20}$$

Nevertheless, it is troublesome to find a closed-form expression using this integral. Thus, we provide the upper and lower bounds for this integral to show the behavior of delay. A lower bound for the expected message delay between A and B is obtained as

$$E\{\tau_M\} > \frac{1 - (1-P_d)^{N_P N_M + 1} - P_d (N_P N_M + 1)(1-P_d)^{N_P N_M}}{\xi P_d (N_P N_M + 1) P_r}. \tag{5.21}$$

To arrive to this bound let us define a new CDF, $F_{\tau^{(u)}}(t)$, which is the CDF of a uniform random variable $\tau^{(u)}$,

$$F_{\tau^{(u)}}(t) = \begin{cases} t/\xi, & \text{if } t \in (0, \xi) \\ 1, & \text{if } t \geq \xi \\ 0, & \text{else} \end{cases}, \tag{5.22}$$

where ξ is mode of the pdf of τ, i.e., the point where the peak of the pdf occurs, which can be calculated by differentiating $f_\tau(t)$ and equating to zero as follows:, i.e.,

$$\xi = -\frac{3D}{v^2} + \frac{\sqrt{9D^2 + d^2 v^2}}{v^2} > 0. \tag{5.23}$$

Note that compared to the infinite duration pdf of τ, which is inverse Gaussian distribution, we observe that the uniformly distributed $\tau^{(u)}$ has a much narrower pdf. However, its density is greater than $f_\tau(t)$ for $t \in (0, \xi)$. Hence, the CDF $F_{\tau^{(u)}}(t)$ is larger than $F_\tau(t)$ for every t value in (0, ∞).

Hence, uniform distribution approximation of $f_\tau(t)$ yields an upper bound on the propagation delay pdf, which, in turn, yields the lower bound for $E\{\tau_M\}$ in (5.21) calculated by substituting (5.22) into $F_\tau(t - iT_M)$ for each i in (5.20).

Similar to lower bound in (5.21), an upper bound is obtained as

$$E\{\tau_M\} < -\frac{(1-P_d)^{N_P N_M}}{P_r} + \frac{(1-P_d N_P N_M/\mu)^{N_P N_M+1} - (1-P_d(N_P N_M+\mu)/\mu)^{N_P N_M+1}}{\mu P_d (N_P N_M+1) P_r}. \tag{5.24}$$

To get this bound, we define a new CDF, $F_{\tau^{(v)}}(t)$, which is the CDF of a uniform random variable $\tau^{(v)}$,

$$F_{\tau^{(v)}}(t) = \begin{cases} t/\mu, & \text{if } t \in (0,\mu) \\ 1, & \text{if } t \geq \mu \\ 0, & \text{else} \end{cases}, \tag{5.25}$$

where μ is the expected value of the pdf of τ.

Note that for the expected value, μ, $F_\tau(t)$ reaches 0.99 which is sufficiently close to 1 so that we can assume $F_\tau(t)$ is 1 for $t > \mu$. Besides, $F_{\tau^{(v)}}(t)$ increases very slowly compared to $F_\tau(t)$ for $t \in (0,\mu)$. Hence, the CDF $F_{\tau^{(v)}}(t)$ is smaller than $F_\tau(t)$ for every t value in $\in(0, \infty)$. To simplify (5.20), we replace $F_\tau(t - iT_M)$ by $F_{\tau^{(v)}}(t - N_P T_M)$ for all i, since $F_{\tau^{(v)}}(t - N_P T_M) \leq F_\tau(t - N_P T_M) \leq F_\tau(t - iT_M)$ for all i. Thus, this approximation yields a lower bound on the propagation delay CDF, which, in turn, yields the upper bound for $E\{\tau_M\}$ in (5.24).

Using (5.19), we obtain

$$E\{T_D\} < E\{T_{AB}\} P(AB) + \left(E\{T_{ARB}\} + E\left\{T_q\right\}\right) P(\overline{AB}). \tag{5.26}$$

Here, $E\left\{T_q\right\}$ is included in (5.26) to represent the expected queuing delay for message A in the Nano-Relay, which is defined in Section 5.3.1. The expected queuing delay depends on both the utilization factor of Nano-Relay and the reception time of the message.

First, assume that only messages A and B of Alice and Bob, respectively, need to be forwarded by Nano-Relay without coding. In that case, if A is received during the transmission of the message B, the message A waits a period of time, $E\left\{T_q{}^{(\overline{C})}\right\}$, which is expressed by

$$E\left\{T_q{}^{(\overline{C})}\right\} = P\left\{Q^{(\overline{C})}\right\} E\left\{T_q{}^{(\overline{C})} | Q^{(\overline{C})}\right\}, \tag{5.27}$$

where $Q^{(\overline{C})}$ is the event that the message A is received in the transmission period of the message B. The probability of queueing in uncoded case is

$$P\left\{Q^{(\overline{C})}\right\} = Pr\{N_P T_M > \tau_A - \tau_B > 0\}, \tag{5.28}$$

where τ_A and τ_B are the respective propagation delays of messages A and B. We assume that puff propagation delays are exponentially distributed with mean d/ν.

For exponentially distributed propagation delays, the probability $P\left\{Q^{(\overline{C})}\right\}$ is given by

$$P\left\{Q^{(\overline{C})}\right\} = \frac{d_{AR}}{d_{AR}+d_{BR}}\left(1-\exp\left(-\frac{\nu N_P^2 T_M}{d_{AR}}\right)\right). \tag{5.29}$$

Suppose that message streams from Nano-Alice and Nano-Bob have Poisson arrivals with rates α and β, respectively. Then, Nano-Relay can be modeled as an M/G/1 server having a service time distribution with mean μ and variance σ^2. Thus, the expected queueing delay can be derived using the *Pollaczek-Khintchine formula* [83]. Specifically, Nano-Relay becomes an M/D/1 server when network coding is not allowed, i.e. direct forwarding.

For M/D/1 case, the relay throughput is constant with rate $1/N_P T_M$ messages per unit time and the expected queueing for an arbitrary message can be calculated by [83] as

$$E\left\{T_q|Q^{(\overline{C})}\right\} = \frac{1}{2}\frac{(\alpha+\beta)N_P^2 T_M^2}{1-(\alpha+\beta)N_P T_M}. \tag{5.30}$$

Besides, reception rate for this case can be calculated by considering an interval of time beginning with the reception of the first message, t_1, and ending with the reception of the k^{th} message, t_k. Similar to the reception rate calculation in 5.2.4, reception rate of Nano-Alice's messages at Nano-Bob can be calculated as follows;

$$R_{\overline{C}}^{(RX)} = \frac{l_m}{N_P T_M}. \tag{5.31}$$

5.3.2 Rate-Delay Tradeoff for Network Coded Case

Now, consider the case when Nano-Relay uses a network coding mechanism, which is shown in Fig. 5.4. When Nano-Relay receives a message, it starts waiting T_W seconds for the other message to arrive before transmitting the received message. If the other message arrives within T_W seconds or during the transmission of the first message, Nano-Relay starts transmitting the XORed version of two messages. Otherwise, Nano-Relay transmits messages separately.

If Nano-Relay forwards messages with the network coding mechanism described above, the expected queuing delay for message A becomes

$$E\left\{T_q^{(C)}\right\} = P\left\{W^{(C)}\right\} E\left\{T_q^{(C)}|W\right\} + P\left\{\overline{W}^{(C)}\right\} T_W, \tag{5.32}$$

where W is the event when the message B arrives within the waiting time T_W.

The probability that the message B arrives within the waiting time T_W in the coded case, $P\left\{W^{(C)}\right\}$, again can be calculated assuming exponential propagation delays as

$$P\left\{W^{(C)}\right\} = \frac{d_{BR}}{d_{BR}+d_{BR}}\left(1-\exp\left(-\frac{\nu N_P T_W}{d_{BR}}\right)\right). \tag{5.33}$$

Even when each of Nano-Alice and Nano-Bob generates one single message, the advantage of network coding is reflected as reduced resource consumption in Nano-Relay. However, if both Nano-Alice and Nano-Bob generate message streams, then the forwarding efficiency of Nano-Relay can significantly affect the delay amounts. When both sources continously emit puffs of molecules, Nano-Relay continously combines the molecules. Since there are always molecules ready to combine arriving from the other source, no molecule waits up to T_W seconds for its conjugate to arrive. Hence, the total waiting time which adversely affects the delay decreases.

In the network coding case, the relay throughput can be assumed to have a bi-modal distribution. Assume that only messages transmitted at the same time can be coded with each other. When a message is going to be transmitted and its conjugate message is in the queuing buffer, then these messages can be forwarded together meaning that the relay throughput is $2/N_P T_M$ messages per unit time. Otherwise, they are transmitted with rate $1/N_P T_M$ messages per unit time.

Similar to the uncoded case, the expected queueing delay for an arbitrary message in network coded case can be calculated by

$$E\left\{T_q^{(C)}|W\right\} = \frac{(1-0.75P_{AXB})(\alpha+\beta)N_P^2 T_M^2}{2(1-(\alpha+\beta)(1-0.5P_{AXB})N_P T_M)}, \tag{5.34}$$

where P_{AXB} is the probability of coding the messages of A and B.

Note that as the probability P_{AXB} increases, $E\left\{T_q\right\}$, i.e., the expected queueing delay, decreases. However, the probability P_{AXB} is also a function of the queueing delay T_q since longer queueing delays increase the chance for coding of conjugate messages. Therefore, the probability P_{AXB} can be defined as

$$P_{AXB} = Pr\left\{|\tau_A - \tau_B| < T_q\right\}, \tag{5.35}$$

where τ_A and τ_B are the reception times of conjugate messages from Nano-Alice and Nano-Bob.

Table 5.1: Simulation parameters.

Parameter	**Symbol**	**Value**
Diffusion coefficient	D	$2.2 \times 10^{-11}\ m^2/s$
Drift velocity	v	$0.2 \times 10^{-9}\ m/s$
Distance b/w two transceivers	d	$10^{-5}\ m$
Puff preparation time	T_M	$10^{-3}\ s$
Probability of coding messages	P_{AXB}	1
Poisson arrival rate of Alice	α	$0.1\ s^{-1}$
Poisson arrival rate of Bob	β	$0.1\ s^{-1}$
Distance b/w Alice and Relay	d_{AR}	$10^{-6}\ m$
Distance b/w Bob and Relay	d_{BR}	$10^{-6}\ m$
Distance b/w Alice and Bob	d_{AB}	$2 \times 10^{-6}\ m$
Area of perfect reception	A	$10^{-10}\ m^2$
Number of molecules in a puff	N_M	10

Besides, reception rate for this case can be calculated by considering an interval of time beginning with the reception of the first message, t_1, and ending with the reception of the k^{th} message, t_k. Similar to the reception rate calculation in 5.2.4, reception rate of Nano-Alice's messages at Nano-Bob can be calculated as follows;

$$R_C^{(RX)} = \frac{l_m}{N_P T_M} \left(2P\left\{W^C\right\} + (1 - P\left\{W^C\right\})\right). \tag{5.36}$$

5.4 Simulations

In this section, we evaluate rate and delay expressions found in Section 5.2 and 5.3 with the necessary simulation parameters given in Table 5.1. In our implementation, the simulation parameters are chosen in agreement with [54]. Subsequently, the uncoded and the network coded cases are compared to reveal the rate-delay tradeoff.

5.4.1 Simulation for Uncoded Case

We investigate the rate-delay tradeoff of an uncoded case without a relay with increasing N_P in Fig. 5.5. The rate expression in (5.9) is utilized to evaluate the rate variation. Our analysis is not based on the exact expressions of the delay. However, lower and upper bounds for propagation delay, given respectively in (5.21) and (5.24) are compared to observe the variation of delay with increasing N_P. Although the two bounds follow the same trend, the lower bound

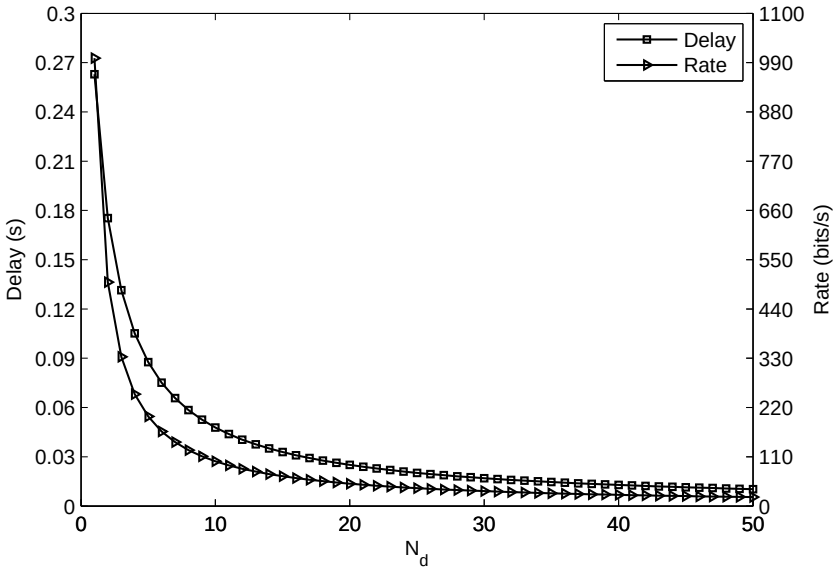

Figure 5.5: Delay and rate characteristics with N_P.

is far beyond the realistic propagation delays in molecular domain, hence, unreliable. Thus, upper bound (5.24) is used for the analysis. The decaying trend of rate and delay estimations is illustrated in Fig. 5.5.

On the one hand, for a single message, as the number of puffs (N_P) increases, the preparation time for the message increases proportionally. Therefore, the transmission rate $R^{(TX)}$ and the reception rate $R^{(RX)}$ increase. On the other hand, increasing N_P augments the message reception probability, causing a descent in expected message propagation delay $E\{\tau_M\}$. Thus, there is a tradeoff between the expected message propagation delay $E\{\tau_M\}$ and the expected reception rate $R^{(RX)}$. These results are also intuitively expected from (5.9), (5.21) and (5.24). The tradeoff between rate and delay is illustrated in Fig. 5.6.

This rate-delay tradeoff analysis is crucial for designing an efficient molecular communication network. An important application of molecular networks is molecular computers which will replace electronic computers in the future for some of the applications requiring huge computing power [101]. This is due to the hundred times smaller size of molecules composing molecular computers with respect to silicon chips of electronic computers and the high parallel computing capacity of molecular computers [117]. The rate and delay characteristics of different molecular communication techniques will be essential criteria for the design of these molecular computers which will boost the computing power to ten-thousandfold of

electronic computers. Especially in gene regulatory applications, molecular computers doing DNA computations are highly investigated in various studies such as [26] and [141].

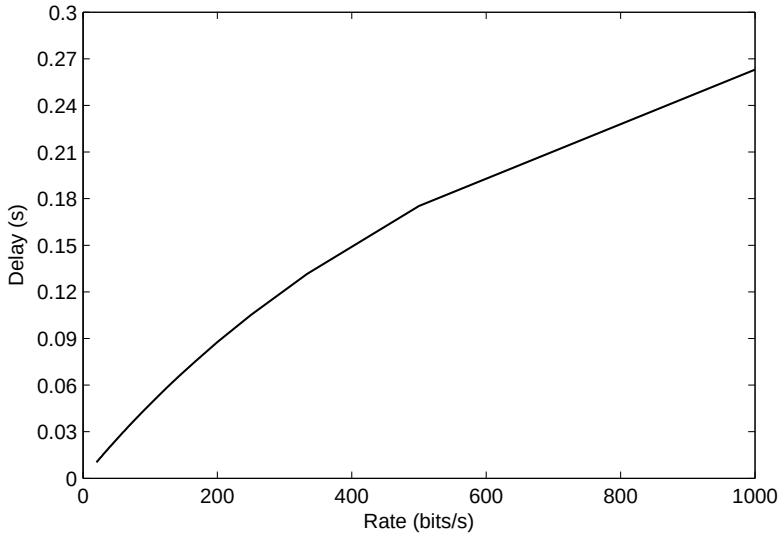

Figure 5.6: Rate vs delay analysis.

5.4.2 Simulation for Network Coded Case

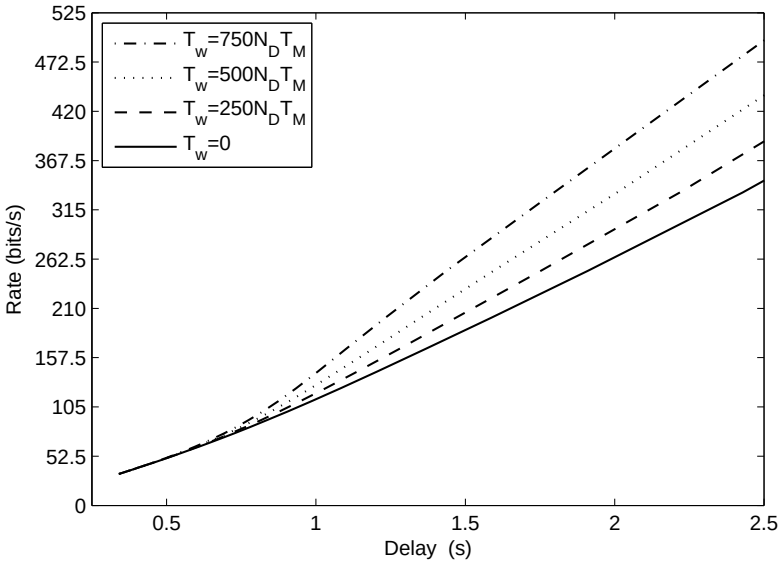

Figure 5.7: Rate vs delay analysis in uncoded and coded network cases.

In Fig. 5.7, reception rates with respect to delay of both uncoded and network coded cases

with different waiting times in Nano-Relay, denoted by T_W, are illustrated. $T_w = 0$ represents the uncoded case. On the one hand, as T_W increases, the waiting interval for conjugate messages increases, which, in turn, increases the probability of coding. Therefore, total delay increases due to the extra delay introduced by Nano-Relay before coding takes place. On the other hand, as the probability of coding increases, the reception rate increases since Nano-Relay combines the incoming messages to decrease the number of transmitted messages.

As illustrated in Fig. 5.7, by increasing the waiting time T_w, 40% higher reception rate compared to uncoded case, i.e, $T_w = 0$, is achievable for a given delay. Thus, it is seen that network coding provides an efficient operation for molecular nanonetworks.

The network coding technique is a beneficial tool to overcome long propagation delay problem for molecular communication in vast different applications. For medical applications, to improve the intervention time of nanomachines placed in the human body, the communication rates between those nanomachines may be ameliorated by network coding. For example, the molecular communication between nanorobots described in [30] may be accelerated by network coding to correlate the nanorobots sensory data and to improve the collaboration between the nanorobots in order to identify the tumor cells effectively. Another medical application can be stated as the regulation of the behaviours of engineered bacteria used in cancer therapy [7]. These bacteria form quorum sensing networks by communicating via signaling molecules to sense the environment of a tumourous cell, invade that cell and release cytotoxic agents. The efficient operation of these bacteria arises from their proper synchronization. To synchronize, a low delay molecular network may be established by network coding.

CHAPTER 6

CONCLUSIONS AND FUTURE RESEARCH DIRECTIONS

Incredible improvements in the field of nanotechnologies have yielded integrated functional devices consisting of nanoscale components, i.e., nanomachines. Enabling nanomachines to communicate with each other, and thus, forming nanonetworks will help realize envisioned complex nanotechnology applications such as intelligent collaborative drug delivery, glucose, sodium, and cholesterol monitoring, detecting the presence of different infectious agents, jointly executing an application-specific task as nanocomputers. Several communication paradigms are considered for use in nanonetworks, but the most promising is molecular communications, where molecules are used to encode, transmit and receive information. Indeed, the human body is a large-scale heterogeneous communication network of molecular nanonetworks as it is composed of billions of nanomachines, i.e., cells, whose functionalities primarily depend on nanoscale molecular communications. Any communication failure that is beyond the recovery capabilities of this network leads to diseases. Therefore, identifying the intra-body molecular nanonetworks, realistically modeling the molecular communication channels, analyzing and understanding its network and information theoretical capabilities and shortcomings, and ultimately contributing to the development of bio-inspired solutions for nanonetworks and information and communication and technology (ICT)-inspired solutions for certain diseases are the interdisciplinary objectives of our research. Furthermore, through the multiple-access synaptic communication channel model of neurons, it is possible to analyze the failures in neurons via action potential transmission characteristics. It is also possible to understand the main mechanisms behind learning, such as the effect of correlation and interference among multiple neurons. Moreover, through the molecular puffing-based nanomachine model, we mimic and extract the communication mechanism behind the alarm situations that require a sudden release of a limited amount of pheromones. In the subsequent

sections, we summarize our contributions and specify open issues in molecular communication nanonetworks and their performance analysis.

6.1 Contributions

In this section, we sum up the contributions of each chapter and underline the important results.

6.1.1 Molecular Communication Nanonetworks inside Human Body

Molecular communication has been a promising field for nanoscale communication applications, and state-of-the-art technology enables the production of nanomachines, i.e., simple nano devices capable of a wide range of tasks, especially for ICT and nanomedicine applications.

Human body itself has never been predicated on a resource for ICT field although it houses different kinds of communication channels, and nanonetworks of sensory, signaling and molecular pathways. Besides, the overall internal network, that we term as human internal Internet in this thesis, supports the integrity of all biological systems by various controlling mechanisms through communication of molecules and signals, as information carriers.

6.1.2 Synaptic Multiple-Access Channel in Hippocampal-Cortical Neurons

Synaptic communication has a very crucial role in learning and memory processes. In this thesis, we investigate the rate region for SISO synaptic communication channel model, and observe the time course of postsynaptic firing rate, and its dependence on dynamics of vesicle release process and docked pool features. Furthermore, we extend the single terminal model to multiple-access synaptic communication channel model and observe how the total information rate adds up. Moreover, we analyze the contribution of first-order correlation on the information rate at the postsynaptic neuron terminal. Our analysis puts forth the boosting effect of spike correlation on the postsynaptic rate. Finally, investigating the disorders characterized by pre- and postsynaptic and synaptic abnormalities, we reveal the potential relations between neuronal coefficients and disorders.

6.1.3 Adaptive Weight Update in Cortical Neurons and Estimation of Channel Weights in Synaptic Interference Channel

Synaptic communication has a very crucial role in learning and memory processes. In this thesis, we investigate the effect of interference among the presynaptic terminals in SISO and MISO synaptic communication channels. We show that synaptic transmission performance is enhanced as stronger connection strengths are established. Furthermore, in comparison with maximum achievable rates in neuronal synaptic interference channel, we show that actual adaptive synaptic weight update mechanism performs close to best achievable characteristics, and also enables high communication performance in terms of postsynaptic rate.

6.1.4 Rate-Delay Tradeoff in Molecular Nanonetworks

Molecular communication is a promising field open to evolution because of its feasibility in a vast variety of fields, such as environment, industry, military and especially biomedicine. Biomedical applications utilize messenger-based approaches that have crucial roles in intervening in biological processes to artificially control biosystems. For this reason, we build our analysis on a specific case of messenger-based molecular communication model. First, we model the puff propagation using a Brownian motion model. Next, using this model, the mathematical relation between reception rate and message delay is extracted to justify the tradeoff between them. Then, this model is applied to a simple nanonetwork in two different cases, namely, uncoded and network coded cases. Finally, the expressions of rate and delay are evaluated for both cases.

6.2 Future Research Directions

Investigation of the fundamental intra-body communication paths, and their role in providing the integrity of all biological systems through nanonetwork relations broadens the contributions and promotes the development of ICT field. Thus, with this background, ICT is anticipated to give substantial contributions for the development of nanoscale molecular communication networks inspired from human's biological network, and to pave the way for developing ICT inspired curing strategies for intra-body diseases.

The analysis on the synaptic multiple-access channel could be extended to observe the effect of multi-order correlations among presynaptic terminals on the postsynaptic performance.

Open issues also include the detailed analysis of interference among multi-terminal neuronal connections.

Our analysis on rate and delay tradeoffs in molecular nanonetworks shows that high data rate and negligible propagation delay cannot be achieved simultaneously as opposed to an ideal communication system. The tradeoff should be exploited in delay or rate sensitive molecular nanoscale applications. This pioneering work constitutes a basis for rate and delay optimization of future nanomolecular frameworks.

REFERENCES

[1] S. Abadal, I.F. Akyildiz, “Automata modeling of quorum sensing for nanocommunication networks," *Nano Communication Networks (Elsevier) Journal*, vol. 2, no. 1, pp. 74–83, Mar. 2011.

[2] L. F. Abbott, S. Song, “Temporally asymmetric Hebbian learning, spike timing and neuronal response variability," in *Advances in Neural Information Processing Systems 11*, Edited by M. S. Kearns, S. A. Solla, D. A. Cohn, MIT Press, Cambridge MA, pp. 69–75, 1999.

[3] I. F. Akyildiz, F. Brunetti, C. Blázquez, “Nanonetworks: A new communication paradigm," *Computer Networks*, vol. 52, pp. 2260–2279, 2008.

[4] I.F. Akyildiz, J.M. Jornet, M. Pierobon, “Propagation models for nanocommunication networks," in *Proc. of EUCAP 2010, Fourth European Conference on Antennas and Propagation (invited paper)*, Barcelona, Spain, April 2010.

[5] I. F. Akyildiz, J.M. Jornet, “Electromagnetic wireless nanosensor networks," *Nano Communication Networks (Elsevier) Journal*, vol. 1, pp. 3–19, Jun. 2010.

[6] I.F. Akyildiz, J.M. Jornet, M. Pierobon, “Nanonetworks: A new frontier in communications," *Communications of the ACM*, vol. 54, no. 11, pp. 84–89, Nov. 2011.

[7] J.C. Anderson, E.J. Clarke, A.P. Arkin, and C.A. Voigt “Environmentally Controlled Invasion of Cancer Cells by Engineered Bacteria," *Journal of Molecular Biology*, vol. 355, no. 4, pp.619–627, 2005.

[8] B. W. Andrews, P.A. Iglesias, “Rate distortion theory in cellular signaling," in *41st Annual Conference on Information Sciences and Systems (CISS ’07)*, pp. 172–173, Mar. 2007.

[9] D. Arifler, “Capacity analysis of a diffusion-based short-range molecular nanocommunication channel," *Computer Networks*, vol. 55, no. 6, pp. 1426–1434, 2011.

[10] Y.Z. Arslan, M.A. Adli, A. Akan, M.B. Baslo, “Prediction of externally applied forces to human hands using frequency content of surface EMG signals," *Computer Methods and Programs in Biomedicine*, vol. 98, no. 1, pp. 36–44, Apr. 2010.

[11] B. Atakan, O.B. Akan, “An information theoretical approach for molecular communication," in *Proceedings of ICST/ACM BIONETICS 2007*, pp. 33–40, Dec. 2007.

[12] B. Atakan, O.B. Akan, “On channel capacity and error compensation in molecular communication," *Springer Transactions on Computational Systems Biology*, vol. 10, pp. 59-80, Feb. 2008.

[13] B. Atakan, O.B. Akan, “On molecular multiple-access, broadcast and relay channels in nanonetworks", in *Proceedings of ICST/ACM BIONETICS*, Nov. 2008.

[14] B. Atakan, O.B. Akan, “Single and multiple-access channel capacity in molecular nanonetworks", in *Proceedings of ICST/ACM Nano-Net*, Oct. 2009.

[15] B. Atakan, O.B. Akan, “Deterministic capacity of information flow in molecular nanonetworks," *Nano Communication Networks Journal (Elsevier)*, vol. 1, pp. 31–42, Mar. 2010.

[16] B. Atakan, S. Balasubramaniam, O. B. Akan, “Body area nanonetworks with molecular communications in nanomedicine", *IEEE Communications Magazine*, vol. 50, no. 1, pp. 28–34, Jan. 2012.

[17] B. Atakan, S. Balasubramaniam, O. B. Akan, “Body Area NanoNetworks with Molecular Communications in Nanomedicine," *IEEE Communications Magazine*, vol. 50, no. 1, pp. 28–34, 2012.

[18] A.A. Bachmanov, G.K. Beauchamp, “Taste receptor genes," *Annual Review of Nutrition*, vol. 27, pp. 389–414, 2007.

[19] E. Balevi, “Inter-Neuron Spike Communication", *M.S. Thesis*, Middle East Tech. Univ., Ankara, Turkey, 2010.

[20] E. Balevi, O. B. Akan, “Synaptic Gaussian Multiple Access Channel", 2011.

[21] E. Balevi, O. B. Akan, “A Physical Channel Model for Nanoscale Neuro-Spike Communication," to appear in *IEEE Transactions on Communications*, 2012.

[22] M. Bartos et al., “Synaptic mechanisms of synchronized gamma oscillations in inhibitory interneuron networks," *Nat. Rev. Neurosci.*, vol. 8, pp. 45–56, Jan. 2007.

[23] C. W. Bauschlicher Jr., A. Ricca, R. Merkle, “Chemical storage of data," *Nanotechnology*, vol. 8, no. 1, pp. 1–5, 1997.

[24] M. Beckerman, *Molecular and Cellular Signaling*, 1st edition, Springer, 2005.

[25] J. M. Bekkers et al., “Origin of variability in quantal size in cultured hippocampal neurons and hippocampal slices," in *Proc. Natl. Acad. Sci. USA*, vol. 87 no. 14, pp. 5359–5362, Jul. 1990.

[26] Y. Benenson, B. Gil, U. Ben-Dor, R. Adar, and E. Shapiro, “An autonomous molecular computer for logical control of gene expression," *Nature*, no. 429, pp. 423–429, 2004.

[27] R.A. Bergman, A.K. Afifi, P.M. Heidger, *Atlas of microscopic anatomy: A functional approach companion to histology and neuroanatomy*, Saunders (Philadelphia), 1989.

[28] B. Borhan, M.L. Souto, H. Imai, Y. Shichida, K. Nakanishi, “Movement of retinal along the visual transduction path," *Science*, vol. 288, no. 5474, pp. 2209–2212, Jun. 2000.

[29] T. Brijs et al., “A multivariate Poisson mixture model for marketing applications," *Stat Neerl*, vol. 58, no. 3, pp. 322–348, 2004.

[30] A. Cavalcanti, T. Hogg, B. Shirinzadeh and H.C. Liaw, “Nanorobot Communication Techniques: A Comprehensive Tutorial," in *Proceedings of the IEEE ICARCV 2006 International Conference on Control, Automation, Robotics and Vision*, Singapore, Dec. 2006.

[31] A. Chaudhuri, P.O. Behan, “Fatigue in neurological disorders," *The Lancet*, vol. 363, no. 9413, pp. 978–988, Mar. 2004.

[32] Y. Chen, E. Wu, H. He, X. Liu, “Effectiveness evaluation of audition in human-computer interface," in *IEEE International Conference on Systems, Man, and Cybernetics*, pp. 2074–2077, Oct 1996.

[33] R.R.L. Cisi, A.F. Kohn, “Simulation system of spinal cord motor nuclei and associated nerves and muscles, in a Web-based architecture," *Journal of computational neuroscience*, vol. 25, pp. 520–542, 2008.

[34] L.C. Cobo, I.F. Akyildiz, “Bacteria-based communication in nanonetworks," *Nano Communication Networks Journal (Elsevier)*, vol 1, no. 4, pp. 244–256, Dec. 2010.

[35] T.B. Comeau, J.E. Epstein, C. Migas, “Taste and smell dysfunction in patients receiving chemotherapy: a review of current knowledge," *Support Care Cancer*, vol. 9, pp. 575–580, 2001.

[36] B.W. Connors, M. A. Long, “Electrical synapses in the mammalian brain," *Annu. Rev. Neurosci.*, vol.27, pp. 393–418, Jul. 2004.

[37] S. F. Cooke, T. V. P. Bliss, “Plasticity in the human central nervous system," *Brain*, vol. 129, no. 7, pp. 1659–73, May 2006.

[38] A. Credi, V. Balzani, S.J. Langford, JF Stoddart, “Logic Operations at the Molecular Level. An XOR Gate Based on a Molecular Machine," *J. Am. Chem. Soc.*, vol. 119, no. 11, pp. 2679–2681, 1997.

[39] P. Dalton, “Psychophysical and behavioral characteristics of olfactory adaptation," *Chemical Senses*, vol. 25, no. 4, pp. 487–492, 2000.

[40] P. Dayan and L.F. Abbott, *Theoretical Neuroscience*, vol. 31, Cambridge, MA: MIT press, 2001.

[41] P. Dayan, L. F. Abbott, “Theoretical neuroscience: computational and mathematical modeling of neural systems," Cambridge, MA: MIT Press, 2001.

[42] L. E. Dobrunz, C. F. Stevens, “Heterogeneity of release probability, facilitation, and depletion at central synapses," *Neuron*, vol. 18, pp. 995–1008, June 1997.

[43] L. E. Dobrunz, “Release probability is regulated by the size of the readily releasable vesicle pool at excitatory synapses in hippocampus," *Int. J. Devl Neuroscience*, vol. 20, pp. 225–236, 2002.

[44] K. Eric Drexler, *Nanosystems: Molecular Machinery, Manufacturing, and Computation*, John Wiley & Sons, NY, 1992.

[45] J.M. Dubach, D.I. Harjes, and H.A. Clark, “Fluorescent ion-selective nanosensors for intracellular analysis with improved lifetime and size," *Nano Letters*, vol. 7, pp. 1827–2831, 2007.

[46] A.W. Eckford, “Molecular communication: Physically realistic models and achievable information rates," *0812.1554*, Dec. 2008. [Online]. Available: http://arxiv.org/abs/0812.1554.

[47] F. R. Edwards, S. J. Redman, B. Walmsley, “Statistical fluctuations in charge transfer at 1a synapses on spinal motoneurones," *J Physiol*, vol. 259, no. 3, pp. 665–688, Aug. 1976.

[48] S.A. El-Safty, A.A. Ismail, H. Matsunaga, F. Mizukami, “Optical nanosensor design with uniform pore geometry and large particle morphology," *Chemistry A European Journal*, vol. 13, no. 33, pp. 9245–9255, Nov. 2007.

[49] M. Endo, “Calcium release from the sarcoplasmic reticulum," *Physiological Reviews*, vol. 57, no. 1, pp. 71–108, 1977.

[50] A.A. Faisal, L.P.J. Selen, D.M. Wolpert, “Noise in the nervous system," *Nature*, vol. 9, Apr. 2008.

[51] E. Fanning, V. Klimovich, A.R. Nager, “A dynamic model for replication protein A (RPA) function in DNA processing pathways," *Nucleic Acids Research*, vol. 34, pp. 4126–4137, 2006.

[52] M.J. Farabee, The Endocrine System [Online] 20 June 2001. Available from: `http://www.emc.maricopa.edu/faculty/farabee/BIOBK/BioBookENDOCR.html`.

[53] J.R. Flanagan, S.J. Lederman, “Neurobiology: Feeling bumps and holes," *Nature*, vol. 412, pp. 389–391, Jul. 2001.

[54] R.A. Freitas, *Nanomedicine, Volume I: Basic Capabilities*, Georgetown: Landes Bioscience, 1999, pp. 178–180.

[55] S. Fukuda, “Somatosensory evoked potential," *Masui*, vol. 55, no. 3, pp. 280–293, 2006.

[56] F. Gabbiani, C. Koch, “Coding of time-varying signals in spike trains of integrate-and fire neurons with random threshold," *Neural Comput.*, vol. 8, pp. 44–66, 1996.

[57] J. L. Gaiarsa et al., “Long-term plasticity at GABAergic and glycinergic synapses: mechanisms and functional significance," *Trends Neurosci*, vol. 25, no. 11, pp. 564–570, Nov. 2002.

[58] R.G. Gallager, “An inequality on the capacity region of multiacess multipath channels," *Communications & Cryptography, Two Sides of one Tapestry,* Kluwer Academic Publishers, ed. Blahut, Costello, Maurer, Mittleholzer, 1994.

[59] N. Garralda, I. Llatser, A. Cabellos-Aparicio, M. Pierobon, “Simulation-based evaluation of the diffusion-based physical channel in molecular nanonetworks," in *Proc. of 1st IEEE International Workshop on Molecular and Nano Scale Communication (MoNaCom), INFOCOM*, Shanghai, China, Apr. 2011.

[60] F. Gawin,“Chronic neuropharmacology of cocaine abuse: progress in pharmocotherapy," *J Clin Psychiat*, vol. 49, pp. 11–17, 1988.

[61] R. A. Gonzales, J. N. Jaworski, “Alcohol and glutamate", *Alcohol Health Res World.*, vol. 21, no. 2, pp. 120–127, 1997.

[62] M. Gregori, I.F. Akyildiz, “A new nanonetwork architecture using flagellated bacteria and catalytic nanomotors," *IEEE Journal of Selected Areas in Communications*, vol. 28, no. 4, pp. 612–619, May 2010.

[63] E. Gul, B. Atakan, O.B. Akan, “NanoNS: A nanoscale network simulator framework for molecular communications," *Nano Communication Networks Journal (Elsevier)*, vol. 1, pp. 138–156, Jun. 2010.

[64] R.M. Gulrajani, “Models of the electrical activity of the heart and computer simulation of the electrocardiogram," *Critical Reviews in Biomedical Engineering*, vol. 16, no. 1, pp. 1–66, 1988.

[65] A. Guney, B. Atakan, O. B. Akan, “Mobile Ad Hoc Nanonetworks with Collision-based Molecular Communication," *IEEE Transactions on Mobile Computing*, vol. 11, no. 3, pp. 353-266, Mar. 2012.

[66] A. Guney, B. Atakan, O. B. Akan, “Mobile Ad Hoc Nanonetworks with Collision-based Molecular Communication," *IEEE Transactions on Mobile Computing*, vol. 11, no. 3, pp. 353–266, Mar. 2012.

[67] A.C. Guyton, J.E. Hall, *Textbook of Medical Physiology*, W.B. Saunders (Philadelphia), 2006.

[68] J. Hasty, D. McMillen, F. Isaacs, J.J. Collins, “Computational studies of gene regulatory networks: in numero molecular biology," *Nature Reviews Genetics*, vol. 2, pp. 268–279, Apr. 2001.

[69] S. Hiyama et al., “Molecular communication," in: *Proc. NSTI Nanotechnology Conference*, Oct. 2005.

[70] A.L. Hodgkin, A.F. Huxley, “A quantitative description of membrane current and its application to conduction and excitation in nerve," *The Journal of Physiology*, vol. 117, pp. 500–544, 1952.

[71] S. Li, L. Huang, “Nonviral gene therapy: promises and challenges," *Gene Therapy*, vol. 7, pp. 31–34, 2000.

[72] K.M. Irick, W. Xu, N. Vijaykrishnan, M.J. Irwin, “A nanosensor array-based VLSI gas discriminator," *18th International Conference on VLSI Design*, pp. 241–246, Jan. 2005.

[73] J. S. Isaacson, B. Walmsley “Counting quanta: direct measurements of transmitter release at a central synapse," *Neuron*, vol. 15, pp. 875–884, Oct. 1995.

[74] A. Jabbari, I. Balasingham, “On the modeling of a nano communication network using spiking neural architecture," in *Proc. IEEE International Conference on Communications (ICC)*, pp. 6193–6197, Jun. 2012.

[75] M. Jansen, G. Dannhardt, “Antagonists and agonists at the glycine site of the NMDA receptor for therapeutic interventions," *Eur J Med Chem*, vol. 38, no. 7–8, pp. 661–670, July–Aug. 2003.

[76] H.J. Jongsma, R. Wilders, “Gap junctions in cardiovascular disease," *Circulation Research*, vol. 86, pp. 1193–1197, 2000.

[77] R.W. Joyner, F.J. Van Capelle, “Propagation through electrically coupled cells. How a small SA node drives a large atrium," *Biophysical Journal*, vol. 50, pp. 1157–1164, 1986.

[78] J.W. Kalat, *Biological Psychology*, Wadsworth (CA), 2009.

[79] D.L. Kasper, E. Braunwald, S. Hauser, D. Longo, J.L. Jameson, A.S. Fauci, *Harrison's Principles of Internal Medicine*, McGraw Hill, 2004.

[80] J. P. Keener, F. C. Hoppensteadt, J. Rinzel, "Integrate and fire models of nerve membrane response to oscillatory input," *SIAM Journal on Applied Mathematics*, vol. 41, pp. 503–517, 1981.

[81] J. Keener, J. Sneyd, *Mathematical Physiology,* Springer-Verlag, New York, 1998.

[82] A.G. Kermode, A.J. Thompson, P. Tofts, D.G. Macmanus, B.E. Kendall, D.P.E. Kingsley, I.F. Moseley, P. Rudge, W.I. McDonald, "Breakdown of the blood-brain barrier precedes symptoms and other MRI signs of new lesions in multiple sclerosis: Pathogenic and clinical implications," *Brain*, vol. 113, no. 5, pp. 1477–1489, 1990.

[83] A.Y. Khintchine, "Mathematical theory of a stationary queue," *Mathematicheskii Sbornik*, no. 32, pp. 64–100, 1930.

[84] T.H. Kim, S.H. Lee, J. Lee, H.S. Song, E.H. Oh, T.H. Park, S. Hong, "Single-carbon-atomic-resolution detection of odorant molecules using a human olfactory receptor-based bioelectronic nose," *Advanced Materials*, vol. 21, pp. 91–94. 2008.

[85] R.E. Klabunde, *Cardiovascular physiology concepts*. Lippincott Williams & Wilkins, 2005.

[86] B. W. Knight, "Dynamics of encoding a population of neurons," *Journal of General Physiology*, vol. 59, pp. 734–766, 1972.

[87] C. Koch, I. Segev, "The role of single neurons in information processing," *Nature Neurosci.*, vol. 3, pp. 1171–1177, 2000.

[88] V. Koleshko, N. Khmurovich, Y. Varabei, E. Polynkova, "Biosensor intelligent system of rapid diagnosis," in *5th International Conference on Perspective Technologies and Methods in MEMS Design (MEMSTECH 2009)*, pp. 26–30, Apr. 2009.

[89] M.S. Kuran, H.B. Yilmaz, T. Tugcu, I.F. Akyildiz, "Modulation techniques for communication via diffusion in nanonetworks," in *Proc. of the IEEE International Conference on Communications (ICC) 2011*, Kyoto, Japan, Jun. 2011.

[90] Y. Kurita, M. Tada, Y. Matsumoto,T. Ogasawara, "Simultaneous measurement of the grip/load force and the finger EMG : effects of the grasping condition," in *Proceedings of IEEE International Workshop on Robot and Human Interactive Communication*, pp. 217–222, 2002.

[91] Y. Kurita, M. Tada, Y. Matsumoto,T. Ogasawara, "Simultaneous measurement of the grip/load force and the finger EMG : effects of the object weight," in *Proceedings of IEEE International Conference on Systems, Man and Cybernetics (SMC2002)*, 2002.

[92] M. Kuscu, O. B. Akan, "A physical channel model and analysis for nanoscale molecular communications with Forster Resonance Energy Transfer (FRET)," *IEEE Trans. Nanotechnol.*, vol. 11, no. 1, pp. 200–207, January 2012.

[93] J. Law, F. Regnier, "Pheromones," *Annual Review of Biochemistry*,no. 40, 1971.

[94] W. Leal, *Pheromone reception*, Topics in Current Chemistry, Springer-Verlag, Berlin, Heidelberg, 2005.

[95] J. Li, T. Peng, and Y. Peng, “A cholesterol biosensor based on entrapment of cholesterol oxidase in a silicic sol-gel matrix at a prussian blue modified electrode," *Electroanalysis*, vol. 15, pp. 1031–1037, 2003.

[96] Y. Li, M. Chiang, A.R. Calderbank, and S.N. Diggavi, “Optimal Rate-Reliability-Delay Tradeoff in Networks with Composite Links," *IEEE Transactions on Communications*, vol. 57, no. 5, 2009.

[97] K. Limpaphayom, R.W. Newcomb, “The extended ear type system and possible applications," in *Proceedings of 2010 IEEE International Symposium on Circuits and Systems (ISCAS)*, pp.1795–1798, 2010.

[98] S. Lindsay, *Introduction to Nanoscience*, Oxford University Press, Oxford, UK, 2009.

[99] Glenn Terje Lines, Per Grøttum, Aslak Tveito, “Modeling the electrical activity of the heart: a bidomain model of the ventricles embedded in a torso," *Computing and Visualization in Science*, vol. 5, no. 4, pp. 195–213, Apr. 2003.

[100] J.Q. Liu, T. Nakano, “An information theoretic model of molecular communication based on cellular signaling," in *Bio-Inspired Models of Network, Information and Computing Systems (Bionetics 2007)*, pp. 316 –321, Dec. 2007.

[101] M. S. Livstone, D. Noort, L. F. Landweber, “Molecular computing revisited: a Moore’s Law?," *Trends in Biotechnolgy*, vol. 21, no. 3, pp. 98–101, 2003.

[102] I. Llatser, E. Alarcón, M. Pierobon, “Diffusion-based channel characterization in molecular nanonetworks," in *Proc. of 1st IEEE International Workshop on Molecular and Nano Scale Communication (MoNaCom), INFOCOM,* Shanghai, China, Apr. 2011.

[103] R. Llinàs, I.Z. Steinberg, K. Walton, “Relationship between presynaptic calcium current and postsynaptic potential in squid giant synapse," *Biophysical Journal*, vol. 33, pp. 323–351, 1981.

[104] U. Madhow, M. L. Honig, “MMSE interference suppression for direct-sequence spread-spectrum CDMA," *IEEE Trans. Comm.*, vol. 42, no. 12, pp. 3178–3188, Dec. 1994.

[105] D. Malak, O. B. Akan, “A communication theoretical analysis of synaptic multiple-access channel in hippocampal-cortical neurons," under revision in *IEEE Trans. Commun.*, 2012.

[106] A. Manwani, C. Koch, “Detecting and estimating signals over noisy and unreliable synapses: information-theoretic analysis," *Neural Comput.*, vol. 13, no. 1, pp. 1–33, Jan. 2001.

[107] R.L. Marchetti, L.A. Fiore, K.D. Valente, G. Gronich, A.B. Nogueira, W.H. Tzu, “Surgical treatment of temporal lobe epilepsy with interictal psychosis: results of six cases,"]emphEpilepsy & Behavior, vol. 4, no. 2, pp. 146–152, Apr. 2003.

[108] H. Markram et al., “Physiology and anatomy of synaptic connections between thick tufted pyramidal neurons in the developing rat neocortex," *J Physiol*, vol. 500, no. 2, pp. 409–440, April 1997.

[109] P.S. Masand, L. Culpepper, D. Henderson, S. Lee, K. Littrell, J.W. Newcomer, N. Rasgon, “Metabolic and endocrine disturbances in psychiatric disorders: a multidisciplinary approach to appropriate atypical antipsychotic utilization," *CNS Spectrums*, vol. 10, no. 14, pp. 1–16, 2005.

[110] V. Matveev, X.-J. Wang, “Implications of all-or-none synaptic transmission and short-term depression beyond vesicle depletion: a computational study," *J Neurosci*, vol. 20, no. 4, pp. 1575–88, Feb. 2000.

[111] J. P. Meeks, S. Mennerick, “Action potential initiation and propagation in CA3 pyramidal axons," *J Neurophysiol*, vol. 97, pp. 3460–72, May 2007.

[112] M. Moore, A. Enomoto, T. Nakano, R. Egashira, T. Suda, A. Kayasuga, H. Kojima, H. Sakakibara, K. Oiwa, “A design of a molecular communication system for nanomachines using molecular motors," in *Proceedings of the Fourth Annual IEEE International Conference on Pervasive Computing and Communications (PerCom06)*, Mar. 2006.

[113] M. Moore, T. Suda, K. Oiwa, “Molecular communication: Modeling noise effects on information rate", *IEEE Transactions on Nanobioscience*, vol. 8, pp. 169–180, Jun. 2009.

[114] Y. Moritani, S. Hiyama, T. Suda, “Molecular communication among nanomachines using vesicles," in *Proceedings of NSTI Nanotechnology Conference*, May 2006.

[115] M. Mukai, K. Maruo, J. Kikuchi, Y. Sasaki, S. Hiyama, Y. Moritani, T. Suda, “Propagation and Amplification of Molecular Information using a Photo-responsive Molecular Switch," *Supramol. Chem.*, vol. 21, no. 3-4, pp. 284–291, 2009.

[116] R. Mukkamala, R.J. Cohen, “A forward model-based validation of cardiovascular system identification," *AJP – Heart*, vol. 281, no. 6 , pp. H2714–H2730, Dec. 2001.

[117] T. Munakata. “Guest Editor’s Introduction," in the Special Issue “Beyond Silicon: New Computing Paradigms," *Communications of the ACM*, vol. 50, no. 9, pp. 30–34, 2007.

[118] Dale Muzzey, “The effects of drug and disease on synaptic transmission," Available from Harvard Life Sciences-HHMI Outreach Program [Online]. Available at: `http://outreach.mcb.harvard.edu/animations/synapse.swf`. Accessed July 10, 2012.

[119] T. Nakano, T. Suda, M. Moore, R. Egashira, A. Enomoto, K. Arima, “Molecular communication for nanomachines using intercellular calcium signaling," in *Proceedings of the Fifth IEEE Conference on Nanotechnology*, pp. 478–481, Jun. 2005.

[120] T. Nakano, T. Suda, T. Koujin, T. Haraguchi, Y. Hiraoka, “Molecular communication through gap junction channels: system design, experiments and modeling," in *Proc. 2nd International Conference on Bio-Inspired Models of Network, Information, and Computing Systems*, Budapest, Hungary, 2007.

[121] T. Nakano, and J.-Q. Liu, “Design and Analysis of Molecular Relay Channels: An Information Theoretic Approach," *IEEE Transactions on Nanobioscience*, vol. 9, no. 3, pp. 213–221, 2010.

[122] J.B. O’connell, R.C. Bourge, M.R. Costanzo-Nordin, D.J. Driscoll, J.P. Morgan, E.A. Rose, B.F. Uretsky, “Cardiac transplantation: recipient selection, donor procurement, and medical follow-up. A statement for health professionals from the Committee on

Cardiac Transplantation of the Council on Clinical Cardiology," *American Heart Association, Circulation*, vol. 86, pp. 1061–1079, 1992.

[123] A. Opel, S. Deurloo, C. Robles, D. Harrington, "Severe physical handicaps," California State University, 2010.

[124] M.A. Paradiso, M.F. Bear, B.W. Connors, *Neuroscience: Exploring the Brain*, Lippincott Williams & Wilkins, 2007.

[125] L. Parcerisa, I.F. Akyildiz, "Molecular communication options for long range nanonetworks," *Computer Networks Journal (Elsevier)*, vol. 53, no. 16, pp. 2753-2766, Nov. 2009.

[126] M.G. Parker, "Mechanism of steroid hormone action," *Cancer Surveys*, vol. 5, no. 3, pp. 625-633, 1986.

[127] V. I. Pidoplichko et al., "Nicotine activates and desensitizes midbrain dopamine neurons," *Nature*, vol. 390, pp. 401–404, 1997.

[128] M. Pierobon, I.F. Akyildiz, "A physical channel model for molecular communication in nanonetworks", *IEEE Journal on Selected Areas in Communications*, vol. 28, pp. 602–611, May 2010.

[129] M. Pierobon, I.F. Akyildiz, "A physical end-to-end model for molecular communication in nanonetworks," *IEEE Journal of Selected Areas in Communications*, vol. 28, no. 4, pp. 602–611, May 2010.

[130] M. Pierobon, I.F. Akyildiz, "Information capacity of diffusion-based molecular communication in nanonetworks," in *Proc. of IEEE International Conference on Computer Communication, INFOCOM, Miniconference,* Shanghai, China, Apr. 2011.

[131] M. Pierobon, I.F. Akyildiz, "Diffusion-based noise analysis for molecular communication in nanonetworks," *IEEE Transactions on Signal Processing*, vol. 59, no. 6, pp. 2532–2547, Jun. 2011.

[132] M. Pierobon, I.F. Akyildiz, "Noise analysis in ligand-binding reception for molecular communication in nanonetworks," *IEEE Transactions on Signal Processing*, vol. 59, no. 9, pp. 4168–4182, Sep. 2011.

[133] A. Pigoń-Wegiel, J. Sroczyński, A. Wegiel, D. Znamirowska, K. Biskupek, F. Zych, "Effect of mechanical vibration and noise on adrenal cortex hormone secretion," *Pol Arch Med Wewn*, vol. 68, no. 5, pp. 329–335, Nov. 1982.

[134] J.P.J. Pinel, *Biopsychology*, Pearson Education Inc., 2006.

[135] P. Poirazi, T. Brannon, B. W. Mel, "Arithmetic of subthreshold synaptic summation in a model CA1 pyramidal cell," *Neuron*, vol. 37, pp. 977–987, Mar. 2003.

[136] D. Purves, G.J. Augustine, D. Fitzpatrick, W.C. Hall, A.-S. LaMantia, J.O. McNamara, L.E. White, *Neuroscience*, Sinauer Associates Inc., 2008.

[137] M. Raastad, G. Shepherd, "Single axon action potentials in the rat hippocampal cortex," *J Physiol*, vol. 548, pp. 745–52, 2003.

[138] W. Rall, "Distinguishing theoretical synaptic potentials computed for different soma-dendritic distributions of synaptic input," *J. Neurophysiol.*, vol. 30, pp. 1138–68, 1967.

[139] L. A. Raymond et al., “Pathophysiology of HuntingtonÕs disease: time-dependent alterations in synaptic and receptor function," *Neuroscience*, vol.198, pp. 252–273, Dec. 2011.

[140] J. A. Ribeiro et al., “Adenosine receptors in the nervous system: pathophysiological implications," *Prog Neurobiol*, vol. 68, no. 6, pp. 377–392, Dec. 2002.

[141] J.L. Richard, E.B. Baum, “DNA Based Computers," in *Proc. of a DIMACS Workshop*, vol. 27, 1995.

[142] S.O. Rizzoli, W.J. Betz, “Synaptic vesicle pools," *Nature Reviews Neuroscience*, vol. 6, pp. 57–69, Jan. 2005.

[143] S. Rohr, “Role of gap junctions in the propagation of the cardiac action potential," *Cardiovascular Research*, vol. 62, pp. 309–322, 2004.

[144] C. Rose, S. Ulukus, R. D. Yates, “Wireless systems and interference avoidance," *IEEE Trans. Wireless Commun.*, vol. 1, no. 3, pp. 415–428, Jul. 2002.

[145] M. C. W. van Rossum, G. Q. Bi, G. G. Turrigiano, “Stable Hebbian learning from spike timing-dependent plasticity," *The Journal of Neuroscience*, vol. 20, no. 23, pp. 8812–8821, Dec. 2000.

[146] M.C.W. van Rossum, G.G. Turrigiano, “Correlation based learning from spike timing dependent plasticity," *Neurocomputing* vol. 38–40, pp. 409–415, June 2001.

[147] P.B. Sargent et al., “Rapid vesicular release, quantal variability, and spillover contribute to the precision and reliability of transmission at a glomerular synapse," *J Neurosci*, vol. 25, no. 36, pp. 8173–87, Sep. 2005.

[148] Y. Sasaki, T. Ishikawa, M. Hashizume, J. Kikuchi, Y. Moritani, S. Hiyama and T. Suda, “Molecular communication using artificial cells (1): Controlled propagation of molecular capsules," in *Proceedings of International Symposium on Nanoscience and Photoscience*, p-41, Jul. 2007.

[149] Y. Sasaki, Y. Shioyama, W. Tian, J. Kikuchi, S. Hiyama, Y. Moritani, T. Suda, “A Nano Sensory Device Fabricated on a Liposome for Detection of Chemical Signals," *Biotechnol. Bioeng.*, vol. 105, no. 1, pp. 37–43, 2010.

[150] T.D. Schneider, “Sequence logos, machine/channel capacity, Maxwell’s demon, and molecular computers: a review of the theory of molecular machines," *Nanotechnology*, vol. 5, no. 1, pp. 1–18, Jan. 1994.

[151] J. Schnupp, I. Nelken, A. King, *Auditory neuroscience*, MIT Press, 2011.

[152] G. Schram, M. Pourrier, P. Melnyk, S. Nattel, “Differential distribution of cardiac ion channel expression as a basis for regional specialization in electrical function," *Circulation Research*, vol. 90, pp. 939–950, 2002.

[153] R. Shabetai, O. Noble, W.G. Guntheroth, “The hemodynamics of cardiac tamponade and constrictive pericarditis," *The American Journal of Cardiology*, vol. 26, no. 5, pp. 480–489, Nov. 1970.

[154] R.M. Shaw, Y. Rudy, “Ionic mechanisms of propagation in cardiac tissue: Roles of the sodium and L-type calcium currents during reduced excitability and decreased gap junction coupling," *Circulation Research*, vol. 81, pp. 727–741, 1997.

[155] R.M. Shaw, Y. Rudy, “Electrophysiologic effects of acute myocardial ischemia: A mechanistic investigation of action potential conduction and conduction failure," *Circulation Research*, vol. 80, pp. 124–138, 1997.

[156] E.P. Simoncelli, L. Paninski, J. Pillow, O. Schwartz, “Characterization of neural responses with stochastic stimuli," in *“The New Cognitive Neurosciences,"* edited by M. Gazzaniga, MIT Press, 2004.

[157] S. Song, K. D. Miller, L. F. Abbott, “Competitive Hebbian learning through spike-timing-dependent synaptic plasticity," *Nature Neurosci.*, vol. 3, pp. 919–926, 2000.

[158] R.S. Adve, and A.W. Eckford, “Molecular Communication Using Brownian Motion With Drift," *IEEE Transactions on Nanobioscience*, vol. 11, no.2, pp. 89–99, 2012.

[159] C. F. Stevens, Y. Wang, “Facilitation and depression at single central synapses," *Neuron*, vol. 14, pp. 795–802, April 1995.

[160] T. Strand, B. Lamb, H. Thistle, E. Allwine and H. Peterson, “A simple model for simulation of insect pheromone dispersion within forest canopies," *Ecological Modelling*, vol. 220, no. 5, pp. 640-656, 2009.

[161] T. Swift, “Disorders of neuromuscular transmission other than Myasthenia Gravis," *Muscle & Nerve*, vol. 4, pp. 334–353, 1981.

[162] P. Tallury, A. Malhotra, L.M. Byrne, and S. Santra, “Nanobioimaging and sensing of infectious diseases," *Advanced Drug Delivery Reviews*, vol. 62, pp. 424–437, Mar. 2010.

[163] C. M. Tang et al., “Saturation of postsynaptic glutamate receptors after quantal release of transmitter," *Neuron*, vol. 13, no. 6, pp. 1385–93, Dec. 1994.

[164] H. L. Van Trees, *Detection, Estimation, and Modulation Theory, Part I.* Wiley, New York, 1968.

[165] S.K. Vashist, R. Tewari, I. Kaur, R.P. Bajpai, L.M. Bharadwaj, “Smart-drug delivery system employing molecular motors," in *Proceedings of International Conference on Intelligent Sensing and Information Processing*, pp. 441–446, Jan. 2005.

[166] A. Vázquez, A. Flammini, A. Maritan, A. Vespignani, “Global protein function prediction in protein-protein interaction networks," *Nature Biotechnology*, vol. 21, pp. 697–700, 2003.

[167] M. Vehkaperä, M. Médard, “A Throughput-Delay Trade-Off in Packetized Systems With Erasures," in *Proc. of ISIT*, Sept. 2005, pp. 1858–1862.

[168] S. Verdu, *Multiuser Detection,* Cambridge University Press, 1998.

[169] B.T. Walsh, “Endocrine disturbances in anorexia nervosa and depression," *Psychosomatic Medicine*, vol. 44, no. 1, pp. 85–91, Mar. 1982.

[170] J.M. Walsh, S. Weber, C.W. Maina, “Optimal Rate Delay Tradeoffs for Multipath Routed and Network Coded Networks," in *Proc. of ISIT*, July 2008, pp. 682–686.

[171] X.-J. Wang, D. Golomb, J. Rinzel, “Emergent spindle oscillations and intermittent burst firing in a thalamic model: Specific neuronal mechanisms," *Proc. Natl. Acad. Sci. USA*, vol. 92, pp. 5577–81, June 1995.

[172] W.-D. Wang, Z.-T. Chen, B.-G. Kang, R. Li, “Construction of an artificial intercellular communication network using the nitric oxide signaling elements in mammalian cells," *Experimental Cell Research*, vol. 314, pp. 699–706, 2008.

[173] T. D. Wyatt, *Pheromones and animal behaviour: communication by smell and taste*, New York: Cambridge University Press, 2003, pp. 9–10.

[174] K. Yasuhara, Z. Wang, T. Ishikawa, J. Kikuchi, Y. Sasaki, S. Hiyama, Y. Moritani, T. Suda, “Specific delivery of transport vesicles mediated by complementary recognition of DNA signals with membrane-bound oligonucleotide lipids," *Supramol. Chem*, vol. 23, no. 3-4, pp. 218–225, 2011.

[175] T. Yoshida, K. Nakadai, H.G. Okuno, “Automatic speech recognition improved by two-layered audio-visual integration for robot audition," in *9th IEEE-RAS International Conference on Humanoid Robots (Humanoids 2009)*, pp. 604–609, Dec. 2009.

[176] T.F. Zuck, J.G. Riess, “Current Status of Injectable Oxygen Carriers," *Critical Reviews in Clinical Laboratory Sciences*, vol. 31, no. 4, pp. 295–324, 1994.

[177] R. S. Zucker, “Short-term synaptic plasticity," *Ann. Rev. Neurosci.*, vol. 12, pp. 13–31, 1989.

CURRICULUM VITAE

Derya Malak received her B.Sc. degree in Electrical and Electronics Engineering from Middle East Technical University, Ankara, Turkey, in 2010. She is currently a research assistant in the Next-generation and Wireless Communication Laboratory (NWCL) and received her M.Sc. degree in the Department of Electrical and Electronics Engineering, Koc University under the supervision of Prof. Özgür B. Akan. Her current research interests include molecular communications, nanoscale networks, information theory and coding.